学位論文

The carbon cycle in the Himalayan river basins
on both modern and geological timescales:
evidence for a role of CO_2 release from river surface water
and chemical weathering

（ヒマラヤの河川流域における現代および
地質学的時間スケールの炭素循環の解明:
河川表層からの CO_2 放出と化学風化が果たす役割について）

平成 27 年 12 月博士（理学）申請

東京大学大学院理学系研究科

地球惑星科学専攻

眞中 卓也

Abstract

The carbon cycle in terrestrial rivers plays an important part in the Earth-surface environment, transporting vast amounts of material from the land to the ocean and providing essential waters and nutrients for terrestrial biota. On modern timescales of 1-100 years, recent studies have reported that abundant CO_2 generated by biological activity in river basins is released from surface waters to the atmosphere. In contrast, on geological timescales of 10^4 to 10^6 years, chemical weathering of silicate rocks in the basins consumes atmospheric CO_2. In this study, I focused on the Himalayan rivers, where active weathering occurs and large spatial variations in geology and land use are observed between the upper and lower basins. In this setting, the riverine carbon cycle on multiple timescales and its significance within the Earth-surface environment was examined, through the following three studies.

(1) Modern timescale: spatial and seasonal variations in surface water pCO_2.

The Ganges, Brahmaputra, and Meghna rivers together have the second largest water discharge in the world. However, few studies have analyzed the partial pressure of CO_2 (pCO_2) and CO_2 degassing fluxes in these rivers. I investigated the carbonate systems of these rivers, including spatial and seasonal variations in pCO_2, and determined their potential importance. Although pCO_2 was low in the upper reaches of these rivers, owing to active chemical weathering, values were higher than atmospheric pCO_2 along the lower reaches, where deep soils have developed and where high air temperatures promote active soil respiration. Using a simple mixing calculation, it was found that seasonal variations in these river water carbonate systems are controlled by subsurface water flows, which originate in the lowlands and are influenced by soil respiration. In the rainy season, most of the lowlands are inundated, and the contribution of subsurface flow to river water carbonate systems increases, resulting in higher pCO_2 values. Total CO_2 fluxes from the Ganges and Brahmaputra River waters were calculated to be 0.45-1.7 × 10^{11} mol yr^{-1} and 0.62-2.4 × 10^{11} mol yr^{-1}, respectively. In future research, more detailed spatial and seasonal investigations are required to clarify the role of terrestrial ecosystems in the short-term global carbon cycle.

(2) Geological timescale: chemical weathering and long-term CO_2 consumption reconstructed from major ion chemistry.

The role of Himalayan river systems in the long-term global carbon cycle has been a subject of great interest, especially in the context of past climate change such as global cooling during the Cenozoic. However, there are few reliable geochemical data from the Ayeyarwady River. This study focused on reevaluating chemical weathering in the Himalayan watersheds by carrying out chemical analyses of the composition of dissolved substances in samples taken from the Ayeyarwady, Mekong, and Chao Phraya rivers. Comparisons of water quality showed that, unlike in previous studies, the total alkalinity budgets of the Ayeyarwady are dominated by carbonate rather than silicate weathering. Long-term CO_2 consumption by silicate weathering in the Ayeyarwady is estimated to be only 63-145 $\times 10^9$ mol yr^{-1}, which is only 10 % of the previous estimate. The results of this study also suggest that all Himalayan watersheds only account for approximately 10 % of the total global CO_2 consumption by silicate weathering. Although further studies are needed, chemical weathering and associated CO_2 uptake in the Himalayas likely played a lesser role in past long-term global cooling than previously thought.

(3) Geological timescale: development of analytical procedures of magnesium and silicon isotope ratio measurement to gain further insight into chemical weathering.

Magnesium and silicon isotope ratios ($\delta^{26}Mg$, $\delta^{30}Si$) are new potential proxies for gaining insight into Mg- and Si-related processes including chemical weathering in river basins. In this study, I examined the availability of $\delta^{26}Mg$ for the carbon cycle, by investigating the spatial and seasonal variations in concentrations and isotope ratios of Mg and Sr in the Ganges, Brahmaputra, and Meghna rivers. $\delta^{26}Mg$ values of these river waters reflected the upstream lithology (dolostone/silicate) throughout the year. The spatial and seasonal variations in the major ion concentrations of the water suggested that the ions may originate from different sources. This result implies that $\delta^{26}Mg$ ratios are the best tool for identifying Mg sources and their chemical reaction histories, which can impact on the global carbon cycle. Additionally, the Ganges, Brahmaputra, and Meghna rivers were found to play an important role in the Mg isotope budget of the ocean, transporting as much as 4 % of the total riverine flux of Mg^{2+} to the ocean, with a $\delta^{26}Mg$ value slightly lower (-1.2 ‰) than the global river average. I also developed a Si separation method, which is essential for $\delta^{30}Si$ measurements. I revised the cation exchange methods reported by a previous study, and conducted repeated pilot studies. The Si recovery rate of this study was 102.3 ± 4.2 % (n = 24), suggesting that separation was successfully carried out in the laboratory environment.

Contents

Chapter 1. Background and objectives

1.1. Introduction

1.1.1. Overview of the global carbon cycle

Carbon is an important element controlling the Earth-surface environment. The carbon cycle describes the exchange of carbon between the biosphere, pedosphere, geosphere, hydrosphere, and atmosphere (Figure 1-1). Carbon dioxide (CO_2) is one of the main forms of carbon in the atmosphere (e.g., CO_2, methane, and chlorofluorocarbon). It is a greenhouse gas that traps significant heat inside the Earth's atmosphere, affecting the global climate [IPCC, 2013]. Terrestrial vegetation absorbs atmospheric CO_2 and sunlight, and converts CO_2 into organic matter. This process, photosynthesis, is shown in the following simple equation:

$$CO_2 + H_2O \rightarrow CH_2O + O_2 \quad (1\text{-}1)$$

In turn, respiration by both heterotrophic and autotrophic organisms, including human beings, decomposes organic matter into CO_2:

$$CH_2O + O_2 \rightarrow CO_2 + H_2O \quad (1\text{-}2)$$

Besides these biological processes, chemical weathering of terrestrial rocks consumes CO_2. Chemical weathering of silicate and carbonate rocks (e.g., calcite) can be expressed by the following equations:

$$CaSiO_3 + 2\ CO_2 + H_2O \rightarrow Ca^{2+} + 2\ HCO_3^- + SiO_2 \quad (1\text{-}3)$$

$$CaCO_3 + CO_2 + H_2O \rightarrow Ca^{2+} + 2\ HCO_3^- \quad (1\text{-}4)$$

In silicate weathering processes, the bicarbonate (HCO_3^-) generated originates solely from the atmosphere. Conversely, in carbonate weathering processes, 50 % of generated HCO_3^- comes from the parent rock.

Both photosynthesis and respiration are active processes in the surface ocean, and the organic matter produced here sinks to the deeper waters below. These successive processes are known as the "biological pump". Inorganic and organic carbonate mineralization also occurs (e.g., corals and foraminifera generate calcite and aragonite) and CO_2 is released back to the atmosphere [Hartmann, 2009; Ushie et al., 2010; Feely et al., 2009]. This process is shown in the following simplified equation:

$$Ca^{2+} + 2\ HCO_3^- \rightarrow CaCO_3 + CO_2 + H_2O \quad (1\text{-}5)$$

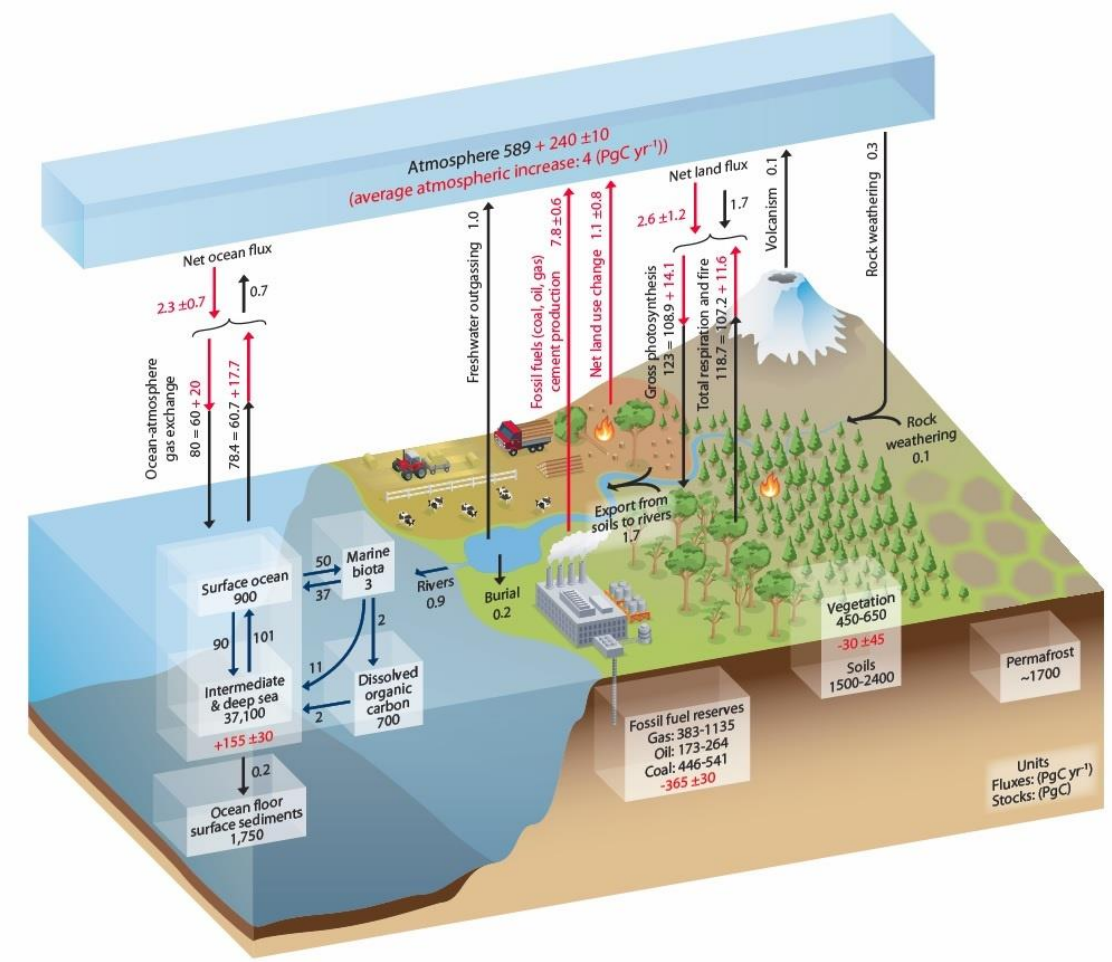

Figure 1-1.

Simplified schematic of the global carbon cycle reported by IPCC [2013] (IPCC Fifth Assessment Report, Climate Change 2013: The Physical Science Basis, 6. Carbon and Other Biogeochemical Cycles, Figure 6.1). Numbers represent reservoir mass, also called “carbon stocks” in PgC and annual carbon exchange fluxes (in PgC yr^{-1}). Black numbers and arrows indicate reservoir mass and exchange fluxes estimated for the time prior to the Industrial Era, in about 1750. Red arrows and numbers indicate annual “anthropogenic” fluxes averaged over the 2000–2009 time period.

Although about 80 % of biologically generated calcium carbonate will dissolve in the deep sea, referred to as the "alkalinity pump", the rest will be fixed in marine sediments [Archer, 2003].

In order to understand the global carbon cycle and successive changes to climate, it is necessary to determine the timescales of each process. On modern timescales of 1-100 years, both human activities post Industrial Revolution and biological activities (photosynthesis and respiration) are important. In recent years, 7.8 Pg C yr^{-1} of CO_2 has been emitted by either fossil fuel combustion in the pedosphere or cement production [IPCC, 2013] (Figure 1-1). Although about half the anthropogenic CO_2 is absorbed by gross photosynthesis and physical CO_2 exchange between the ocean and the atmosphere, partial pressure of CO_2 (pCO_2) in the atmosphere has increased from 280 μatm in the pre-industrial era to 395 μatm nowadays, leading to global warming (Figure 1-2). In addition, human activities directly impact continental and oceanic biota. For example, the increase in anthropogenic nutrient loading from urban sewage and agricultural runoff over the last several decades has caused eutrophication in aquatic ecosystems around the world, resulting in highly active photosynthesis [Vollenweider, 1968; National Research Council, 1992; Nixon 1995]. As much as 1.1 PgC yr^{-1} of CO_2 is released by anthropogenic land use, mainly deforestation [IPCC, 2013] (Figure 1-1).

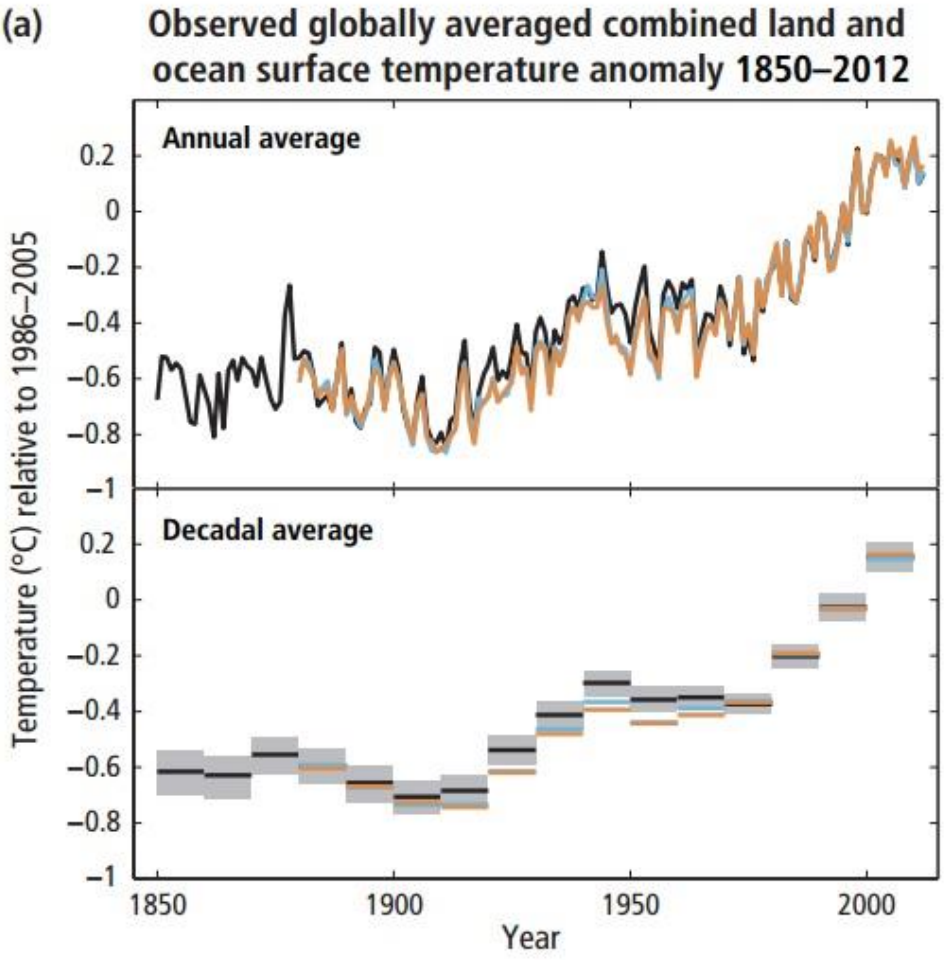

Figure 1-2.

Observed globally averaged combined land and ocean surface temperature anomalies (relative to the mean of 1986 to 2005 period, as annual and decadal averages) with an estimate of decadal mean uncertainty included for one data set (grey shading), reported by IPCC [2013] (IPCC Fifth Assessment Report, Climate Change 2014: Synthesis Report, 1. Observed Changes and their Causes, Figure 1.1).

On geological timescales of 10^4 to 10^6 years, however, most organic matter, including plant and animal matter, is decomposed and returned back to the atmosphere in the form of CO_2. On this timescale, chemical weathering of terrestrial rocks is important; 0.29 PgC yr^{-1} of atmospheric CO_2 is converted to HCO_3^- (equation 1-3 and 1-4), which is transported to the ocean via rivers [Gaillardet et al., 1999]. Equation 1-5 shows that a portion of HCO_3^- in the ocean would be released back to the atmosphere in the form of gaseous CO_2. Through the silicate weathering process, two molars of atmospheric CO_2 are converted to two molars of HCO_3^- (equation 1-3), while only one molar of atmospheric CO_2 is consumed through the carbonate weathering process (equation 1-4). In equation 1-5, two molars of HCO_3^- are consumed and only one molar of CO_2 is released. Therefore, only silicate weathering contributes to a net reduction in atmospheric CO_2 concentration, which contributes to long-term climate change as shown by Raymo and Ruddiman [1992] and Zachos et al. [2001] (Figure 1-3).

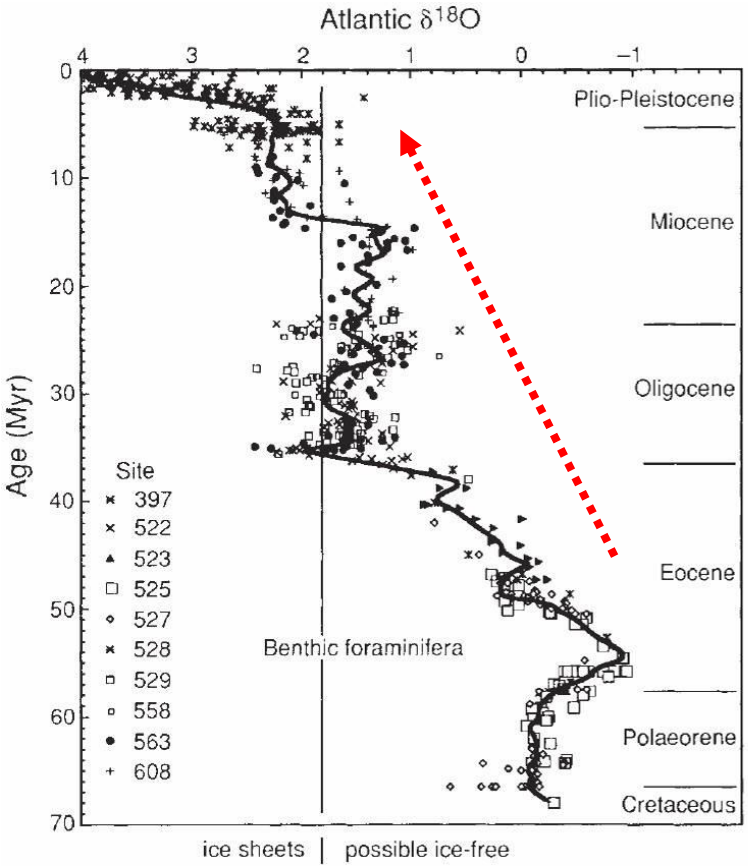

Figure 1-3.
Benthic $\delta^{18}O$ record from Deep Sea Drilling Program Sites since 70 Ma compiled modified from Raymo and Ruddiman [1992].

1.1.2. The importance of rivers

As a reservoir of "liquid water" on the Earth-surface, terrestrial waters are very small; rivers and lakes constitute only 0.0001 % and 0.01 % of the world's total water, respectively [Berner and Berner, 1987]. However, they are important in supporting terrestrial biota, due to high nutrient and oxygen concentrations and abundant sunlight. Net primary production of the land (107 PgC yr^{-1}) is larger than that of the ocean (55 PgC yr^{-1}) [Whittaker and Likens, 1973]. In addition, human beings are also one part of the terrestrial ecosystem supported by terrestrial waters. It is well known that the great ancient civilizations of the world (e.g., Mesopotamia, Egypt, Indus, and China) formed along major rivers, and flourished owing to active agriculture using fertile soils and water in the river basin.

This thesis focuses on the carbon cycle in terrestrial waters, in particular river waters. Terrestrial waters work as the sole transporter of abundant material from the land to the ocean. The IPCC [2013] reported that rivers transport as much as 0.9 PgC yr^{-1} of carbon (for details, see Sections 1.3 and 1.4). Other ions, such as calcium and magnesium, nutrients from organic materials, and particulates are also transported. Rivers enhance biological production not only in river basins but also in oceans, and coastal zones in particular [Siegenthaler and Sarmiento, 1993; Kawahata et al., 2000]. Therefore, a comprehensive understanding of the role of rivers in the carbon cycle is of great importance.

1.1.3. Aims of this chapter

The focus of this thesis is Himalayan rivers, namely the Ganges, Brahmaputra, Ayeyarwady, and Mekong rivers (Figure 1-4). These rivers are among the world's largest and play an important role in both the water and the carbon cycles. The river basins include regions of active physical and chemical weathering of rocks, owing to the uplift of the Himalayan-Tibetan Plateau and the high rainfall associated with strong monsoons [Molnar et al., 1993; Yin and Harrison, 2000]. In addition, the lower basins of these rivers are covered by the Himalayan alluvium characterized by well-developed soils [Kuehl et al., 2005]. These lowlands have the highest population density supported by active agriculture in the world. For example, downstream of the Ganges and Brahmaputra flows in Bangladesh, three rice crops are commonly grown each year [Catling et al., 1983]. Active biological activity in the thick soils and waters is expected in this area.

This chapter focuses on three chemical components of the river water. The first two are dissolved CO_2 and HCO_3^-, both important forms of dissolved inorganic carbon (DIC) whose

concentrations in the river are pH-dependent (see Section 1.3 and equation 1-6 to 1-8). Dissolved CO_2 is closely related to biological activity in the basin. Recent studies revealed that abundant CO_2 is released from surface waters of major rivers to the atmosphere, which may play an important role in the global carbon cycle on modern timescales [Cole et al., 2007; Aufdenkampe et al., 2011; Raymond et al., 2013]. In contrast, HCO_3^- is mainly derived from chemical weathering and is the dominant contributor to total water alkalinity. Determination of HCO_3^- concentration, along with other major dissolved ions, can provide insights into weathered rock types (in particular, silicate or carbonate) and produce estimates of how much CO_2 was consumed on a geological timescale [Gaillardet et al., 1999; Sarin, 2001]. The third chemical component studied here is stable isotope ratios of light elements such as magnesium and silicon. Recently, developments in multicollector inductively coupled plasma mass spectrometry (MC-ICP-MS) have allowed these new isotope systems to be explored in terrestrial systems. Through the measurement of isotope ratios in the river water, a more accurate estimation can be made of the sources and chemical reactions involved in the weathering processes of each element, that is, the types of rock that have been weathered within the catchment area.

Here, I review previous research on the role of these three chemical components in Himalayan rivers (the Ganges, Brahmaputra, Ayeyarwady, and Mekong rivers) in order to more fully understand the carbon cycle on both modern and geologic timescales.

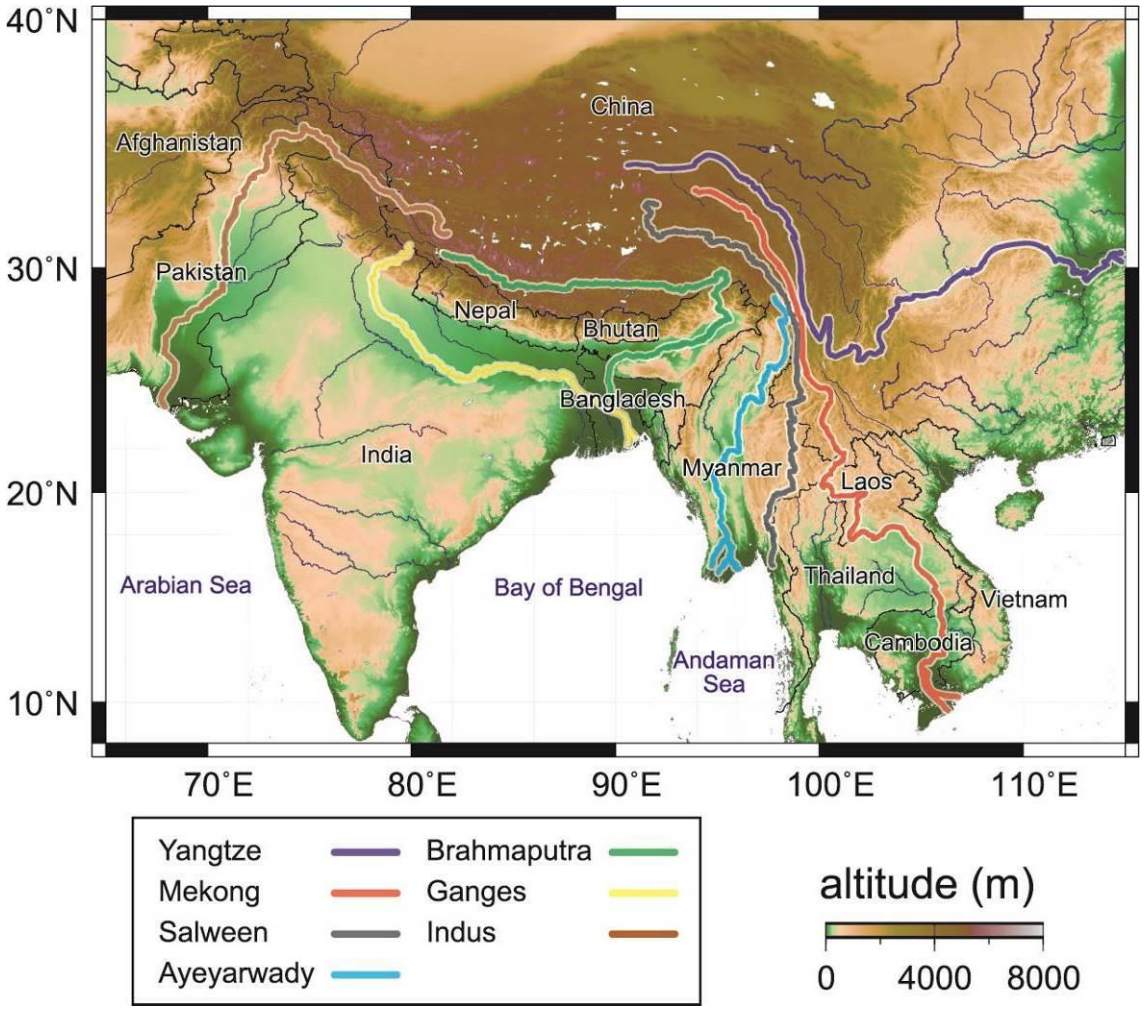

Figure 1-4.

Locations of major Himalayan rivers. Topography data are from Amante and Eakins [2009].

1.2. Overview of studied rivers

This Chapter discusses the general characteristics, such as geology and river size, of the studied rivers. The climate of these Himalayan river basins is mainly tropical and controlled by the summer monsoon. Precipitation during the rainy season accounts for more than 80 % of the total annual rainfall, resulting in extreme discharge of water at this time. I also focus on one local non-Himalayan river in Thailand, the Chao Phraya River, to compare its chemical components to those of the Himalayan rivers.

1.2.1. The Ganges, Brahmaputra, and Meghna rivers

The transboundary river basin of the Ganges, Brahmaputra, and Meghna River system drains a total area of approximately 1.6×10^6 km^2 in India, China, Bhutan, Nepal, and Bangladesh [Milliman et al., 1995]. The Ganges and Brahmaputra rivers originate from the northwest and northeast parts of the high Himalayas, respectively. Tributaries joining these two rivers along their upper reaches flow across various rock types, including Precambrian metamorphics (high-grade schists, gneisses, quartzites, and metamorphosed limestones), felsic intrusives, and Paleozoic to Mesozoic sandstones, shales, and limestones [Huizing, 1971; Heroy et al., 2003; Kuehl et al., 2005] (Figure 1-5). This area is also divided into four lithotectonic units: the Tethyan Sedimentary Series (TSS), with widespread limestone and black shales, the High Himalayan Crystalline Series (HHCS), with biotite muscovite paragneiss and calc-silicates, the Lesser Himalayan Series (LHS), with dolostone, and the Sub-Himalaya (SH), consisting of siliciclastic sediments. Because of the regional metamorphism of limestone and silicate rocks in the Himalayas, chemical weathering in this area greatly contributes to global CO_2 consumption [Galy and France-Lanord, 1999; Sarin et al., 2001]. The lower basins are characterized by Pleistocene alluvium plains, which mainly consist of massive beds of clay, sand and gravel. Illite is ubiquitous in both the Ganges and Brahmaputra rivers, indicating erosion from relatively unweathered granitic or metamorphic terrain of the Himalayas [Heroy et al., 2003]. In addition, the plain contains alkaline and saline soils with calcareous concretion, which is locally known as “kankar” [Sarin et al., 1989]. This soil may result from cyclic wetting and drying in the middle streams.

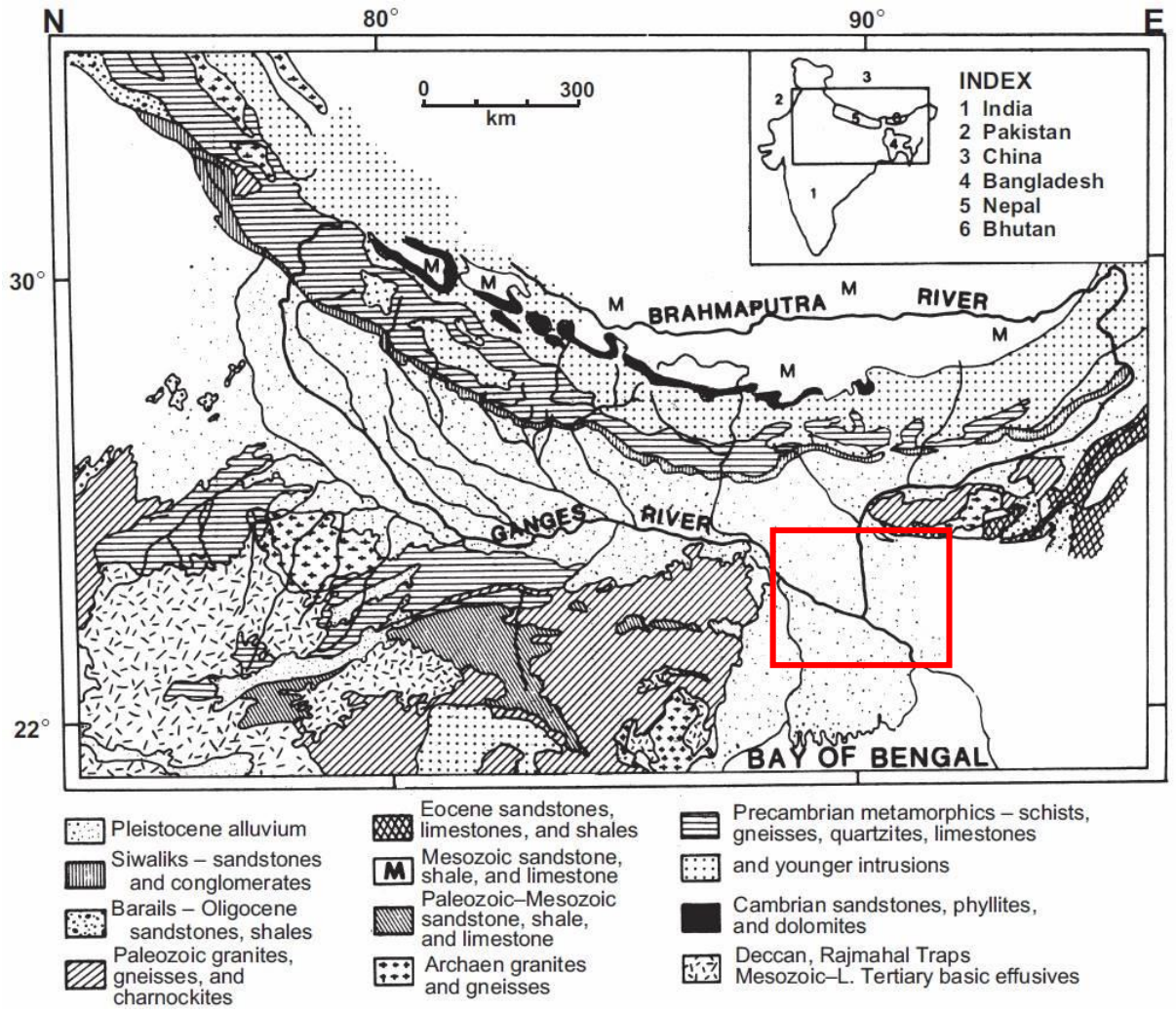

Figure 1-5.

Geological map of drainage basins for the Ganges and Brahmaputra rivers, modified from Kuehl et al. [2005] and references therein. Open red square indicates my sampling stations.

The Ganges flows southeast across India into Bangladesh. Its total length is 2520 km [Parua, 2010] and it drains an area of 1.1×10^6 km^2 [Meybeck and Ragu, 2012]. The mean annual discharge of the Ganges at the Hardinge Bridge station, above its confluence with the Brahmaputra River, is 1.1×10^4 m^3 s^{-1}, and maximum flood discharges of 5.5×10^4 m^3 s^{-1} occur during the rainy season [Webster et al., 2010]. The annual sediment discharge of the Ganges River is 330-550 Tg yr^{-1} [River Survey Project, 1996; Aucour et al., 2006]. This river crosses most of the Himalayan lithotectonic units i.e., TSS, HHCS, and LHS, as well as alluvial plains in India and Bangladesh.

The Brahmaputra flows eastward from its source in the Tibetan Plateau (where it is called the Yarlung Tsangpo River) and then southwest into eastern India (the Eastern Syntaxis zone with high denudation rate) and south to Bangladesh. It meets the Ganges at Goalondo in central Bangladesh. The total length of the Brahmaputra River is 2840 km and its drainage area is 5.8×10^5 km^2 [Parua, 2010; Meybeck and Ragu, 2012]. The mean annual discharge of this river at the Bahadurabad station is 2.0×10^4 m^3 s^{-1}, and maximum flood discharges of 6.4×10^4 m^3 s^{-1} occur during the rainy season [Webster et al., 2010]. The annual sediment discharge of the Brahmaputra River is 400-600 Tg yr^{-1} [River Survey Project, 1996; Aucour et al., 2006]. This river also crosses the TSS, HHCS, and LHS Himalayan lithotectonic units as well as the alluvial plains of Assam and Bangladesh. The Yarlung Tsangpo River drains turbidites and ophiolities from the Indus-Tsangpo Suture Zone, and its major tributaries drain sedimentary rocks, gneisses, and gabbroic to granodioritic rocks of the Tibetan Plateau. Several tributaries of the Brahmaputra River drain from Bhutan Himalaya (northern part of HHCS), which is dominated by migmatites, gneisses, mica schists, marbles, and in some places amphiboles. The main channel of the Brahmaputra River flows over the alluvial plain of Assam and Bangladesh, which consists of Neogene molasses sediments including cherty quartzites and phyllites.

In contrast, the Meghna River, the headstream of which rises in the hills of eastern India, mainly flows across lowland deposits of the Himalayan alluvium. The Meghna River itself is formed by the convergence of the Surma and Kusiyara rivers in Bangladesh and flows southwest within Bangladesh until it joins the Ganges at Chandpur. The combined rivers then flow southward into the Bay of Bengal (also called the lower Meghna River at this point). The total length and average annual discharge of the upper Meghna River system (before confluence with the Ganges) are only 930 km and 3510 m^3 s^{-1}, respectively [Parua, 2010].

The upper basins of these rivers exist in an alpine climate, while the lower basins are under tropical climates controlled by the summer monsoon. The mean annual air temperature at Lhasa, Tibet

was 9.9 °C in 2012, whereas it was 26.7 °C at Dhaka, Bangladesh [National Oceanic and Atmospheric Administration, 2013]. Annual rainfall at Dhaka in 2014 was 1400 mm [Bangladesh Meteorological Department, 2016]. As much as 80 % of this annual precipitation is received during the rainy season.

1.2.2. The Ayeyarwady River

The Ayeyarwady River flows mainly through Myanmar. The drainage basin extends northward to the southwest sector of Yunnan, China. The tributaries of the Ayeyarwady eventually converge at Mandalay, where the mainstream of the Ayeyarwady forms and flows southward, eventually emptying into the Andaman Sea. To the northwest of this river basin lies the Indian subcontinent, the tectonic movement of which has been responsible for uplift of the continental landmass, including the Himalayan range. The Indo-Australia/Eurasia plate boundary runs longitudinally through the central plain of Myanmar and extends into the Indonesian island arc. The terrain to the east and west of the Ayeyarwady are hilly as a result of plate collision and there is a wide area of lowland in between. The processes responsible for the formation of the basin are reflected by its geological characteristics: mainly late Cretaceous to Paleogene sedimentary rock layers on the western terrains, Cenozoic sedimentary rock layers in the middle, and folded Paleozoic strata with intrusive granites and limestones in the eastern terrains [Bender, 1983; Wandrey and Law, 1997; Hadden, 2008; Chapman et al., 2015] (Figure 1-6). Because the Ayeyarwady River receives all the runoff from these geological provinces, the chemical composition of its water reflects their geochemistry. The length, drainage basin area, and annual discharge of this river are 2300 km, 4.1×10^5 km^2, and 1.5×10^4 m^3 s^{-1}, respectively [Meybeck and Ragu, 2012]. The annual sediment discharge of this river is 260 Tg yr^{-1} [Meybeck et al., 2012].

The climate of the Ayeyarwady basin is also very much influenced by the summer monsoon. The mean annual rainfall is 2700 mm at Yangon [Department of Meteorology and Hydrology (Myanmar), 2014]. As much as 80 % of this annual precipitation is received during the summer monsoon (rainy) season.

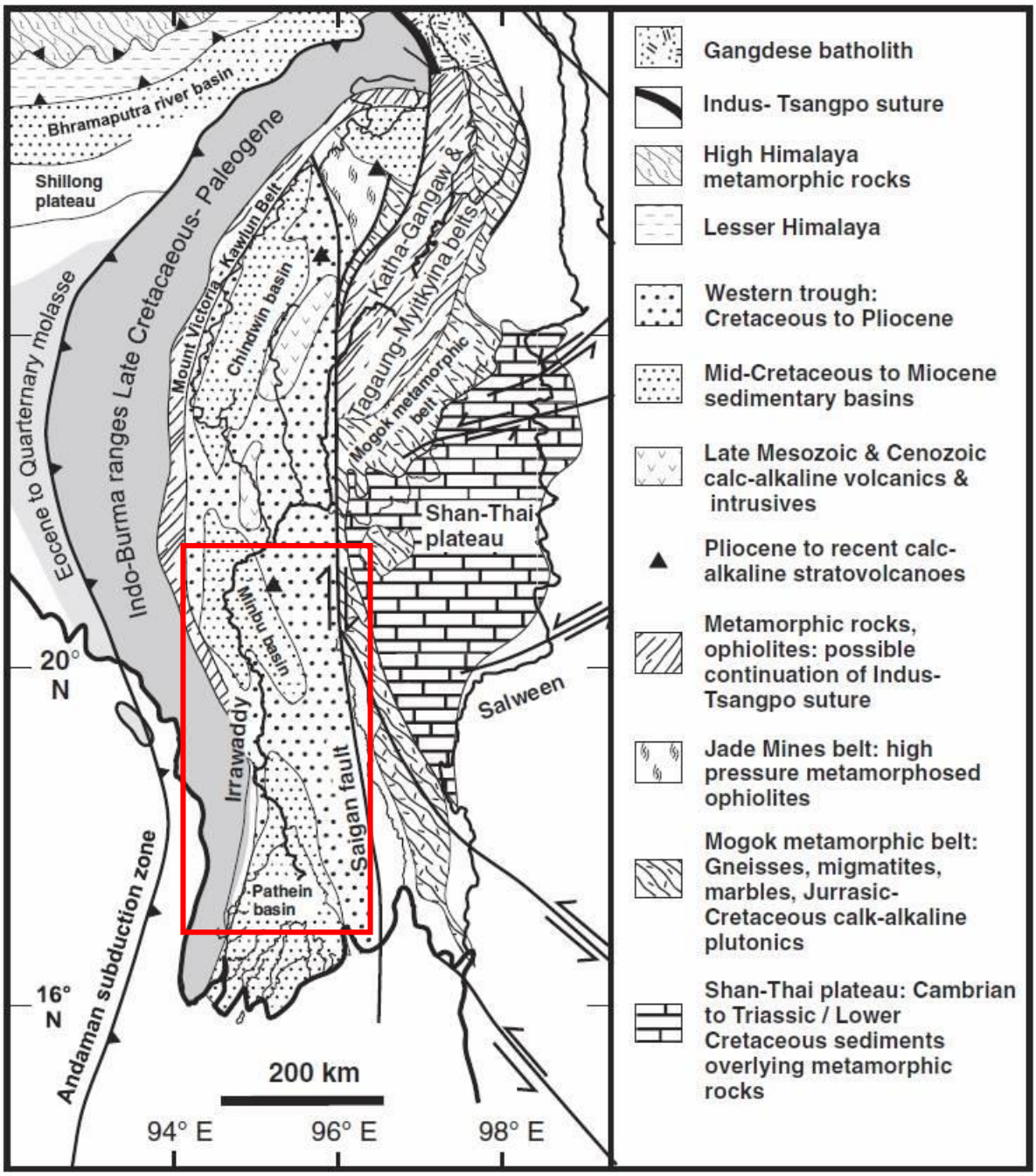

Figure 1-6.

Geological map of the Ayeyarwady River basin modified from Chapman et al. [2015] and references therein. Open red square indicates my sampling stations.

1.2.3. The Mekong River

The Mekong River is one of the longest rivers of the Himalayan watersheds. It originates in the eastern part of the Tibetan Plateau and its drainage basin includes parts of China, Myanmar, Laos, Thailand, Cambodia, and Vietnam. The river flows through relatively steep and narrow gorges in its upper reaches, but the rate of descent becomes more gradual as it approaches the South China Sea. The upper reach of the river on the eastern Tibetan Plateau consists mainly of Mesozoic sedimentary rocks, with minor Precambrian metamorphic and extrusive igneous rocks. The middle reach is covered mainly by Paleozoic-Mesozoic sedimentary rocks and intrusive igneous rocks that produce bisiallitic and ferrallitic soils. Sampling sites used in Chapter 2 and 3 are located within the lower reach of the river in Thailand. This area is also called the Indochina terrain or the Khorat Plateau, and is characterized by wide areas of flat land. The northern and southern halves of the plateau are drained by the Chi River and Mun River, respectively. Both rivers are characterized by very low gradients until they eventually merge with the Mekong. The basin is covered mainly by Mesozoic to Quaternary shales and sandstones [Löffler et al., 1984; Dheeradilok et al., 1992; Mouret, 1994; Liu et al., 2005] (Figure 1-7). In addition, salt-affected soils cover a wide area of the plateau [Shrestha, 2006; Wongpokhom et al., 2008]. The total area of the drainage basin is approximately 8.0×10^5 km^2 and the total length of the river is 4650 km [Meybeck and Ragu, 2012]. The rate of water and sediment discharge flux of the river is 1.5×10^4 m^3 s^{-1} and 150 Tg yr^{-1}, respectively.

The climate of the Mekong sampling sites from Chapter 2 and 3 is mainly tropical and also strongly controlled by the monsoon. Most of the basin area experiences annual precipitation of 1300-2000 mm [Thailand Meteorological Department, 2014]. The monthly precipitation average hits its minimum in January and reaches its maximum in August and September. Precipitation during the rainy season accounts for 80 % of the total annual rainfall.

1.2.4. The Chao Phraya River

The Chao Phraya River flows through northwestern Thailand and the Bangkok delta. The mainstream is formed by the confluence of four tributary rivers at Nakhon Sawan, which, from west to east, are the Ping, Wang, Yom, and Nan rivers. All of these rivers originate in the northwestern mountains of Thailand. The river eventually discharges into the Gulf of Thailand. The Chao Phraya basin is widely known as the Shan-Thai terrain [Dheeradilok et al., 1992] and is an extension of the eastern terrain of Myanmar. This tectonically active terrain is a result of the obduction of Paleozoic and Mesozoic rocks that consist mainly of carbonates and limestones. [Metcalfe, 1988]. The terrain

has also experienced four periods of granite magmatism associated with the Southeast Asia batholithic intrusions [Nakapadungrat and Putthapiban, 1992]. The topography of the Shan-Thai terrain, which has contributed to the formation and characteristics of the Chao Phraya River system, is mostly mountainous with outcropping areas. The area of its drainage basin is 1.1×10^5 km^2, and the total length of the river is approximately 1200 km [Meybeck and Ragu, 2012]. The total water discharge is 882 m^3 s^{-1} and the annual sediment discharge is 11 Tg yr^{-1}. The Chao Phraya basin experiences the same climatic conditions as the lower Mekong.

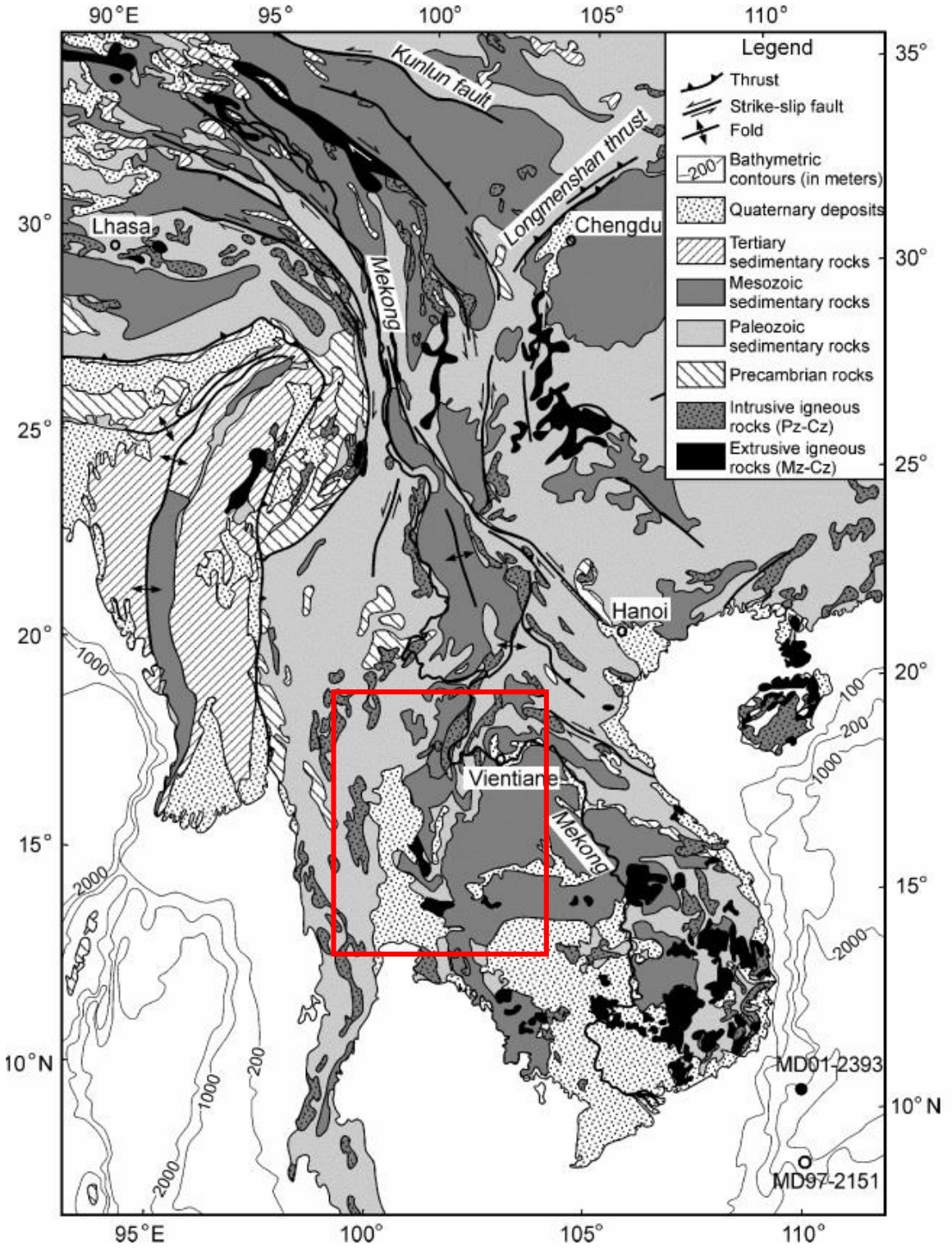

Figure 1-7.

Geological map of the Mekong River basin modified from Liu et al. [2005] and references therein.

Open red square indicates my sampling stations.

1.3. Dissolved CO_2

1.3.1. Overview

Carbon in the river water is classified into dissolved and particulate fractions, each of which has an inorganic and organic form. The most abundant form of global riverine carbon is dissolved inorganic carbon (DIC) (0.39 PgC yr^{-1}), followed by dissolved organic carbon (DOC) (more than 0.20 PgC yr^{-1}), particulate organic carbon (POC) (about 0.20 PgC yr^{-1}), and particulate inorganic carbon (PIC) (0.17 PgC yr^{-1}) [Meybeck, 2003].

There are three types of DIC in the river waters: dissolved CO_2, HCO_3^-, and CO_3^{2-}. Chemical equilibria of these forms are described as follows:

$$CO_2(g) \rightarrow CO_2(aq) \quad (1\text{-}6)$$

$$H_2O + CO_2(aq) \rightarrow HCO_3^- + H^+ \quad (1\text{-}7)$$

$$HCO_3^- \rightarrow CO_3^{2-} + H^+ \quad (1\text{-}8)$$

The concentration of DIC (C_T) can be described as follows:

$$C_T = [CO_2(aq)] + [HCO_3^-] + [CO_3^{2-}] \quad (1\text{-}9)$$

In the pH range of most major rivers ($6 < pH < 8.2$), HCO_3^- is the dominant form of DIC [Meybeck, 2003]. For example, HCO_3^- concentration accounts for more than 95 % of total DIC concentration in samples from the Ganges River (for details, see Chapter 2). Total alkalinity (A_T) is a measure of the capacity of water to neutralize strong acids and/or bases. This value is often used as a proxy for chemical weathering and is defined as the difference in the concentrations of strong acids and bases, as follows:

$$A_T = C_{cation} - C_{anion} \quad (1\text{-}10)$$

In the case of freshwater, this equation is simplified as follows:

$$A_T = [HCO_3^-] + 2[CO_3^{2-}] + [OH^-] - [H^+] \quad (1\text{-}11)$$

pH, pCO_2, C_T, and A_T are four measureable parameters of the CO_2 system. If two of these parameters are measured, along with temperature and pressure, concentrations of the two remaining CO_2 parameters can be calculated. Recent advances in the calculation program of carbonate systems such as CO_2calc [Robbins et al., 2010] and PHREEQC [Parkhurst and Appelo, 2013] have greatly increased the ease with which these parameters are calculated.

Dissolved CO_2 is a relatively minor form of DIC. In the case of rainwater, CO_2 is dissolved in equilibrium with the atmosphere; pCO_2 is only about 395 µatm. However, for many major rivers in the world, recent studies have shown that pCO_2 in the surface water is much higher than atmospheric

pCO_2 level (Table 1-1). Rivers receive abundant organic carbon from ecosystems in the basins, most of which is decomposed and returned back to the atmosphere as a form of CO_2 before being transported to the ocean.

The CO_2 degassing flux from surface river waters to the atmosphere can be simply calculated as follows:

$$F = k (C_{air} - C_{water}) \quad (1\text{-}12)$$

where F represents the degassing flux rate, and (C_{air} - C_{water}) is the concentration difference in CO_2 between the overlying air and the bulk of the water. "k" is the gas exchange velocity between the water and the atmosphere [Telmer and Veizer, 1999; Yao et al., 2007]. This value is affected by many physical factors such as wind speed, fetch, water current velocity, and water depth [Alin et al., 2011 and references therein].

Table 1-1.

Published pCO_2 data for large rivers of the world.

River	Sampling Year	pCO_2 (μatm)	Basin Area[1] (km^2)	Discharge[1] ($km^3\ yr^{-1}$)	References
Amazon	1995–1996	4350	6112000	6590	Richey et al. [2002]
Columbia	1964–1976	1150	669000	236	Kempe [1982]
Congo	2010–2011	2020–6850	3698000	1200	Wang et al. [2013b]
Elbe	1975–1977	4220	146000	23.7	Kempe [1982]
Hudson	1992–1999	1010	34500	17.3	Cole and Caraco [2001]
Indus	1994–1995	70–2090	916000	57	Karim and Veizer [2000]
Mekong	2004–2005	700–1600	795000	467	Alin et al. [2011]
	1972-1998	1090	795000	467	Li et al. [2013]
Mississippi	2000–2001	1340	3217000	687	Dubois et al. [2010]
Ottawa[2]	1991–1994	1200	(see St. Lawrence River)		Telmer and Veizer [1999]
Paraná	1982–1984	3700	2783000	568	Depetris and Kempe [1993]
Rhine	1988–1989	3400–5100	224000	101	Buhl et al. [1991]
Rhône	1996	180–3720	95600	54	Aucour et al. [1999]
Seine	1975–1979	1980	78600	15.8	Kempe [1982]
St. Lawrence[2]	1998–1999	1300	1020000	337	Hélie et al. [2002]
Xijiang[3]	2005–2006	600–7200	437000	363	Yao et al. [2007]
Yangtze	2003–2006	610–1450	1808000	928	Zhai et al. [2007]
Yukon	1976–1979	2790	849000	200	Kempe [1982]

[1]: Basin area and discharge data are from Meybeck and Ragu et al. [2012].

[2]: Ottawa River is a tributary of St. Lawrence River.

[3]: Basin area and discharge data for the Zhujiang River [Meybeck and Ragu, 2012] are used for the Xijian River data.

Figure 1-8 represents CO_2 degassing rate to the atmosphere from various land types [Raich and Schlesinger, 1992] and major rivers worldwide [Dubois et al., 2010; Alin et al., 2011; Li et al., 2013]. The rates from river waters are relatively high. In addition, as discussed in Section 2.4.3, the photosynthesis processes should be less active in rivers. Thus, river waters should efficiently release ecosystem-originated carbon to the atmosphere.

The number of studies that focus on the total CO_2 degassing flux from major rivers remains relatively small. For example, Cole et al. [2007] reported the overall magnitude of CO_2 efflux as the sum of estimates from previous studies (e.g., large rivers [Cole and Caraco, 2001] and lakes [Sobek et al., 2003]). In their study, terrestrial waters (rivers, lakes, reservoirs, and wetlands) receive 2.7 PgC yr^{-1} of carbon from the land. However, as much as 0.75 PgC yr^{-1} of carbon is released to the atmosphere (0.23 PgC yr^{-1} from river waters alone), and only 0.9 PgC yr^{-1} of carbon is transported to the ocean (Table 1-2). Aufdenkampe et al. [2011] estimated the degassing flux from inland waters in each latitude zone. They reported the largest degassing flux from waters in low latitudes and tropical climates, resulting in a global degassing flux from river waters of 0.56 PgC yr^{-1}. Raymond et al. [2013] reconsidered the impact of small and/or frozen rivers and revised gas exchange velocity values for their calculation (related discussion can be found in Alin et al. [2011] and Section 1.3.2). They proposed a much larger global degassing flux from river waters of 1.8 PgC yr^{-1}, which is more than seven times and three times higher than Cole and Aufdenkampe's estimates, respectively.

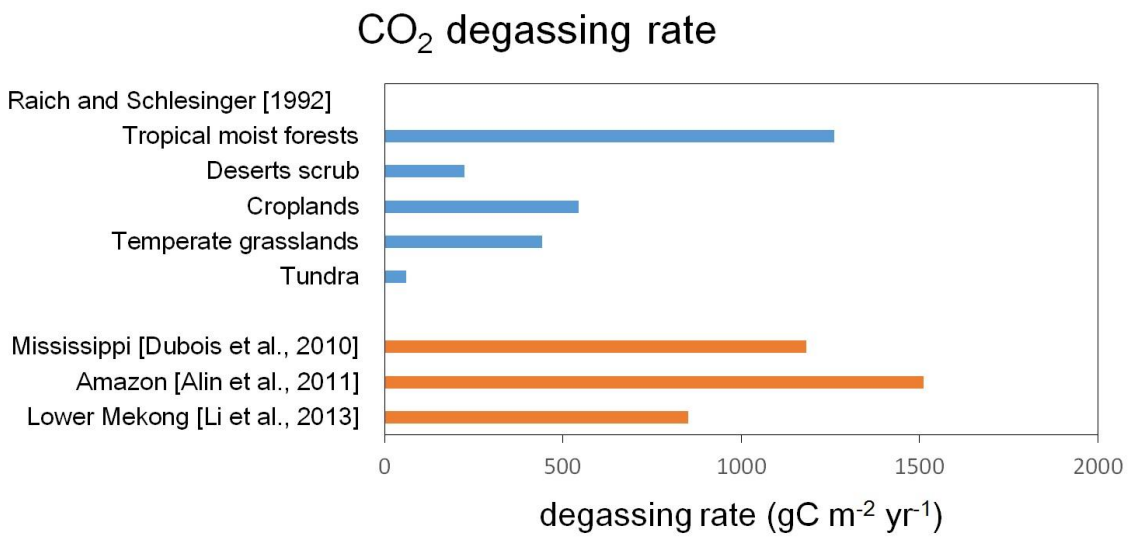

Figure 1-8.

CO_2 degassing rate from various land types [Raich and Schlesinger, 1992] and major rivers [Dubois et al., 2010; Alin et al., 2011; Li et al., 2013] to the atmosphere.

Table 1-2

Global degassing flux of CO_2 from rivers and total terrestrial waters.

Global Degassing Flux (PgC yr^{-1})		References
From River Waters	From Total Terrestrial Waters	
0.23	0.75	Cole et al. [2007]
not stated	1.20	Battin et al. [2009]
0.56	3.28	Aufdenkampe et al. [2011]
1.80	2.10	Raymond et al. [2013]
not stated	1.10	Regnier et al. [2013]

It should be noted that, on modern timescales, terrestrial rivers never work as a simple "pipeline" connecting the land to the ocean. CO_2 degassing from river waters to the atmosphere is not insignificant compared to other anthropogenic forms of CO_2 release (e.g., 7.8 PgC yr^{-1} by fossil fuel combustion and cement production [IPCC, 2013]). Therefore, carbon fluxes from river water to the atmosphere are potentially of considerable importance. However, a large degree of uncertainty is associated with the estimation of CO_2 evasion because it is based on data from only a limited number of river systems. Data from more major rivers are needed to improve estimates of CO_2 evasion and to comprehend the global carbon cycle on modern timescales.

1.3.2. CO_2 evasion from Himalayan rivers

The Himalayan rivers transport abundant water and organic carbon to the ocean. In the upper streams, active physical and chemical weathering of rocks occurs. In contrast, Himalayan alluvium and well-developed soils cover the lower basins, where soil erosion enhances carbon export from soils to terrestrial waters, although most is released to the atmosphere before reaching the open ocean [Regnier et al. 2013]. Thus, these river waters should have a unique and important CO_2 evasion system in the global carbon cycle. Although Raymond et al. [2013] estimated one of the largest CO_2 degassing fluxes in these rivers, few studies have examined actual pCO_2 variations [Regnier et al., 2013].

Alin et al. [2011] conducted sampling surveys in the Amazon and Mekong rivers and measured the gas transfer velocity, pCO_2, and degassing flux in surface waters using floating chambers with an internal fan. They conducted sampling surveys in the lower Mekong River and its tributaries (including Tonle Sap Lake) in September and October in 2004-2005. In large rivers (river width: > 100 m), the temperature-normalized gas transfer velocity values (k_{600}) were moderate (14.7 ± 8.6 cm

h^{-1}) compared to previous studies (e.g., the Amazon River by Richey et al. [2002]: 9.6 ± 3.8 cm h^{-1}) and were largely controlled by wind speed. On the other hand, in small rivers and streams (river width: < 100 m), they observed larger k_{600} values with large variations (10.9 ± 14.4 cm h^{-1}) compared to previous studies (e.g., 5.0 ± 2.1 cm h^{-1} by Richey et al. [2002]). They proposed that water current velocity and depth become increasingly important for k_{600} values and degassing flux estimation as channels get progressively smaller. Small river channels constitute the majority of the net river system. Thus, a doubling of k_{600} values in their study alone could increase the basin-wide degassing flux estimate by as much as ~50-75 %. Although more detailed analysis is necessary, they highlighted the importance of incorporating scale-appropriate k values into basin-wide models in order to determine degassing fluxes in each river.

Using k values estimated by Alin et al. [2011], Li et al. [2013] analyzed pCO_2 and the degassing flux of the lower Mekong River. They conducted monthly sampling from 1972 to 1998 at 11 sampling stations. The average pCO_2 value in their study was 1090 ± 290 µatm, comparatively lower than other major global rivers (Table 1-1). A significant increase in pCO_2 values was observed from upper to lower streams. With regard to seasonal variations, pCO_2 started to increase from the beginning of the wet season (May) until July or even September. Calculated CO_2 degassing flux from the river surface water to the atmosphere was 6.8 TgC yr^{-1}. Surprisingly this value is much larger than the DIC, DOC, and POC fluxes (4.5 TgC yr^{-1}, 2.2 TgC yr^{-1}, and 2.1-3.2 TgC yr^{-1}, respectively). They highlighted the potential importance of rivers as an essential atmospheric CO_2 source in the global and regional carbon cycle.

To the best of my knowledge, there are few studies about pCO_2 and CO_2 degassing fluxes in the Ganges, Brahmaputra, and Ayeyarwady rivers. Sarma et al. [2012] reported pCO_2 values in the inner estuaries of the Bay of Bengal and found that pCO_2 levels of the rivers in the northwestern bay were higher (5000-17000 µatm) compared to the Ganges (500 µatm). However, more detailed studies in the inland area are needed because the carbonate system and buffering capacity differs between freshwater and seawater. In Chapter 2, pCO_2 is measured in river water samples from the Ganges, Brahmaputra and Meghna rivers in Bangladesh during both the dry and rainy seasons. There the roles of biogeochemical processes and the exchange of CO_2 between river water and the atmosphere are examined.

1.4. HCO_3^- and other major ion concentrations

1.4.1. Overview

HCO_3^- is the most abundant form of DIC in river waters, thereby controlling CO_2 parameters. According to Meybeck [2003], in weighted global average river water, the concentration of HCO_3^- (798 μmol kg^{-1}) is higher than that of any other major ions (Table 1-3). Riverine HCO_3^- is derived from both silicate and carbonate weathering in the basin, as shown in equation 1-3 and 1-4, and then transported to the ocean. Total flux of riverine HCO_3^- to the ocean is estimated to be 31.9×10^{12} mol yr^{-1} [Galy and France-Lanord, 1999; Meybeck, 2003].

To understand the long-term global carbon cycle and chemical weathering in river basins, it is important to estimate the amount of CO_2 consumed by weathering of silicate or carbonate rocks. HCO_3^- is derived from both silicate and carbonate and it is difficult to distinguish its source. A common and effective approach to overcome this problem is to use "the forward model", that is, quantifying the contributions of precipitation input (atmosphere) and various source rocks (silicate, carbonate, and evaporate) for various dissolved major ions other than HCO_3^-: Na^+, Mg^{2+}, K^+, Ca^{2+}, Cl^-, and SO_4^{2-} [e.g., Gaillardet et al., 1999]. The mass balance for the element X concentration is expressed as follows:

$$[X]_{river} = [X]_{atmosphere} + [X]_{silicate} + [X]_{carbonate} + [X]_{evaporite} \quad (1\text{-}13)$$

Table 1-3.

Concentrations of major ions in weighted global average river water [Meybeck, 2003] and seawater [Millero, 2003 and references therein].

	Na^+	Mg^{2+}	K^+	Ca^{2+}	Cl^-	SO_4^{2-}	HCO_3^-
	(μmol kg^{-1})						
River Water	240	123	44	297	167	88	798
Seawater	469070	52820	10210	10280	545880	28240	1750

In this calculation, each ion can be derived from a unique source (Table 1-4). For example, carbonate dissolution provides mainly Mg^{2+} and Ca^{2+}. Cl^- and SO_4^{2-} are derived from atmospheric inputs and evaporate dissolution. In addition, the atmospheric input of each ion can be easily calculated by multiplying the chemical composition of rainwater by rainfall amount, which is reported by local meteorological observatories. Chemical compositions of some source rock endmembers are already known; Li et al. [2011] and references therein reported molar ratios of $[Ca/Na]_{silicate}$ and $[Mg/K]_{silicate}$ in the global river waters of between 0.17-0.84 and 0.16-0.88, respectively. In some studies, contributions from anthropogenic inputs and sulfide dissolution are also considered [e.g., Galy and France-Lanord, 1999; Li et al., 2014]. CO_2 consumption by silicate and carbonate weathering can be calculated as follows:

$$[\Phi CO_{2silicate}] = [HCO_3^-]_{silicate} \times \text{discharge}$$
$$= ([Na^+]_{silicate} + [K^+]_{silicate} + 2\,[Ca^{2+}]_{silicate} + 2\,[Mg^{2+}]_{silicate}) \times \text{discharge} \quad (1\text{-}14)$$
$$[\Phi CO_{2carbonate}] = 1/2\,[HCO_3^-]_{carbonate} \times \text{discharge}$$
$$= ([Ca^{2+}]_{carbonate} + [Mg^{2+}]_{carbonate}) \times \text{discharge} \quad (1\text{-}15)$$

In Chapter 3, using the sample datasets, CO_2 consumption by silicate and carbonate weathering in the Ayeyarwady River basins are calculated.

According to Gaillardet et al. [1999], CO_2 consumption by silicate and carbonate weathering in continental rocks is estimated to be 8.7×10^{12} mol yr^{-1} and 12.3×10^{12} mol yr^{-1}, respectively. In addition, 3.0×10^{12} mol yr^{-1} of CO_2 is consumed by silicate weathering in oceanic and volcanic arcs. In total, 24.0×10^{12} mol yr^{-1}, that is, 0.29 PgC yr^{-1} is consumed. Although Meybeck [1987] reported that the abundance of carbonate sedimentary rocks on land is only 15.9 % (Table 1-5), such a high consumption rate of CO_2 from carbonate rocks in global river basins indicates that the relative chemical weathering rate of carbonate is much higher i.e., the relative rate of granite to carbonate rocks is 1:12 [Meybeck, 1987]. Amiotte Suchet et al. [2003] reported that the CO_2 consumption rate due to silicate and carbonate weathering for 39 selected major rivers is 1.1×10^5 mol km^{-2} yr^{-1} and 7.7×10^4 mol km^{-2} yr^{-1}, respectively.

Table 1-4.

Potential sources of major dissolved ions (Na^+, Mg^{2+}, K^+, Ca^{2+}, Cl^-, and SO_4^{2-}) in river waters.

	Potential Source			
	Atmosphere	Silicate	Carbonate	Evaporite
Na^+	+	+		+
Mg^{2+}	+	+	+	
K^+	+	+		
Ca^{2+}	+	+	+	+
Cl^-	+			+
SO_4^{2-}	+			+

Table 1-5.

Outcrop abundance of major rock types on land reported by Meybeck [1987].

	Abundance (%)
Plutonic Rocks	11.0
Metamorphic Rocks	15.0
Volcanic Rocks	7.9
Sandstones	15.8
Shales	33.1
Carbonate Sedimentary Rocks	15.9
Evaporite	1.3
Total	100.0

The most abundant dissolved cations and anions in river waters are Ca^{2+} followed by Na^+ and Mg^{2+}, and HCO_3^-, followed by Cl^- and SO_4^{2-}, respectively [Meybeck, 2003] (Table 1-4). From a chemical weathering point of view, Ca, Na, and Mg are more soluble compared to K, Si, Al, and Fe. However, in seawater, the most abundant dissolved cations and anions are Na^+ followed by Mg^{2+} and Ca^{2+}, and Cl^- followed by SO_4^{2-} and HCO_3^-, respectively [Millero, 2003 and references therein]. This difference is attributed to the relatively conservative behavior of Na^+ and Cl^-: dissolved ions of Ca^{2+}, Mg^{2+}, and HCO_3^- are removed by carbonate mineral formations as shown in equation 1-5. Ca, Mg, and K are major essential elements for biota. In contrast, Na and Cl do not tend to be involved in such inorganic and organic processes, instead remaining as dissolved forms in seawater.

1.4.2. Chemical weathering in the Himalayan river basins

Gaillardet et al. [1999] reported CO_2 consumption due to both silicate and carbonate weathering in global river basins: 471×10^9 mol yr^{-1} and 236×10^9 mol yr^{-1} in the Ganges, 87×10^9 mol yr^{-1} and 199×10^9 mol yr^{-1} in the Brahmaputra, 832×10^9 mol yr^{-1} and 24×10^9 mol yr^{-1} in the Ayeyarwady, and 194×10^9 mol yr^{-1} and 409×10^9 mol yr^{-1} in the Mekong, respectively (Table 1-6). Along with the Indus and Yangtze rivers (unfortunately the Salween is not stated in this study), the

total CO_2 consumption by silicate and carbonate weathering in the Himalayan river basins is estimated at 1745×10^9 mol yr^{-1} and 1924×10^9 mol yr^{-1}, respectively (as much as 20 %, and 15 %, respectively, of the global CO_2 consumption by continental silicate weathering). Amiotte Suchet et al. [2003] also reported high chemical weathering rates in Himalayan rivers, compared to 39 major rivers. Therefore, this area plays an important part in the global carbon cycle on a long timescale.

The total flux of HCO_3^- in the Ganges-Brahmaputra Rivers is estimated as 1.19×10^{12} mol yr^{-1} (3.7 % of the global flux) [Galy and France-Lanord, 1999] (Table 1-6). Galy and France-Lanord [1999] analyzed chemical components of the Ganges-Brahmaputra Rivers from upper streams to lower streams. They reported $[Ca/Na]_{silicate}$ molar ratios of 0.18-0.3, based on the whole-rock chemical composition of silicate rocks in the area, and $[Mg/K]_{silicate}$ molar ratios of 0.3-0.7, based on the $[Mg/K]_{river}$ ratios of rivers draining only silicate formations. These estimated values are widely used in many studies of chemical weathering in the Himalayan region [e.g., Noh et al., 2009], including in this study (Chapter 3). They used the forward model along with ^{13}C and sulfide contributions, which Gaillardet et al. [1999] did not take into account, and estimated alkalinity flux derived from silicate weathering to be 2.7×10^{11} mol yr^{-1}. Sulphuric acid, which does not contribute to the CO_2 uptake, controls 6-9 % of the weathering reaction in the Ganges and as much as 20-30 % in the Brahmaputra. They also estimated that net CO_2 consumption over long timescales in these river basins is 6.4×10^{11} mol yr^{-1} (only 1.3 % of the global uptake), attributed to a low proportion of Ca- and Mg-silicates in the Himalayas.

Table 1-6.

Chemical weathering properties in the Himalayan rivers reported in previous studies.

	Area	Discharge	Silicate Weathering		Carbonate Weathering		Sampling Site	References
	10^4 km^2	km^3 yr^{-1}	CO_2 cons.		CO_2 cons.			
			10^3 mol km^{-2} yr^{-1}	10^9 mol yr^{-1}	10^3 mol km^{-2} yr^{-1}	10^9 mol yr^{-1}		
Ganges	105	493	449	471	225	236	Total Basin	Gaillardet et al. [1999]
	~0.96	10.8	400-700				Upper Tributaries (the Upper Yamuna)	Dalai et al. [2002]
	1.96	22.4	230	5			Upper Streams (at Rishikesh)	Tripathy and Singh [2010]
Brahmaputra	58	510	150	87	343	199	Total Basin	Gaillardet et al. [1999]
	45.5	510	~600	~272			Lower Streams (at Dhubri)	Singh et al. [2005]
			20-1520				Upper Streams (as the Yarlung Tsangpo)	Hren et al. [2007]
	15.3	30.9	170	26	127	19	Upper Streams (as the Yarlung Tsangpo)	Jiang et al. [2015]
Ganges-Brahmaputra	164		190	312	240	394	Total Basin	Amiotte Suchet et al. [2003]
	164	1071		270*			Total Basin	Galy and France-Lanord [1999]
Ayeyarwady	41	486	2029	832	59	24	Total Basin	Gaillardet et al. [1999]
	40		197	79	710	284	Total Basin	Amiotte Suchet et al. [2003]
Mekong	80	467	244	194	515	409	Total Basin	Gaillardet et al. [1999]
	82		237	194	240	197	Total Basin	Amiotte Suchet et al. [2003]
	45.6		103-121	55			Upper Streams of the Yangtze, Mekong, and Saleween	Noh et al. [2009]
	80	470	191	152	286	228		Li et al. [2014]
Global Average				8700		11700	Based on 60 Largest Rivers	Gaillardet et al. [1999]
			110		77		Based on 39 Selected Rivers	Amiotte Suchet et al. [2003]

*: reported as alkalinity flux derived from silicate weathering

For the Ganges, Dalai et al. [2002] conducted sampling surveys in an upper tributary, the Yamuna River. Their reported value of CO_2 consumption rates by silicate weathering is 4-7 × 10^5 mol km^{-2} yr^{-1} (Table 1-6). This value is higher than for the southern lowlands of the Himalayas and is attributed to rapid physical erosion in this region. Tripathy and Singh [2010] also focused on the upper streams and conducted forward and inverse modeling, along with strontium isotope measurements. "The inverse model" calculates not only the contribution of various sources to riverine dissolved load but also the best values of elemental ratios for each endmember [Negrel et al., 1993]. These models showed that the extent of Ca^{2+} loss was 25 % at Rishikesh (upper mainstream) due to calcite precipitation. They also estimated higher erosion rates of both silicate and carbonate rock, and CO_2 consumption rates by silicate weathering of 2.3 × 10^5 mol km^{-2} yr^{-1} at Rishikesh.

For the Brahmaputra, Singh et al. [2005] used the forward model and reported CO_2 consumption rates as a result of silicate weathering of ~6 × 10^5 mol km^{-2} yr^{-1} in lower streams at Dhubri and ~1.9 × 10^6 mol km^{-2} yr^{-1} in the middle streams (Eastern Syntaxis zone with highly metamorphosed rocks) (Table 1-6). They proposed that the sulphuric acid contribution to silicate weathering is negligible in this area, and that relatively higher values of consumption compared to those of Galy and France-Lanord [1999] are attributed to differences in endmember estimates of $[Ca/Na]_{silicate}$. Hren et al. [2007] focused on the middle and upper streams (the Yarlung Tsangpo River). They also report high consumption rates due to silicate weathering, in particular in the Syntaxis zone: 0.2 to 15.2 × 10^5 mol km^{-2} yr^{-1}. Their data shows that 15-20 % of total CO_2 consumption by silicate weathering in the Brahmaputra basins is derived from their studied area, which accounts for only 4 % of the total land area of the basin. They also measured the calcite and dolomite saturation indices, revealing that most samples are undersaturated. Jiang et al. [2015] describe consumption rates by silicate and carbonate weathering of 1.7 × 10^5 mol km^{-2} yr^{-1} and 1.3 × 10^5 mol km^{-2} yr^{-1}, respectively.

Few studies have examined chemical weathering rates in the Ayeyarwady River (Table 1-6). Although Gaillardet et al. [1999] reported extremely active silicate weathering, Amiotte Suchet et al. [2003] suggested that total CO_2 consumption and consumption rate by silicate weathering is only 7.9 × 10^{10} mol yr^{-1} and 2.0 × 10^5 mol km^{-2} yr^{-1}, respectively. Recently, Champan et al. [2015] described the chemical composition of river waters, but they have not calculated CO_2 consumption due to silicate weathering.

With regard to the Mekong, Noh et al. [2009] analyzed chemical weathering rates in the upper stream along with two other Himalayan rivers (the Yangtze and Salween) (Table 1-6). They used

both the forward and inverse models, and calculated a CO_2 consumption rate by silicate weathering of 1.0-1.2 × 10^5 mol km^{-2} yr^{-1}. Li et al. [2014] used data obtained during 1972-1996 in the lower Mekong River basins. Their consumption rates by silicate and carbonate weathering are 1.9 × 10^5 mol km^{-2} yr^{-1} and 2.9 × 10^5 mol km^{-2} yr^{-1}, respectively. The total flux of HCO_3^- in this river is estimated at 3.7 × 10^{11} mol yr^{-1}. Although this value is small compared to the Ganges-Brahmaputra [Galy and France-Lanord, 1999], it accounts for as much as 1.2 % of the global HCO_3^- flux.

By and large, although previously reported CO_2 consumption rates by silicate and carbonate weathering in the Himalayan rivers show significant variation, attributed to differences in sampling sites and/or calculation methods, they are larger than the global average. In order to elucidate the global carbon cycle over long timescales, a more detailed understanding of chemical weathering is needed, through continuous and high-density sampling of river waters and geological endmembers, and the application of various models and methods. In Chapter 3, the major focus is the Ayeyarwady River, specifically reported chemical components of the river water and weathering rates.

1.5. Stable isotope ratios of light elements

1.5.1. Advantage of using stable isotope ratios

In Section 1.4, I reviewed CO_2 consumption by silicate and carbonate weathering in the Himalayan river basins. Most previous studies have employed the forward model using concentrations of dissolved major ions including HCO_3^-. However, there is an issue with this calculation: not all dissolved ions derived from weathered rocks are preserved during transportation downstream. Some ions are removed by "intra-river processes" such as biological uptake, formation of secondary minerals, adsorption/desorption/exchange reactions with particulate materials, and/or inorganic mineralization in the basins. Thus, non-conservative behavior of dissolved constituents could lead to misestimation of CO_2 consumption in river basins. Calculation of saturation indices of each secondary mineral can reveal whether or not inorganic precipitation has occurred in the basin. In addition, it is possible to quantify the loss of each ion using one of the following three methods.

The first approach is to use both the forward and inverse models. Sources of each dissolved ion are determined in the forward model [Gaillardet et al., 1999]. In contrast, the inverse model constrains the relative contribution of each endmember to the total dissolved load [Negrel et al., 1993]. Tripathy and Singh [2010] used these two models in the upper Brahmaputra basins and revealed the extent of Ca^{2+} loss based on differences in the results obtained from these models.

The second method is analyzing spatial variations in the concentration of elements, both dissolved and particulate. Mobile to immobile ratios of major elements in the sediment are used to trace and quantify chemical weathering. Lupker et al. [2012] also used hydration of sediments as a sensitive tracer of secondary mineral formations and silicate weathering, and reported cation fluxes derived from silicate and carbonate weathering in the Ganges River basin. In addition, Galy and France-Lanord [1999] estimated $[Mg/K]_{river}$ ratios by measuring the chemical composition of rivers draining only silicate formations. This value reflects Mg^{2+} and K^+ loss after each ion is released from the bedrock. If the relationship of Mg^{2+} and K^+ concentrations can be applied to other basins, CO_2 consumption can be more accurately estimated.

The third approach, and the one I will examine in this thesis, is to measure isotope ratios. Isotope fractionation effects are widely used as a tool to identify differences in element sources and transport processes. Variations in stable isotope ratios are induced in natural samples both by biological and abiological processes. Recent studies reported mineral-specific fractionation factors for each element [e.g., Schmitt et al., 2012], using an atomic-scale spectroscopy technique that yields chemical

reaction histories for the element of interest. For example, when dissolved Mg is adsorbed onto the secondary silicate minerals, heavy Mg is preferentially removed from the dissolved load. In contrast, carbonate precipitation preferentially incorporates light Mg from the dissolved load (for details, see Section 1.5.3). Thus, this method enables examination of not only the extent but also the type of intra-river processes in river basins. In addition, isotope ratios of each ion can be used to identify the source rocks, that is, the extent of silicate and/or carbonate which has weathered in the basin. Tracing behaviors of each ion through isotope analysis can provide direct information about chemical weathering and intra-river processes in the basin, which play an important role in the long-term carbon cycle.

I focus on the isotope system of Mg and Si. These ions are major components of both terrestrial rocks and river waters and are closely related to chemical weathering processes. Recent developments in inorganic mass spectrometry have allowed us to quantify Mg and Si isotopes, which have recently been examined as potential tools for understanding chemical weathering and intra-river processes. Here I review the latest studies concerning these isotopes in the Himalayan river basins. I also discuss Sr isotope ratios ($^{87}Sr/^{86}Sr$), which have traditionally been used as a proxy for chemical weathering in river basins.

1.5.2. Sr isotope ratios: a traditional proxy for chemical weathering

Sr is a minor element, with a concentration of only 320 μg g^{-1} in the bulk continental crust [Rudnick and Gao, 2003] and 0.68 μmol kg^{-1} in average river water [Gaillardet et al., 2003]. Sr has four naturally occurring stable isotopes: ^{84}Sr (approximate abundances: 0.56 %), ^{86}Sr (9.87 %), ^{87}Sr (7.04 %), and ^{88}Sr (82.53 %). Only ^{87}Sr can be derived from the radioactive decay of rubidium-87 (^{87}Rb) with a half-life of 4.88×10^{10} yr, while the other three forms are only produced by cosmic nucleosynthesis. Compared to Rb, Sr is a more compatible element. During formation of the continental crust in subduction zones, Rb tends to be concentrated in the crust, while Sr remains in the mantle. Thus, the concentration of ^{87}Sr tends to be higher in the continental crust; the $^{87}Sr/^{86}Sr$ ratio is 0.716 on average for continental crust, and 0.704 in oceanic island basalts [Capo et al., 1998]. In addition, Sr is an alkaline earth element often replacing Ca in the rock-forming process, while Rb is an alkali element with properties similar to K. Many limestones on land tend to have higher concentrations of Sr with a low $^{87}Sr/^{86}Sr$ ratio (< 0.709), while silicate rocks have lower Sr contents with a high $^{87}Sr/^{86}Sr$ ratio (> 0.710). Therefore, this isotope and its ratio is a useful proxy for tracing

source rocks. More detailed information can be found in Capo et al. [1998] and Tripathy et al. [2012].

Raymo [1991] has reconstructed the Sr isotope composition of Phanerozoic seawater based on analysis of biological carbonate in the deep-sea sediment. This study reported an increase in the $^{87}Sr/^{86}Sr$ ratio from the early Eocene, which occurs concurrently with global cooling. Raymo proposed that this variation can be attributed to uplift of the Himalayan-Tibetan Plateau and ongoing silicate weathering [Raymo et al., 1988; Raymo, 1991; Raymo and Ruddiman, 1992]. Extremely high $^{87}Sr/^{86}Sr$ ratios are observed in the Himalayan rivers, in particular the Ganges (0.729) and Brahmaputra (0.719), while the average Sr concentration of global rivers is 939 nmol kg^{-1} with a $^{87}Sr/^{86}Sr$ ratio of 0.7112 [Tripathy et al., 2012]. Therefore, these high $^{87}Sr/^{86}Sr$ ratios are important evidence in support of the work of Raymo [1991].

However, recent studies have suggested that the $^{87}Sr/^{86}Sr$ ratio is not an appropriate proxy for tracing bedrock in the case of the Himalayan region. In this area, LHS contains metamorphosed impure carbonate with high Rb/Sr ratios, and metamorphism and diagenesis has caused exchange of Sr between carbonate and silicate [Palmer and Edmond, 1992; Bickle et al., 2001, 2003; Oliver et al., 2003]. This has resulted in extremely high $^{87}Sr/^{86}Sr$ ratios in carbonate as well as silicate rock; for example, Singh et al. [1998] reported that $^{87}Sr/^{86}Sr$ ratios in carbonate collected across LHS was in the range of 0.7064-0.8935. Therefore, in this region, it is difficult to use $^{87}Sr/^{86}Sr$ ratio as a tracer of silicate-versus-carbonate weathering in the watershed area.

1.5.3. Mg isotope ratios

Mg is the eighth most common element on the Earth's surface. This ion is contained in both silicate and carbonate rocks and released to river waters through chemical weathering processes. It has a weighted global average river water concentration of 123 μmol kg^{-1} [Meybeck, 2003] (Table 1-3). Mg is a major alkaline-earth element and also plays an important role in the biosphere, that is, it is incorporated during growth of biogenic carbonate minerals, along with Ca. Mg participates in the activation of not only abundant enzymes but also chlorophyll, which is essential for organic matter synthesis [Wilkinson et al., 1990; Schmitt et al., 2012]. Thus, this element plays a fundamental role in the global carbon cycle.

Mg has three naturally occurring stable isotopes: ^{24}Mg (approximate abundances: 78.99 %), ^{25}Mg (10.00 %), and ^{26}Mg (11.01 %). The per mil notation for Mg isotope ratios is defined as follows:

$$\delta^{x}Mg = \{(^{x}Mg / {}^{24}Mg)_{sample} / (^{x}Mg / {}^{24}Mg)_{standard} - 1\} \times 1000 \quad (1\text{-}16)$$

where x is either 25 or 26. Recent studies use DSM-3 (Dead Sea Magnesium) as the standard material.

δ^{26}Mg is a potential tracer for the source of Mg in the Earth-surface environment. Several studies have reported that Mg isotope fractionation during melt-rock interaction at high temperature is negligible [Teng et al., 2007, 2010a, b; Liu et al., 2010]. The average value of upper continental crust is -0.22 ‰ [Bourdon et al., 2010; Li et al., 2010] and igneous rocks and minerals have δ^{26}Mg values within a relatively narrow range (-0.9 ‰ to +0.1 ‰) [Young and Galy, 2004; Pogge von Strandmann et al., 2008a; Bolou-Bi et al., 2009; Huang et al. 2009, 2012: Teng et al., 2010a, b; Yang et al., 2012; Liu et al., 2014]. Limestone and dolostone show relatively lower values between -4.6 ‰ and -2.7 ‰ and -2.3 ‰ and -1.1 ‰, respectively [Galy et al., 2002; Chang et al., 2003; Young and Galy, 2004; Bolou-Bi et al., 2009]. The average value of seawater is -0.82 ‰ [Foster et al., 2010]. These datasets were compiled by Manaka and Yoshimura [2015] and shown in Figure 1-9.

Figure 1-9.

Ranges of measured δ^{26}Mg values for seawater, rocks, minerals, weathering products, plants, and river water, reported by Manaka and Yoshimura [2015] and references therein.

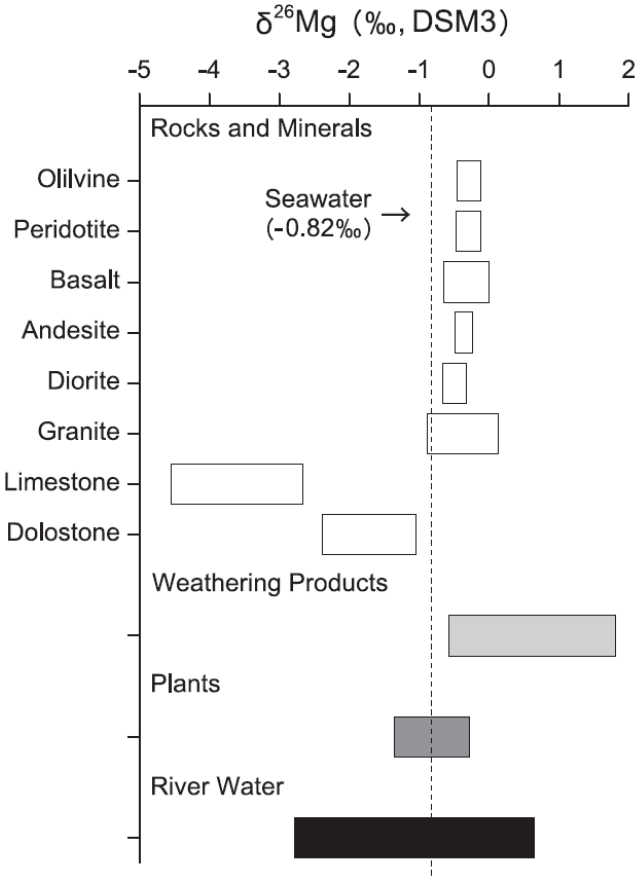

Mg-related processes occurring at low temperature in the terrestrial environment can be identified through δ^{26}Mg analysis. Heavy Mg isotopes are preferentially incorporated into the structure of clay minerals or absorbed into soil. For example, Opfergelt et al. [2012] examined Mg isotope behavior during chemical weathering and clay mineral formation processes in Guadeloupe. They investigated, for the first time, isotope variations in both bulk soils and clay fractions relative to their parent andesite and in different weathering stages. Their data provided evidence that Mg retained on the soil exchange complex contributed to the shift to relatively lighter Mg isotope compositions in the bulk soils. This result may be applicable to other fields; δ^{26}Mg values of most river waters draining a silicate catchment are generally lower than those of the bedrock [Tipper et al., 2006, 2012a, b; Brenot et al., 2008; Teng et al., 2010a; Huang et al., 2012; Opfergelt et al., 2012; Pogge von Strandmann et al., 2012; Lee et al., 2014], with some exceptions such as the findings of Pogge von Strandmann et al. [2008b] in Iceland.

During inorganic precipitation of carbonate minerals (e.g., calcite), light Mg is preferentially incorporated into solid forms [Immenhauser et al., 2010; Saulnier et al., 2012; Mavromatis et al., 2013; Wang et al., 2013a]. Yoshimura et al. [2011] reported not only the same kind of Mg fractionation during biogenic carbonate formation (e.g., deep-sea corals) but also a clear temperature dependence of the fractionation. However, many river waters draining a carbonate catchment show similar Mg isotope compositions to the bedrock [Brenot et al., 2008; Lee et al., 2014]. In Chapter 4, I discuss the impact of secondary carbonate precipitation on the riverine Mg isotope composition.

Vegetation in the basin can also induce isotope fractionation of Mg. Bolou-Bi et al. [2010] cultivated higher plant species under laboratory conditions and reported that they preferentially incorporate heavy Mg isotopes from the water. Bolou-Bi et al. [2012] reported the potential influence of plants on the Mg isotope composition of soils and waters in a small forested catchment. However, in larger catchments its impact may be minor compared to that of chemical weathering and soil formation [Tipper et al., 2008; Mavromatis et al., 2014].

Recently, Mg isotope composition has been studied in river waters around the world in an attempt to discuss its potential importance as a tracer of Mg-related processes, including chemical weathering in the river basin. However, the number of studies remains limited (Figure 1-9). Tipper et al. [2006] studied Mg isotope composition of 45 rivers around the world (including 16 major rivers) with different climatic and geologic conditions. Mg isotope composition of large rivers is affected by various lithology and biogeochemical processes in the basin. By and large, δ^{26}Mg values of river

waters vary between -2.8 ‰ and 0.6 ‰ (average: -1.09 ‰).

Regarding the Himalayan rivers, Tipper et al. [2006] reported δ^{26}Mg values between -1.54 ‰ and -1.19 ‰ in the major tributaries of the Ganges. For the Brahmaputra, lower Meghna, and Ayeyarwady, the values are -0.98 ‰, -1.10 ‰, and -0.86 ‰, respectively. For the Mekong, two samples were taken in August 1992 (-1.12 ‰) and September 2003 (-1.03 ‰), respectively. These river waters show relatively low δ^{26}Mg values with a high Mg^{2+} concentration, thereby lowering the average δ^{26}Mg value in global rivers.

Tipper et al. [2008] focused on upper tributaries of the Ganges in the Himalaya-Tibetan-Plateau region. The δ^{26}Mg value of river waters draining TSS was -1.41 ‰, higher than bedrock limestone. In this area, where Mg is a trace element in limestone, tributary Mg^{2+} was strongly influenced by the small amounts of silicate mineral dissolution. The δ^{26}Mg value of rivers draining HHCS was -1.25 ‰, lower than the average silicate rock. Here, Tipper et al. [2008] proposed incongruent silicate weathering with a $^{26}Mg/^{24}Mg$ isotope fractionation factor of 0.99937. In contrast, tributaries draining the dolomitic LHS showed a δ^{26}Mg value of -1.31 ‰. This value was within the analytical uncertainty of the dolostone, suggesting a congruent dissolution of dolostone in the area. The study also reported a negligible impact of vegetation and spring water on the riverine isotope composition. These results highlight the impact of heterogeneity in source rocks and isotope fractionation processes during chemical weathering on the δ^{26}Mg value of river waters.

In Chapter 4, I focus on the downstream part of the Ganges as well as the Brahmaputra and Meghna, and analyze the Mg isotope compositions of these rivers. Through comparisons with the results of Tipper et al. [2008], I include a detailed discussion on the spatial variations of chemical weathering and related processes, which play an important part in the global carbon cycle.

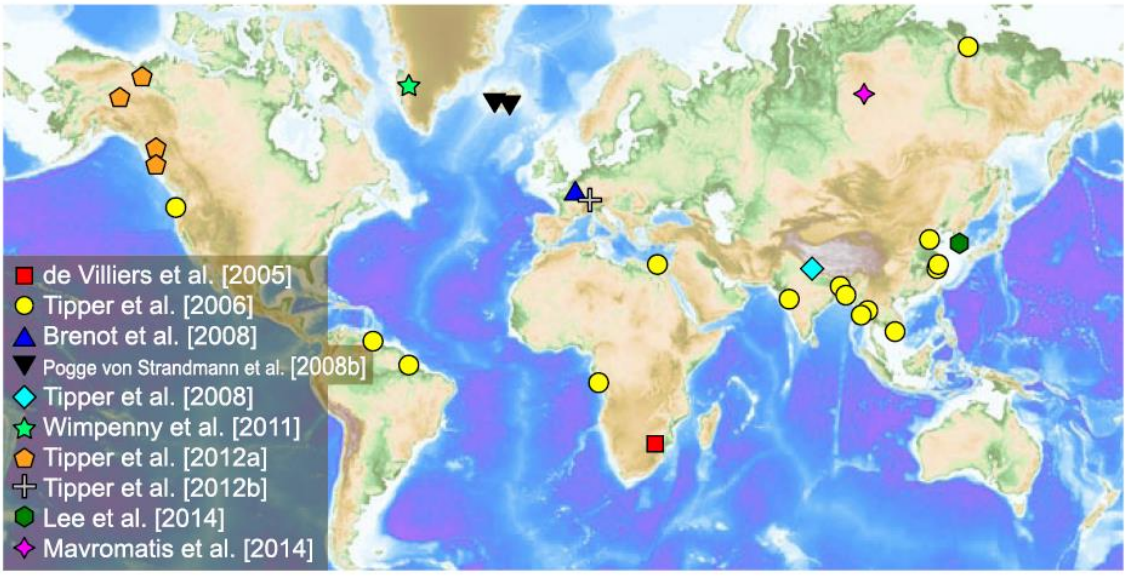

Figure 1-10.

Map showing the location of rivers reported in previous Mg isotope studies (modified from Manaka and Yoshimura [2015]).

1.5.4. Si isotope ratios

Si is the second most common element on the Earth's surface. Chemical weathering of silicate rocks, which acts as a net CO_2 consumption process, releases Si to river waters with an average concentration of 145 μmol kg^{-1} [Meybeck, 2003]. Silicon is always bound to oxygen in rocks. The speciation of dissolved Si in river waters is pH-dependent: at pH lower than 8, $Si(OH)_4$ (in equilibrium with $H_3SiO_4^-$) is the dominant species [Fujii et al., 2015]. Si is an essential nutrient for biota and marine diatoms, which form opal shell, account for up to 75 % of the new primary production in high nutrient and coastal regions of the ocean [Nelson et al., 1995]. Thus, this element has a vital role in the global carbon cycle.

Si has three naturally occurring stable isotopes: ^{28}Si (approximate abundances: 92.23 %), ^{29}Si (4.68 %), and ^{30}Si (3.09 %). The per mil notation for Si isotope ratios is defined as follows:

$$\delta^{x}Si = \{(^{x}Si / ^{28}Si)_{sample} / (^{x}Si / ^{28}Si)_{standard} - 1\} \times 1000 \quad (1\text{-}17)$$

where x is either 29 or 30. NBS-28 quartz is used as a standard material.

In contrast to Mg, Si isotopes are affected by high temperature fractionation. Felsic rocks

have higher isotope ratios than mafic rocks [André et al., 2006; Hoefs, 2015] (Figure 1-10). δ^{30}Si values of Precambrian rocks are extremely high, ranging between -1.8 ‰ and 5.0 ‰ [Robert and Chaussidon, 2006; Hoefs, 2015]. The average value of upper continental crust is -0.25 ‰ [Savage et al., 2013]. River waters have relatively heavy Si: δ^{30}Si values are 0.4 ‰ to 4.7 ‰. The highest values are reported in the Nile (0.5-4.7 ‰ [Cockerton et al., 2013]) or Yangtze rivers (0.7-3.4 ‰ [Ding et al., 2004]).

Both inorganic and organic processes can induce isotope fractionation of Si. When chemical weathering occurs, the dissolved phase tends to be isotopically enriched [e.g., Ziegler et al., 2005; Ding et al., 2004; Cockerton et al., 2013]. Oelze et al. [2014] conducted adsorption experiments and reported preferential adsorption of ^{28}Si on Al- hydroxide. In contrast, plants and diatoms tend to incorporate light Si isotopes. Large horizontal and depth variations in δ^{30}Si values are observed in the open ocean, resulting from dissolved Si concentration and biological uptake at each sampling station [Reynolds, 2006; Beucher et al., 2008]. Such biological activity can affect δ^{30}Si values even in river waters [Ding et al., 2004; Sun et al., 2013] and coastal areas (e.g., the Bay of Bengal [Singh et al., 2015]).

In Himalayan rivers, several studies have focused on δ^{30}Si as a potential tool for tracing the bedrock and chemical weathering processes in river basins. Georg et al. [2009] took samples from not only the Ganges and Brahmaputra rivers but also groundwater within the basin. δ^{30}Si values of the rivers range between 1.3 ‰ and 1.7 ‰, while those of the shallow groundwater were relatively higher (about 1.3 ‰) and those of the deep groundwater were lower (at least -0.2 ‰). Annual Si flux from rivers and groundwater to the Bay of Bengal was 9.3×10^{10} mol yr^{-1} and 1.3×10^{11} mol yr^{-1}, respectively. This highlights the potential importance of groundwater on biological activity in the ocean and the global Si cycle. In addition, Fontorbe et al. [2013] and Frings et al. [2015] conducted a sampling survey from the upper to lower streams (both the mainstream and tributaries) of the Ganges and reported detailed spatial variations of δ^{30}Si values. δ^{30}Si values ranged between 0.5 ‰ and 3.0 ‰. Si concentrations were high and δ^{30}Si values were low in the upper streams, and vice versa in the lower streams, which was attributed to incorporation of preferentially light Si into secondary minerals and vegetation. Frings et al. [2015] also took account of the hydrographic network of the main tributaries of the Ganges. By using both Rayleigh distillation and batch equilibrium models, they suggested that the majority (75 %) of Si mobilized during decomposition of the bedrock occurs in the Indian Peninsula and the Ganges alluvial plain. They highlight that active chemical weathering can

occur even in the lower stream basins, a hypothesis also suggested by Lupker et al. [2012].

Although several studies have already focused on the Ganges, there are still relatively few studies on Si isotope compositions in terrestrial river waters. To better understand chemical weathering and Si-related processes, I aim to measure δ^{30}Si values in various Himalayan rivers. In Chapter 4, I describe the methods developed for the measurement of δ^{30}Si values in river waters.

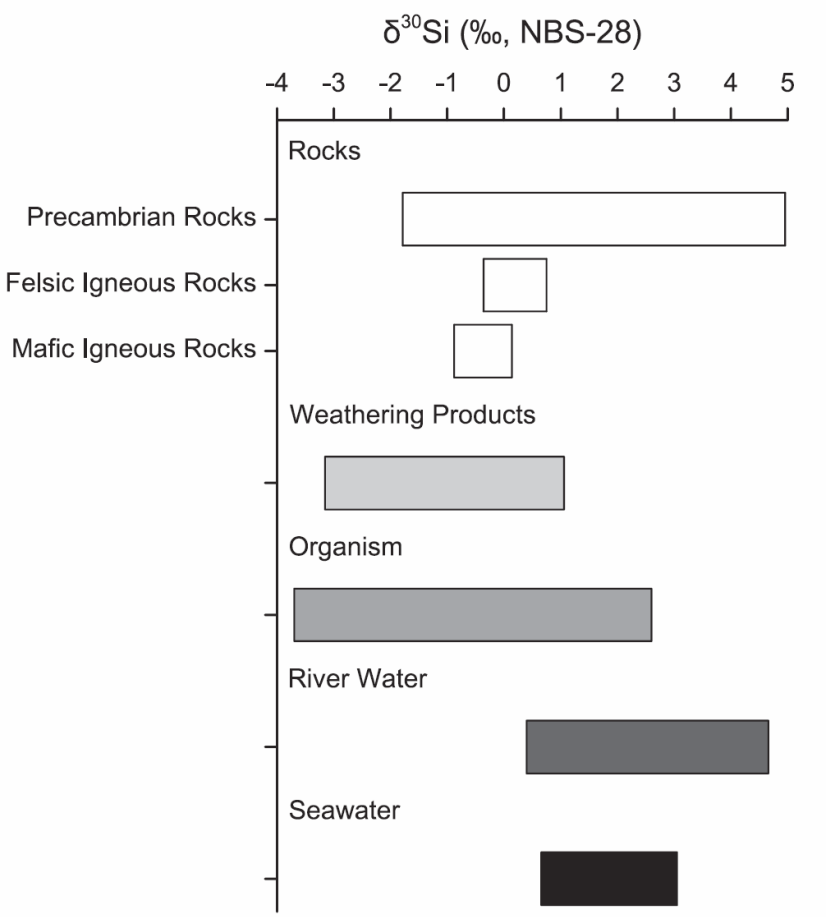

Figure 1-11.
Range in measured δ^{30}Si values of rocks, minerals, weathering products, organisms, river waters, and seawater, reported by Basile-Doelsch [2006], Cockerton et al. [2013], Hoefs [2015], and references therein.

Chapter 2. Spatial and seasonal variations in surface water pCO_2 in the Ganges, Brahmaputra, and Meghna rivers

2.1. Introduction

Terrestrial waters, including rivers, are important components of the global carbon cycle [Sarmiento and Gruber, 2006]. Previous studies on the carbon cycle in rivers have focused mainly on chemical weathering and the horizontal transport of dissolved and particulate carbon to the oceans [e.g., Milliman and Meade, 1983; Aitkenhead and McDowell, 2000]. Among the dissolved forms of carbon in river water, the concentration and flux of total alkalinity and HCO_3^-, which is a proxy for the intensity of chemical weathering, has received the most attention [Galy and France-Lanord, 1999; Sarin et al., 2001]. Dissolved CO_2 is another important form of carbon that is affected by both chemical weathering and biological activity, such as decomposition of terrestrially derived organic matter—in other words, respiration. Recent studies have shown that in many rivers, pCO_2 in the surface water is much higher than the atmospheric pCO_2 level (395 μatm) and that abundant carbon is released from river waters into the atmosphere over a short timescale [Telmer and Veizer, 1999; Richey et al., 2002; Yao et al., 2007]. Rivers receive abundant carbon from terrestrial ecosystems, and before being transported to oceans, a large portion of this carbon is returned to the atmosphere as a form of CO_2, the flux of which is not insignificant compared to that of fossil fuel combustion [Cole et al., 2007; Butman and Raymond, 2011; Aufdenkampe et al., 2011; Raymond et al., 2013]. Thus, in order to comprehend the global carbon cycle and associated global warming on timescales of 1-100 years, it is important to improve our understanding of the direct evasion of CO_2 from surface river water to the atmosphere.

In this chapter, I investigate surface water pCO_2 in the Ganges, Brahmaputra, and Meghna rivers. These rivers together have the second largest water discharge in the world after the Amazon, approximately 3 % of the world's total riverine discharge [Galy and France-Lanord, 1999]. The upper parts of the Ganges and Brahmaputra River basins include regions of active physical and chemical weathering of rocks, owing to the uplift of the Himalayan-Tibetan Plateau and the high rainfall. These processes increase the alkalinity of river water and thus decrease its pCO_2 [Molnar et al., 1993; Yin and Harrison, 2000]. The lower basins of these rivers are in lowlands in Bangladesh covered by

Himalayan alluvium with well-developed soils [Kuehl et al., 2005]. In addition, these lowlands have the highest population density in the world supported by active agriculture owing to the thick soils. Therefore, the production of CO_2 by respiration in these lowlands should be expected to increase organic carbon concentration and pCO_2 of the water in local rivers [Islam and Weil, 2000]. However, few studies have focused on pCO_2 in these river waters and the associated biogeochemical processes [Regnier et al., 2013]. In contrast, the Meghna River flows across only lowland deposits of Himalayan alluvium and exhibits a unique water chemistry.

I also report surface water pCO_2 in two other major Himalayan rivers, the Ayeyarwady and Mekong rivers, and one local non-Himalayan river in Thailand: the Chao Phraya River.

Water samples from the lower parts of the Ganges and Brahmaputra, and the northern part of the Meghna River (above its confluence with the Ganges: also called the upper Meghna at this point) in Bangladesh were collected during both the dry and rainy seasons. Those from the Ayeyarwady, Mekong, and Chao Phraya rivers were collected only during the rainy season. Using these samples, I evaluate their chemical and physical properties. The evaluation is based on a limited number of samples, however, and more samples are required for future study. By comparing the resulting dataset with previously published data from the upper basins of the Ganges and Brahmaputra rivers in particular, I investigate the spatial variations in the carbonate systems. pCO_2 is calculated based on pH and total alkalinity measurements, although the method is less precise compared to the direct measurement of pCO_2. On the basis of the results, I examine the roles of biogeochemical processes and the exchange of CO_2 between river water and the atmosphere on short timescales in the global carbon cycle.

2.2. Analytical procedures

To evaluate seasonal and annual variations in the discharge of the Ganges, Brahmaputra, and Meghna rivers and in the chemical composition of their waters, I conducted sampling surveys during two dry seasons (11-18 January 2011 and 16-23 February 2012) and two rainy seasons (5-9 September 2011 and 22-25 September 2012) in lowland areas in Bangladesh (about 300-500 km from the river mouth). Samples were collected at three stations along both the Ganges (Stations G-1 to G-3) and Brahmaputra rivers (Stations B-1 to B-3) and at four stations along the Meghna River, above its confluence with the Ganges River: Station S-1, Surma River; Station K-1, Kusiyara River; and Stations M-1 and M-2, Meghna River (Figure 2-1). At some of these sampling stations, more than two water samples were taken in different seasons (Table 2-1).

With regard to the Ayeyarwady, Mekong, and Chao Phraya rivers, I conducted the sampling survey only during the rainy season, when the river discharge was at its annual peak (Table 2-1). During 12-21 July 2013, I collected 14 samples in total. Four samples were collected from the middle to lower reaches of the Ayeyarwady (about 50-650 km from the river mouth) in Myanmar (A-1 to A-4) (Figure 2-2). One sample was taken from the mainstream of the Mekong, approximately 1500 km from the river mouth (Me-1), and two samples were collected from its two tributaries: the Chi River (Me-2) and Mun River (Me-3). Samples from the Chao Phraya River system were taken along its entire length. Five samples were taken from its four upstream tributaries (the Ping, Wang, Yom, and Nan rivers) (C-1 to C-5) and two samples from the mainstream, which covers the lower half of the system (C-6 and C-7). These sampling points were chosen to encompass the spatial variations in water quality due to convergence of the rivers and differences in flow rates.

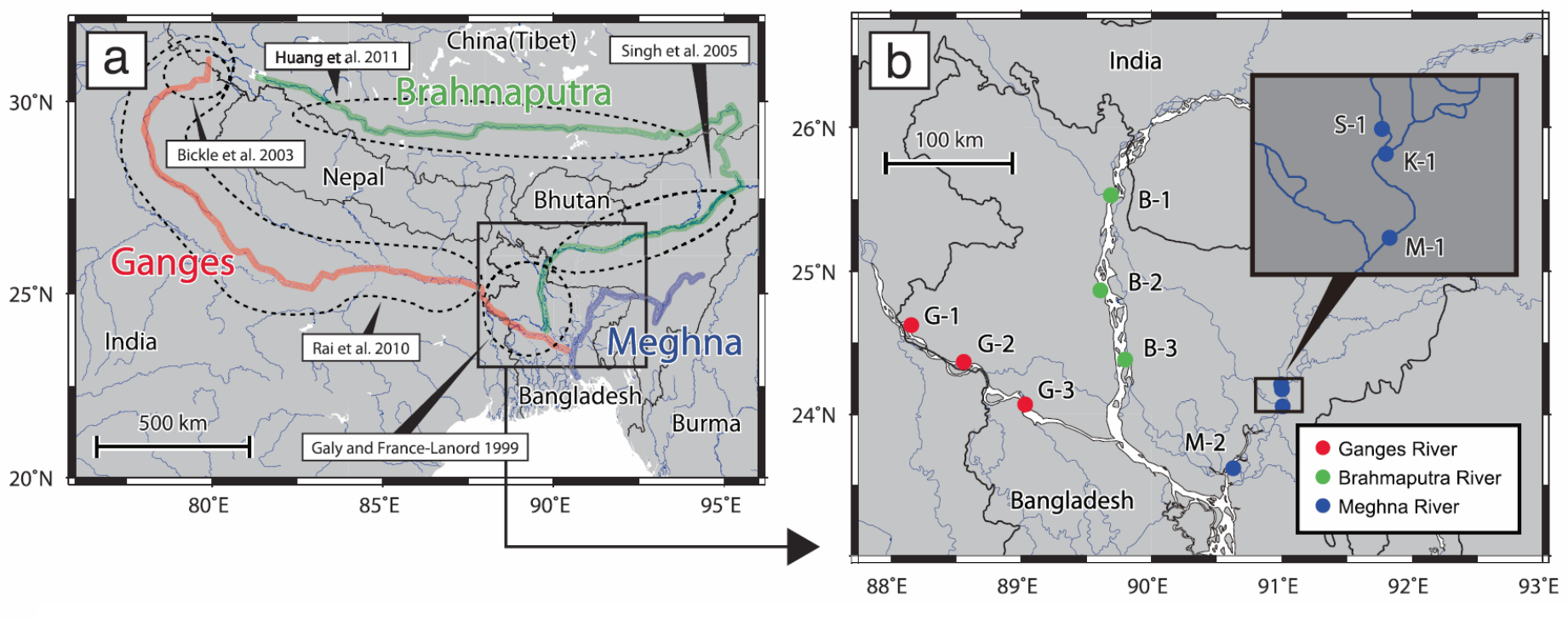

Figure 2-1.

(a) Locations of the Ganges, Brahmaputra, and Meghna rivers and the sampling stations of previous studies; the lower streams of the Ganges (Rajshahi) and Brahmaputra (Chilmari and Aricha Ghat) [Galy and France-Lanord, 1999], the headwaters of the Ganges in the Garhwal Himalaya [Bickle et al., 2003], the middle and lower streams of the Brahmaputra (from Dibrugarh to Chilmari) [Singh et al., 2005], the upper and middle streams of the Ganges (from Devprayag to Rajmahal) [Rai et al., 2010], and the upper and middle Yarlung Tsangpo River [Huang et al., 2011]. (b) Locations of sampling stations in this study.

Table 2-1.

Physical properties, inorganic carbonate chemistry, concentrations of major ions, DOC, and phosphate and strontium isotope ratios of the river water samples.

Sampling Station	Date	Temp.	pH	Total Alkalinity	pCO_2	DIC	Na^+	Mg^{2+}	K^+	Ca^{2+}	Sr^{2+}	F^-	Si	Cl^-	NO_3^-	SO_4^{2-}	HCO_3^-	PO_4^{3-}	$^{87}Sr/^{86}Sr$	DOC
	(dd/mm/yyyy)	(°C)		($\mu mol\ kg^{-1}$)	(μatm)	($\mu mol\ kg^{-1}$)														($\mu mol\ kg^{-1}$)
Ganges River																				
G-1	11/01/2011	16.0	8.31	3033	857	3046	717	453	104	965	2.02	11.2	142	291	14.6	181	2985	0.09	0.7286329	114
G-2	11/01/2011	17.4	8.43	2989	649	2984	494	434	107	1105	1.76	10.1	125	203	1.7	156	2925	0.02	0.7287156	152
G-3	12/01/2011	16.5	8.61	2685	377	2658	682	430	101	759	1.69	10.2	89	292	1.2	172	2602	0.20	0.7286908	123
G-3	07/09/2011	30.6	8.02	1875	1270	1901	290	209	92	693	1.13	10.2	152	85	33.8	96	1853	-	0.7256897	131
G-3	20/02/2012	22.0	8.61	2931	440	2893	750	538	92	858	1.77	10.3	54	256	0.2	164	2827	-	0.7268390	112
G-3	24/09/2012	29.6	7.84	1738	1763	1784	253	218	73	621	1.00	8.5	142	79	36.8	86	1725	-	0.7248720	112
Brahmaputra River																				
B-1	13/01/2011	16.5	7.97	1658	1040	1697	213	205	59	640	1.09	7.1	181	35	7.5	183	1646	0.45	0.7193583	48
B-2	12/01/2011	16.7	8.20	1673	617	1689	208	261	60	644	1.09	7.4	188	35	8.3	174	1652	0.37	0.7200278	46
B-3	14/01/2011	16.1	7.94	1676	1122	1719	211	204	61	632	1.07	7.7	185	35	8.3	173	1665	0.44	0.7206957	44
B-3	06/09/2011	31.3	7.97	1088	836	1105	118	124	60	476	0.76	6.2	160	19	12.3	145	1076	0.60	0.7186717	75
B-3	19/02/2012	21.4	8.07	1692	897	1716	227	280	54	671	1.08	6.8	166	43	0.0	191	1674	-	0.7200691	41
B-3	22/09/2012	27.5	7.70	845	1150	879	84	104	44	353	0.54	4.7	125	14	16.3	98	841	-	0.7178980	81
Upper Meghna River																				
S-1 (Surma)	15/01/2011	18.8	7.45	807	1736	876	230	116	35	224	0.55	4.8	122	59	18.8	62	805	0.17	0.7155291	152
K-1 (Kusiyara)	15/01/2011	19.4	7.71	953	1133	996	321	137	56	218	0.61	6.2	264	82	31.4	36	948	0.43	0.7156579	208
M-1	16/01/2011	19.2	7.52	795	1463	852	234	103	37	220	0.54	4.9	132	59	25.0	60	792	0.28	0.7157216	156
M-1	17/02/2012	22.0	8.01	987	606	1004	315	212	34	277	0.65	4.5	164	86	28.4	76	977	-	0.7156379	159
M-2	17/01/2011	19.4	7.47	767	1588	829	258	103	38	222	0.51	5.4	162	87	27.6	58	765	0.18	0.7162142	149
M-2	05/09/2011	31.6	7.37	374	1159	406	102	50	26	106	0.25	4.3	129	29	3.8	23	373	0.32	0.7163666	130
M-2	25/09/2012	31.0	7.34	396	1303	433	104	60	19	108	0.24	3.2	141	25	8.2	29	395	-	0.7163973	129
Ayeyarwady River																				
A-1	14/07/2013	23.8	7.32	477	1494	529	85	98	24	146	-	3.2	-	15	-	22	476	-	-	90
A-2	13/07/2013	26.8	7.56	656	1225	694	124	142	24	191	-	3.1	-	18	-	35	653	-	-	106
A-3	12/07/2013	26.9	7.15	657	3191	759	124	139	24	191	-	3.3	-	18	-	36	656	-	-	92
A-4	15/07/2013	28.0	7.36	720	2183	787	208	179	33	185	-	3.5	-	82	-	47	718	-	-	103
Mekong River																				
Me-1	18/07/2013	27.7	7.81	1595	1691	1642	336	294	47	657	-	5.5	-	166	-	177	1584	-	-	122
Me-2 (Chi)	17/07/2013	31.7	9.07	2003	109	1876	2621	253	131	612	-	9.7	-	2065	-	122	1763	-	-	374
Me-3 (Mun)	17/07/2013	28.9	7.48	1949	4545	2085	3421	375	260	662	-	9.7	-	3281	-	176	1943	-	-	507
Chao Phraya River																				
C-1 (Ping)	19/07/2013	27.5	7.38	1780	5038	1938	318	258	140	674	-	10.8	-	129	-	90	1775	-	-	310
C-2 (Wang)	19/07/2013	28.2	7.59	2860	5127	3014	638	497	125	1120	-	14.3	-	233	-	205	2848	-	-	517
C-3 (Ping)	19/07/2013	31.4	8.14	1786	916	1797	350	226	97	654	-	11.8	-	109	-	83	1757	-	-	154
C-4 (Yom)	18/07/2013	33.0	7.99	2309	1726	2343	796	374	84	832	-	9.5	-	171	-	284	2283	-	-	243
C-5 (Nan)	20/07/2013	30.8	7.36	1267	3931	1381	412	207	65	407	-	5.8	-	226	-	49	1264	-	-	324
C-6	20/07/2013	30.4	7.59	1437	2628	1511	505	200	78	437	-	9.6	-	180	-	76	1430	-	-	353
C-7	20/07/2013	29.2	7.57	1590	2972	1677	857	265	91	616	-	10.8	-	450	-	210	1583	-	-	368

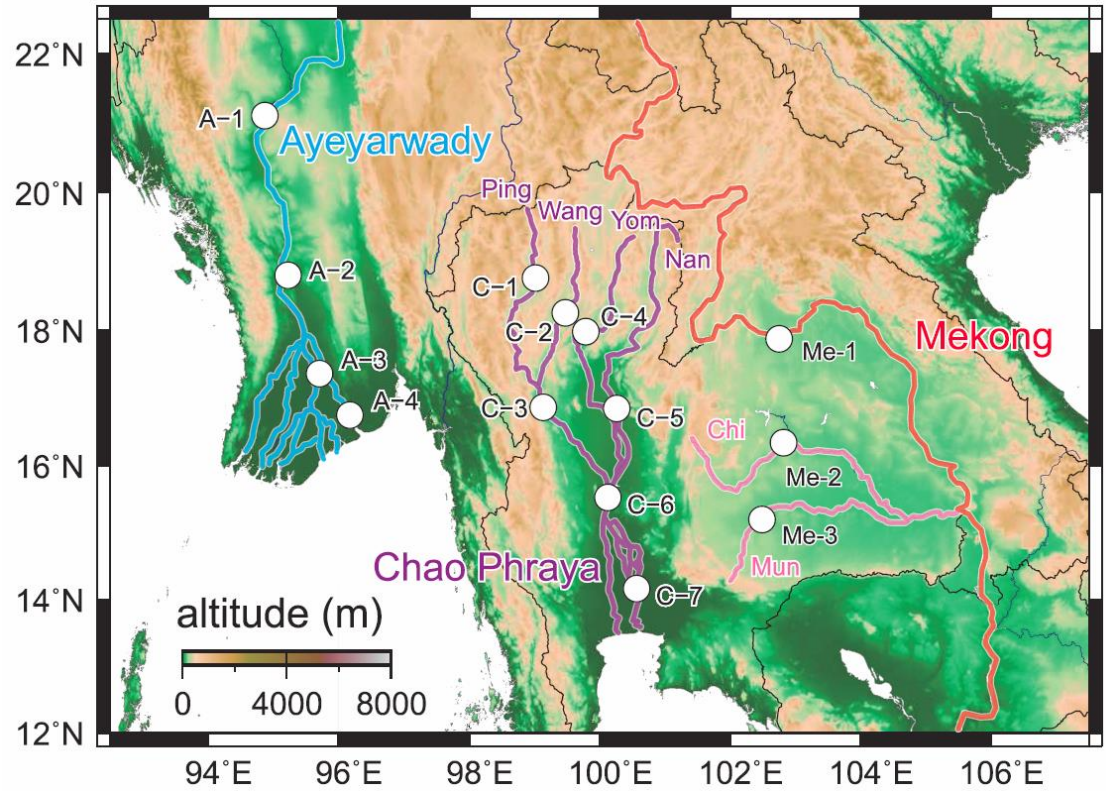

Figure 2-2.

Locations of the Ayeyarwady, Mekong and Chao Phraya rivers and sampling sites. Topography data are from Amante and Eakins [2009].

All collected samples consisted of surface water from the center of the river channel. After each sampling, water temperature and pH were immediately measured in the field. pH was measured with an 826 pH Mobile Meter (Metrohm) equipped with a combination electrode and calibrated every day with buffer solutions of pH 4.01 and 6.86. I measured the pH of each sample at least three times, and the error was within 0.05 in all cases. Samples collected for laboratory analyses were filtered through glass-fiber filters (pore size: 0.7 μm) for DOC measurements and through acetate membrane filters (pore size: 0.45 μm) for other measurements. Subsamples for each measurement procedure were stored separately in glass vials or polypropylene bottles. The filtration for total alkalinity measurements was conducted using syringe filters to minimize CO_2 degassing during the filtration. For other measurements, I filtered samples using an electric pump. Samples for total alkalinity measurements were immediately mixed with $HgCl_2$ to prevent further biological activity. All bottles were sealed and kept in a cool, dark environment until taken out for analysis.

Using an automated titrator (ABU91, Radiometer) I measured total alkalinity by potentiometric acid titration at 25 °C, following the standard procedure for Gran titration [Dickson et al., 2007]. A calibration curve for this measurement was prepared using solutions of sodium bicarbonate. Based on measurements of our laboratory reference solution (drinking water), repeated six times, the analytical error (2SD) was determined to be 10 μmol kg^{-1}. I then calculated pCO_2 and the DIC concentration from the pH and total alkalinity (for details, see Suzuki et al. [1995]), using the carbonate equilibrium calculation program CO_2calc [Robbins et al., 2010] and the DIC system equilibrium constants (K_1 and K_2) of Millero [1979]. I used CO_2calc to evaluate the uncertainties associated with the pCO_2 values, which are attributed to errors associated with the pH (± 0.05) and total alkalinity (± 10 μmol kg^{-1}). When analytical errors in pH are taken into account, uncertainties in pCO_2 values change by 12 % on average. In comparison, analytical errors in total alkalinity affect pCO_2 values by less than 1 % (e.g., a simple simulation is shown in Figure 2-3). The greater the pCO_2 value is, the greater the uncertainty is.

The concentrations of major ions were measured by: ion chromatography (ICS-2000, Dionex, at the Kochi Core Center (KCC), Japan Agency for Marine-Earth Science and Technology (JAMSTEC) and DX-500, Dionex, at the National Institute of Advanced Industrial Science and Technology (AIST)); inductively coupled plasma-atomic emission spectrometry (ICP-AES) (Optima 4300 DV, PerkinElmer, at KCC); or inductively coupled plasma-mass spectrometry (ICP-MS) (ELAN-DRC II, PerkinElmer, at KCC). The uncertainties in these ion measurements were less than ± 3 %, as estimated from the reproducibility (2RSD) of standard solutions [Nishio et al., 2010].

Concentrations of dissolved phosphate (PO_4), an inorganic nutrient, were determined using a continuous-flow autoanalyzer (BRAN+LUEBBE, AACS-II) at the Atmosphere and Ocean Research Institute (AORI) at the University of Tokyo. The maximum analytical error (2SD) was less than 0.16 μmol kg^{-1}.

Sr was recovered from the samples by extraction chromatography using Sr-spec resin (Eichrom). Following chemical exchange separation, 100 and 300 ng of Sr were loaded on a W filament with a Ta oxide activator, and Sr isotope ratios were measured with a Triton thermal ionization mass spectrometer (Thermo Scientific, measurements were made at KCC). The instrumental mass fractionation was corrected by internal normalization using $^{86}Sr/^{88}Sr = 0.1194$ [Steiger and Jäger, 1977]. Repeated measurements of the Sr isotope standard NIST 987 (U.S. National Institute of Standards and Technology) yielded $^{87}Sr/^{86}Sr = 0.7102507 \pm 0.0000066$ (2SD, n = 36) and 0.7102579

± 0.0000014 (2SD, n = 9) for 100 ng and 300 ng runs, respectively. All the Sr isotope data was normalized to NIST 987 = 0.710248 [McArthur et al., 2000]. The error was less than 0.000011 in all samples (Table 2-1).

The DOC concentration was measured with a Total Organic Carbon Analyzer (TOC-VCPH, Shimadzu Corporation) at AORI. Each sample was measured three times, and the error was within 3 μmol kg^{-1} in all cases.

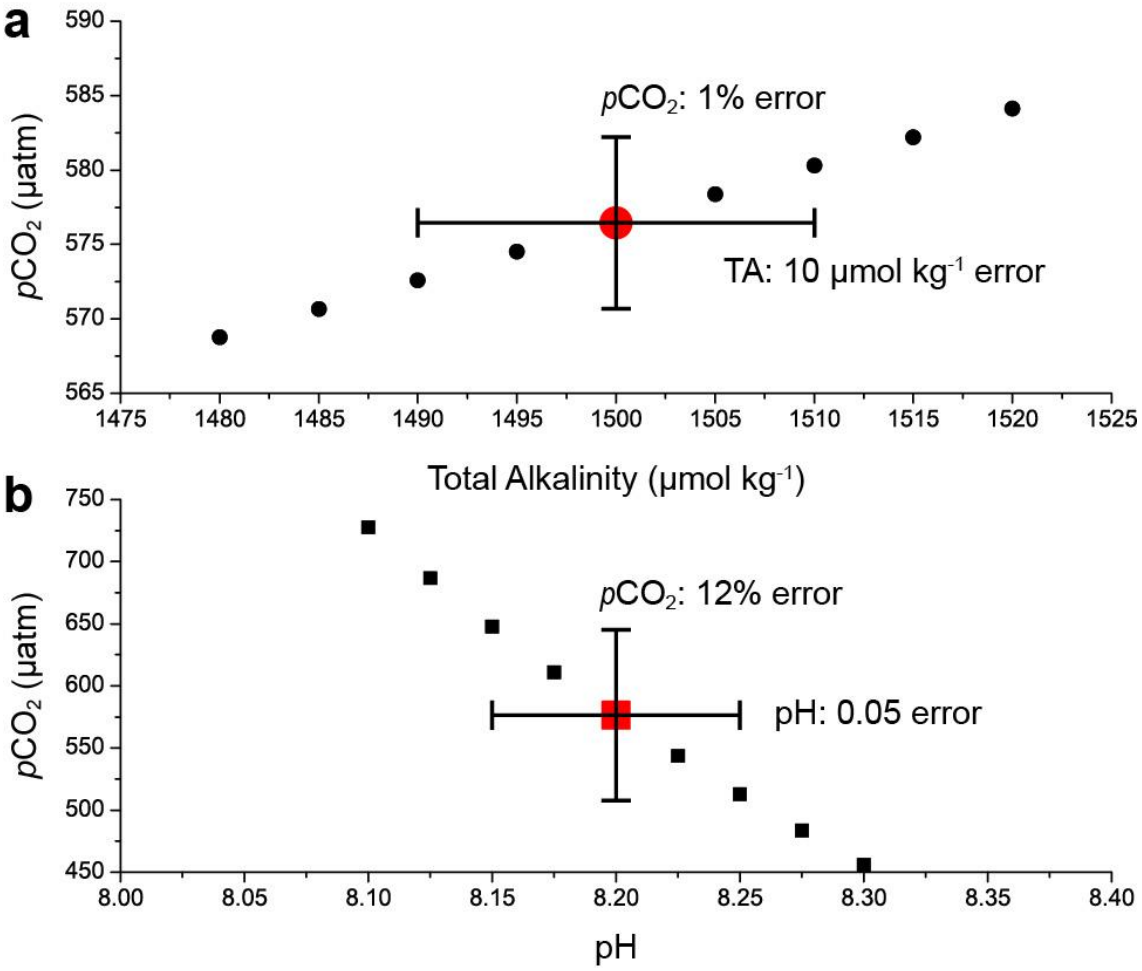

Figure 2-3.

An example showing variations of pCO_2 relative to measurement uncertainties for (a) total alkalinity (TA) concentration and (b) pH. I simulated one freshwater sample (T = 20 °C, pH = 8.2, TA = 1500 μmol kg^{-1}) and calculated its pCO_2 by CO_2calc program (red symbol). Measurement errors of TA (± 10 μmol kg^{-1} in samples) and pH (± 0.05) cause uncertainties in pCO_2 (less than 1 % and 12 % on average, respectively).

2.3. Results

A wide range of seasonal variation in pCO_2 was observed in the Himalayan rivers (Table 2-1). In the Ganges, the range in values for the dry and rainy seasons were 377-857 µatm (average 581 µatm) and 1270-1763 µatm (average 1517 µatm), respectively. In the Brahmaputra, they were 617-1122 (average 919 µatm) and 836-1150 µatm (average 993 µatm), respectively. In the Meghna, they were 606-1736 µatm (average 1305 µatm) and 1159-1303 µatm (average 1231 µatm), respectively. The range in values for the Ayeyarwady, Mekong, and Chao Phraya rivers were 1225-3191 µatm, 109-4545 µatm, and 916-5038 µatm, respectively. The pCO_2 values in most samples were higher than the atmospheric level of 395 µatm, which suggests that these surface waters act as sources of CO_2 to the atmosphere, despite active chemical weathering in these regions. In Bangladesh I measured much lower pCO_2 values in the Ganges and Brahmaputra rivers than in the Meghna River, and in the Ganges River, the pCO_2 values were higher in the rainy season than in the dry season.

The range of total alkalinity in the dry and rainy seasons was 2685-3033 µmol kg^{-1} (average 2909 µmol kg^{-1}) and 1738-1875 µmol kg^{-1} (average 1807 µmol kg^{-1}), respectively, in the Ganges River and 1658-1692 µmol kg^{-1} (average 1675 µmol kg^{-1}) and 845-1088 µmol kg^{-1} (average 967 µmol kg^{-1}), respectively, in the Brahmaputra River. The range of total alkalinity for the Ayeyarwady, Mekong, and Chao Phraya rivers was 477-720 µmol kg^{-1}, 1595-2003 µmol kg^{-1}, and 1267-2860 µmol kg^{-1}, respectively (Table 2-1). Except for the Ayeyarwady River, these values are much higher than the global river average (853 µmol kg^{-1}) [Meybeck, 1987], because of the active chemical weathering of carbonate rocks in the upper basins of these rivers. In Bangladesh, the concentrations of Ca^{2+}, Mg^{2+}, and HCO_3^- were also high in the Ganges and Brahmaputra rivers. In the Meghna River, in contrast, the range in total alkalinity was only 767-987 µmol kg^{-1} (average 862 µmol kg^{-1}) and 374-396 (average 385 µmol kg^{-1}) in the dry and rainy seasons, respectively. HCO_3^- concentrations were relatively low, and Na^+, K^+, and Si concentrations were high. In all these rivers, total alkalinity and the concentrations of most major ions were higher in the dry season than in the rainy season. For more information about major ion results, see Sections 3.3 and 4.3.

The Sr^{2+} concentrations in all samples were higher in the dry season than in the rainy season (Table 2-1). In the Ganges River water samples, the dry and rainy season Sr^{2+} concentrations were 1.69-2.02 µmol kg^{-1} (average 1.81 µmol kg^{-1}) and 1.00-1.13 µmol kg^{-1} (average 1.07 µmol kg^{-1}), respectively. In Brahmaputra River water samples, the values were 1.07-1.09 µmol kg^{-1} (average 1.08 µmol kg^{-1}) and 0.54-0.76 µmol kg^{-1} (average 0.65 µmol kg^{-1}), respectively. In samples from the upper

Meghna River system, the values were 0.51-0.65 μmol kg^{-1} (average 0.56 μmol kg^{-1}) and 0.24-0.25 μmol kg^{-1} (average 0.25 μmol kg^{-1}), respectively. Sr isotope ratios in the three rivers were high compared to the mean global value for major rivers (approximately 0.712) [Tripathy, 2012]. The range in isotope ratios in the dry and rainy seasons was 0.7268-0.7287 and 0.7249-0.7257, respectively, in the Ganges River, and 0.7194-0.7207 and 0.7179-0.7187, respectively, in the Brahmaputra River. In the Meghna River, they were 0.7155-0.7162 in the dry season and 0.7164 in the rainy season. Thus, in the Ganges and Brahmaputra rivers, the ratios were higher in the dry season than in the rainy season, whereas in the Meghna River, they were approximately constant throughout the year.

The concentrations of DOC were high in the Ganges (112-152 μmol kg^{-1}) and Meghna rivers (129-208 μmol kg^{-1}) and low in the Brahmaputra River (41-81 μmol kg^{-1}) (Table 2-1). Values for the Ayeyarwady, Mekong, and Chao Phraya rivers were 90-106 μmol kg^{-1}, 122-507 μmol kg^{-1}, and 154-517 μmol kg^{-1}, respectively.

2.4. Discussion

2.4.1. Spatial variations in river water alkalinity in relation to chemical weathering

The suspended sediment flux of the Ganges River is lower than that of the Brahmaputra River [River Survey Project, 1996; Aucour et al., 2006] because of its smaller runoff and lower discharge, suggesting that less physical weathering occurs in the basin of the Ganges. In general, higher denudation of a watershed tends to accelerate chemical weathering [Riebe et al., 2004; Larsen et al., 2014]. The flux of physically and chemically weathered sediment that enters the Bay of Bengal via the Brahmaputra is enormous because of the rapid uplift of the eastern Himalayan syntaxis [Stewart et al., 2008; Robinson et al., 2014]. Therefore, from a hydrological point of view, the water chemistry of the Ganges might be expected to reflect relatively less active chemical weathering in its basin than in the Brahmaputra basin. In addition, the area of silicate terrain is proportionately higher in the Ganges basin compared to the Brahmaputra basin than the area of carbonate terrane [Galy and France-Lanord, 1999; Gaillardet et al., 1999]. This difference is also reflected in my measurements by the differences in the major ion balance: the Ganges River water is relatively rich in Na^+ and K^+, while the Brahmaputra is rich in Ca^{2+}. Because the dissolution rates of silicates are generally much lower than those of carbonates [Meybeck, 1987; Tripathy et al., 2010], the differences detected in the ion concentrations indicate that chemical weathering occurs more slowly in the Ganges basin than in the Brahmaputra basin.

Unexpectedly, however, the total alkalinity, which can be used as a rough proxy for chemical weathering intensity, was higher in the Ganges River than in the Brahmaputra River, although in both rivers, total alkalinity was more than twice the average value in other rivers of the same size class around the world (Table 2-1). Galy and France-Lanord [1999] reported that the mineralogical composition of the clay fraction of the sediment load differed between these rivers and that the ratio of the physical weathering flux to the chemical weathering flux was higher in the Brahmaputra. One explanation for these results may be the existence of fewer water storage dams (which tend to remove particulate matter from river water) and areas of sediment aggradation along the Brahmaputra [Raymahashay, 1970; Singh et al., 2005]. According to Immerzeel et al., [2010], snow and glacier water in the upper stream contribute more to the water discharge of the Brahmaputra than to that of the Ganges, and these contributions are expected to result in lower total alkalinity.

An approximate evaluation of the spatial variations in total alkalinity was performed along each river over a large area (> 500 km) by comparing data from this study with data collected along

the upper reaches of each river from previous studies (Table 2-2, Figure 2-4). These previous studies were conducted at most 15 years prior to this one. In this study, I assume that significant changes in environmental conditions did not take place in the upper reaches of the rivers in the last few decades because the upper reaches are barren areas with lower population densities than the lower reaches. In addition, these previous studies did not include data from 1987-1988 and 1998, when extensive flooding occurred along both the Ganges and Brahmaputra rivers [Webster et al., 2010].

Although the variations exhibited no clear trends within Bangladesh, which contains a relatively small proportion of the total basin area, unique spatial variations in total alkalinity between the high Himalayas and Bangladesh were observed in each river, despite appreciable seasonal and interannual variation. Along the Brahmaputra, the distribution of total alkalinity was relatively uniform. In the highlands, its mainstream drops steeply and is joined by some tributaries (Figure 2-4). In fact, the annual discharge of the Yarlung Tsangpo River (in Tibet) accounts for up to 25 % of the total discharge of the Brahmaputra at Bahadurabad station in Bangladesh [Huang et al., 2011]. Although groundwater in the upper basin, where chemical weathering occurs, has a long residence time, the flow of the river water from the upper basin to the lower basin is rapid. As a result, weathering and total alkalinity in the middle and lower reaches have little influence on the water chemistry of the lower reaches of the Brahmaputra. Therefore, the total alkalinity observed in Bangladesh mainly preserves the alkalinity that results from active chemical weathering of metamorphosed limestone in the upper basin.

Table 2-2.

Calculated pCO_2 and distance from the river mouth (Bay of Bengal) of sampling stations used in previous studies (see also the caption of Figure 2-1). pCO_2 levels in the upper streams are determined from temperature, pH, and total alkalinity data in the original publications using the CO_2calc carbonate equilibrium calculation program [Robbins et al., 2010] and the DIC system equilibrium constants (K_1 and K_2), proposed by Millero [1979].

River	Reference	Date (dd/mm/yyyy)	Sample numbers (original source)	Distance from the river mouth (km)	pCO_2 (µatm)	Total Alkalinity (µmol kg^{-1})
Ganges	Rai et al. [2010]	01/05/2003	RW03-3	2423	118	801
	Bickle et al. [2003]	17/07/1996	TA4	2363	169	847
		09/1996–02/1997	RK996/RK1096/RK1196/ RK1296/RK197/RK297	2363	279–425	1178–1379
	Rai et al. [2010]	07/05/2004	BR-309	937	2191	4026
	Rai et al. [2010]	09/05/2004	BR-318	559	1618	2892
	Galy and France-Lanord [1999]	02/08/1996	BGP4	453	2566	1492
Brahmaputra	Huang et al. [2011]	4 weeks in fall 2008	A - Z	3354–2166	121–545	1361–2548
	Singh et al. [2005]	01/10/1999	BR-18	1172	292	1194
		01/10/1999	BR-28	902	373	1154
		01/07/2000	BR-65	902	485	851
		01/10/1999	BR-5	748	160	989
		01/07/2000	BR-51	748	1197	1081
		01/07/2000	BR-73	541	1133	1048
	Galy and France-Lanord [1999]	05/08/1996	BGP15	491	1953	1171
		25/02/1997	BGP51	267	400	1614

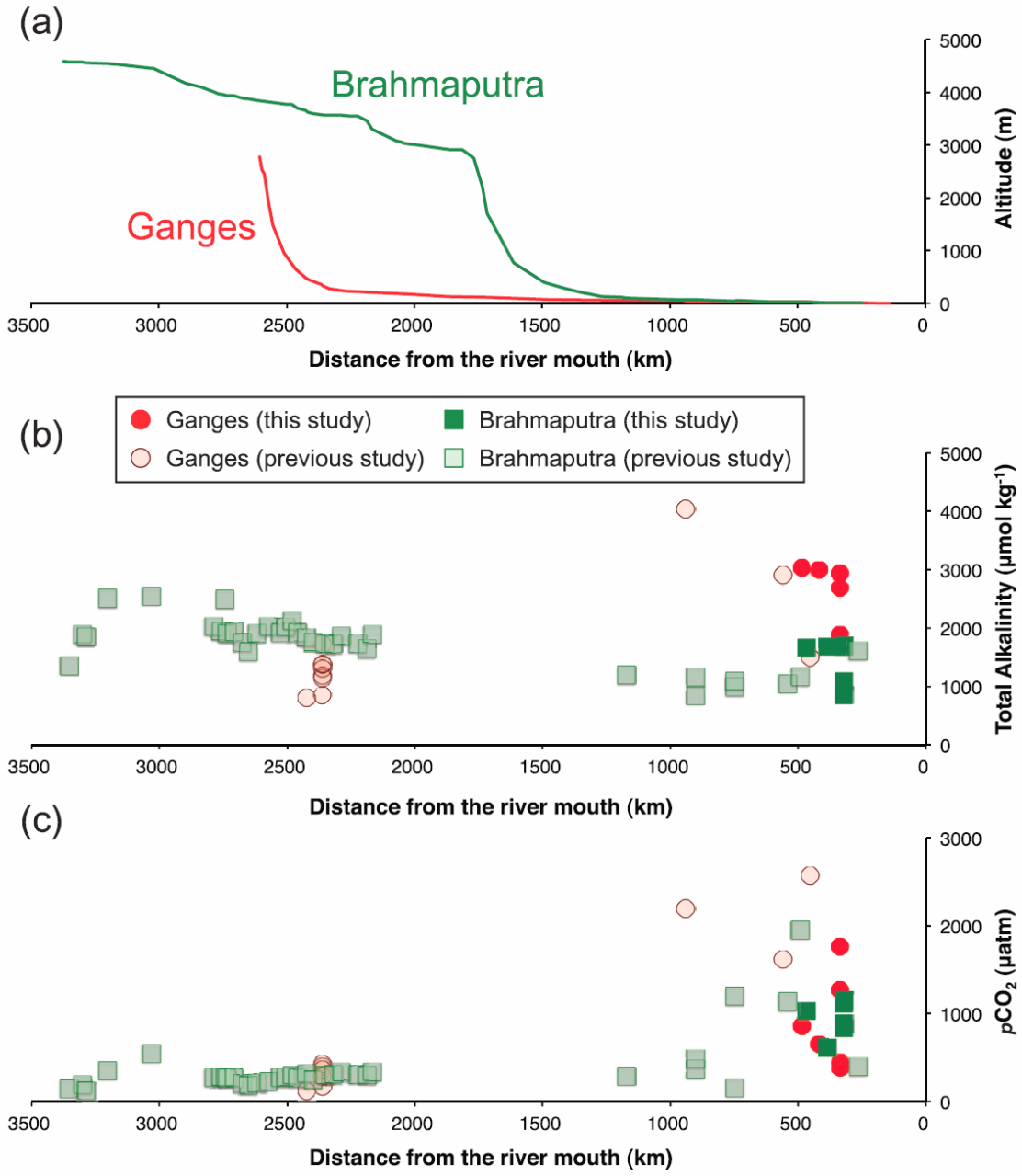

Figure 2-4.

(a) Topographic profiles of the Ganges (red line) and Brahmaputra (green line) rivers and their headstreams. Variations in (b) total alkalinity (μmol kg^{-1}) and (c) calculated pCO_2 (μatm), relative to the distance from the mouth of the Ganges (red circles) and Brahmaputra (green squares) rivers and their headstreams. Dark colors indicate data from this study, and light colors indicate data from previous studies.

In contrast, total alkalinity is low in the upper Ganges and increases by a factor of 2-3 in the lower Ganges (Table 2-1). Numerous large tributaries join the Ganges as it flows southeastward through India. The annual discharge of the Ganges, which is only 7.6×10^2 m^3 s^{-1} at Rishikesh in the upper stream, increases drastically to 4.8×10^3 m^3 s^{-1} at Allahabad in the middle stream [Rai et al., 2010]. Those tributaries that originate in the high Himalayas have high total alkalinity [e.g., Galy and France-Lanord, 1999] because of active chemical weathering. Therefore, when they converge with the Ganges, they increase the total alkalinity of the Ganges mainstream. In addition, cyclic wetting and drying occurs in the basins of lowland tributaries (which drain areas of Mesozoic and Tertiary mafic effusives) and lead to the formation of alkaline and saline soils containing calcareous concretions. Hence, these tributaries also increase total alkalinity in the Ganges [Sarin et al., 1989; Heroy et al., 2003].

In the Meghna River, total alkalinity is lower than in the Ganges and Brahmaputra rivers because the entire course of the Meghna is through Himalayan alluvium in the lowlands, where chemical weathering is less active than in the high Himalayas.

2.4.2. Spatial variations in pCO_2

In general, river water pCO_2 can be influenced by various biological, chemical, and physical processes. Photosynthesis and respiration processes can decrease and increase pCO_2, respectively, although they do not affect total alkalinity values. Chemical weathering processes can convert dissolved CO_2 to bicarbonate ions. Dissolved inorganic carbon can be enriched when some of the water evaporates, and vice versa when it is diluted by rainwater, which contains a small amount of dissolved inorganic carbon. When the residence time of the water in the atmosphere is long enough, the water pCO_2 can be in equilibrium with the atmosphere. In addition, temperature changes can impact the dissolved carbonate system.

The difference in pCO_2 between river water and the atmosphere controls the air-water CO_2 flux [e.g., Alin et al., 2011]. Within Bangladesh, spatial pCO_2 variations did not exhibit any increasing or decreasing trends (Table 2-1), probably because of the influences of local processes, such as biological activity. To understand pCO_2 changes on large spatial scales, I calculated pCO_2 values along the upper reaches of the Ganges and Brahmaputra rivers from previously reported pH and HCO_3^- data and compared these data with observed pCO_2 values in Bangladesh. The calculated pCO_2 values, which range between 222 and 542 μatm at Rishikesh on the upper Ganges and between 121 and 545

µatm along the Yarlung Tsangpo, are less than or comparable to atmospheric pCO_2 values. Therefore, along their upper reaches, these rivers are presumably either sinks or minor sources of CO_2 to the atmosphere. However, along the middle and lower reaches of both the Ganges and Brahmaputra rivers, pCO_2 increases to more than 1000 µatm. Therefore, these rivers are potentially large sources of CO_2 to the atmosphere.

The geological and geomorphological settings of the river basins, rather than local conditions, explain the observed trends. The low pCO_2 values along the upper reaches are attributable to chemical weathering in the upper basin, as evidenced by the high total alkalinity of the river water [Hartmann, 2009]. The upper basins of the Ganges and Brahmaputra rivers are characterized by high elevations, steep relief, and poorly developed soils [Galy and France-Lanord, 1999]. As a result, vegetation is sparse, soil respiration is less active, and the pCO_2 of the river water is low. In contrast, the middle and lower streams drain areas of Himalayan alluvium with well-developed soils. This difference can account for the increased pCO_2 of the river water. In addition, air temperatures are lower in the upper basins. For example, at Lhasa, Tibet, which is near the Yarlung Tsangpo, the mean annual air temperature was 9.9 °C in 2012, whereas at Dhaka, Bangladesh, it was 26.7 °C [National Oceanic and Atmospheric Administration, 2013]. Moreover, based on the solubility of CO_2 gas, which is inversely proportional to the temperature, higher water temperature causes the pCO_2 of water to be higher, assuming constant total alkalinity. For example, in the Yarlung Tsangpo catchment, the average water temperature is 13 °C in fall, and the calculated pCO_2 is 273 µatm [Huang et al., 2011]. In contrast, in Bangladesh, the temperature measured during the same season was approximately 30 °C, and the calculated pCO_2 of the lower Brahmaputra was approximately 1000 µatm. An increase in the temperature of the Yarlung Tsangpo to 30 °C would, assuming carbonate equilibrium, increase the pCO_2 to 504 µatm. However, this value is still small compared to that of the lower streams. The increase of temperature from upper to lower streams can account for only about 30 % of the observed pCO_2 increase., Increased air temperatures, however, also promote biological activity in the soil and, consequently, soil respiration [Hope et al., 2004]. Therefore, higher temperatures in the lowlands cannot by themselves explain the entire downstream increase in pCO_2. Other factors, such as soil respiration, must be taken into account.

Because few previous studies have been focused on the Ganges and Brahmaputra rivers between 750 and 2000 km from the river mouth, it is difficult to pinpoint where the pCO_2 values start increasing along the river. A larger portion (approximately 50 %) of the Brahmaputra drains highland

areas (over 2000 m), where the water is affected by chemical weathering and glacier dissolution in the upper stream [Immerzeel et al., 2010]. Therefore, compared to the Ganges, the pCO_2 levels of the Brahmaputra River may be small, even in the middle streams.

In the high Himalayas, abundant CO_2 degassing ($> 1.3 \times 10^{10}$ mol yr^{-1}) from hot springs has also been observed [Evans et al., 2004; 2008]. However, I considered this degassing to have a minor impact on the riverine pCO_2 for the following reasons. Firstly, calculated pCO_2 values are low for the upper and middle reaches of the Yarlung Tsangpo River [Huang et al., 2011], which, among the sampling stations considered in the previously cited studies, are closest to the hot springs. Therefore, CO_2 derived from the hot springs is probably quickly released to the atmosphere before dissolving and flowing into the Yarlung Tsangpo River. Secondly, the hot spring water exhibits extremely high concentrations of Na^+, Cl^-, and SO_4^{2-}. However, concentrations of these ions are low in the lower streams, indicating that major ion chemistry in the lower streams, including the carbonate system, is not greatly affected by the hot spring water input to the upper streams.

2.4.3. Seasonal variations of carbonate system

In the river water samples, the total alkalinity and the concentrations of most dissolved major ions were lower in the rainy season than in the dry season. In the Ganges River, however, pCO_2 was higher in the rainy season than in the dry season, whereas in the Brahmaputra River, pCO_2 was similar in both seasons (Table 2-1, Figure 2-5).

One of the simplest possible explanations for seasonal variation in the carbonate system is the addition of rainwater to river water. The immense increase in precipitation during the rainy season should considerably dilute river water. For example, the water discharge of the Ganges during the rainy season is more than 10 times greater than the discharge during the dry season [Webster et al., 2010]. To quantify the effect of rainwater on the water quality of the rivers, a simple calculation was performed. I assumed that the mean total alkalinity and pCO_2 values in the Ganges in the dry season (water temperature: 18 °C, DIC: 2895 µmol kg^{-1}, total alkalinity: 2909 µmol kg^{-1}) were typical and that during the rainy season, the river water was locally diluted by rainwater at a dilution ratio of 1:9. For the water quality of the diluting rainwater, I used the HCO_3^- concentration reported by Chatterjee and Singh [2012] for Ahmedabad, India (approximately 50 µmol kg^{-1} in August 2008), a water temperature of 25 °C, and a pCO_2 level of 395 µatm (under the assumption that the pCO_2 of rainwater is at equilibrium with atmospheric pCO_2). Based on these assumptions, I calculated the DIC and total

alkalinity of the rainwater to be 63 and 50 µmol kg^{-1}, respectively. Using these values and CO_2calc, I calculated that the diluted river water would have DIC = 347 µmol kg^{-1}, total alkalinity = 336 µmol kg^{-1}, and pCO_2 = 361 µatm. These values are much lower than the actual values observed during the rainy season. Therefore, these results suggest that, in addition to precipitation, there must be another, completely different source contributing water to the Ganges during the rainy season.

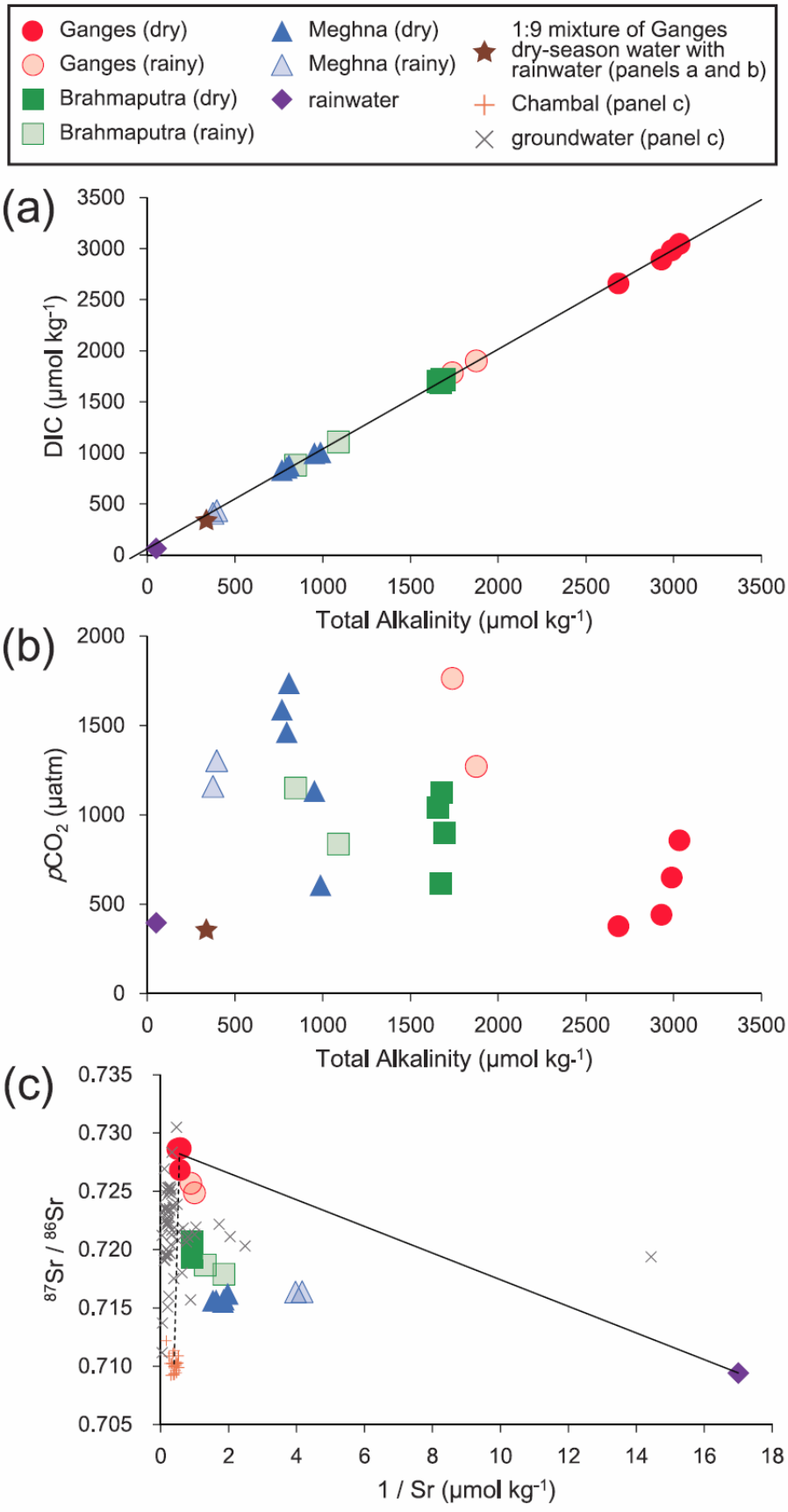

Figure 2-5. (Continued on the following page)

Figure 2-5. (Preceding page)

Variations in (a) DIC (μmol kg^{-1}), (b) pCO_2 (μatm) relative to total alkalinity (μmol kg^{-1}), and (c) the strontium isotope ratio ($^{87}Sr/^{86}Sr$) in relation to 1/Sr. Data from the Ganges, Brahmaputra, and Meghna River water samples are shown by red circles, green squares, and blue triangles, respectively. Dark colors indicate data collected in the dry season, and light colors indicate data collected in the rainy season. Data for rainwater (purple diamonds), (a) 1:9 mixture of the Ganges River water in the dry season and rainwater (brown stars), Chambal River water (orange plus signs), and groundwater in Bangladesh (gray cross signs) are also shown. The solid line in panel (a) represents the slope of total alkalinity and DIC in my samples ($r^2 = 0.99$). The lines in panel (c) represents two component mixtures; the Ganges in the dry season and either rainwater (solid line) or Chambal River water (dashed line), respectively.

Another possible explanation for the observed seasonal variations in the carbonate system is a decrease in pH during the rainy season caused by the addition of acid from soil organic matter to the water, which would increase pCO_2. For example, in Kushiro Mire, Japan, the concentration of humic acid is high, and the pH is relatively low, at 5.1-6.4 [Nagahora et al., 2002; Terai et al., 2002; Senga et al., 2010]. The annual total organic carbon flux in the Ganges and Brahmaputra River system has been calculated as 0.65×10^{12} mol C yr^{-1} [Aucour et al., 2006]. However, in this study, I found very low DOC concentrations (versus DOC concentrations of 800-4000 μmol kg^{-1} in Kushiro Mire) and much higher concentrations of inorganic carbon. These results suggest that acidification by organic acid is unlikely to be a dominant process in the river waters in Bangladesh.

Instead, I suggest that seasonal increases in subsurface flow, influenced by soil respiration, can plausibly explain the seasonal changes observed in the river water. It is expected that groundwater base flow is characterized by high total alkalinity and low pCO_2, owing to its long residence time and origin, mainly in the high Himalayas, where chemical weathering activity is high. In contrast, the subsurface flow originates in the lowlands of Bangladesh, where the soils are well developed, the respiratory activity of soil microorganisms is high, and the residence time of the subsurface flow water is short. The high soil respiratory activity would raise DOC concentrations in the subsurface flow, causing it to have low total alkalinity and high pCO_2.

Because a large area of Bangladesh is typically flooded during the rainy season [Mirza,

2002], the river water is diluted not only by rainwater but also by subsurface flow that has passed through lowland alluvium and soil. I also observed large variations in pCO_2 within the same rivers, which may be attributed to this local dilution of the river water. In addition, in Bangladesh, the rainy season occurs in the summer, when both temperatures and humidity are high, so soil respiration is increased [Hope et al., 2004]. Together, these factors can account for the increased pCO_2 in the rivers in the rainy season. In other words, this extremely high pCO_2 in the rainy season can be explained as a relocation of terrestrial respiration (for details, see Section 2.4.4.).

Observed seasonal changes in the strontium isotope ratios in the river water support this proposed scenario. In the dry season, the strontium isotope ratios in the Ganges and Brahmaputra rivers were high, and 1/Sr was relatively low (Figure 2-5). However, the rainy season data do not fall on the mixing line between the two end members represented by the dry season river water and local rainwater, in particular in the Ganges. This is consistent with the proposal that river water properties in the rainy season cannot be explained by simple dilution of the dry season flow by precipitation. Instead, the results suggest that there must be a third source or end member, which, I suggest, is subsurface flow. In Bangladesh, the lower reaches of the Ganges and the Brahmaputra rivers flow through lowlands composed primarily of Himalayan alluvium transported by the two rivers. However, not all the alluvium is from Himalayan sources; some is from non-Himalayan areas, including the Vindhya Range and the Deccan Plateau of southwestern India and the Tripura Fold Belt of eastern Bangladesh [e.g., Sarin et al., 1989; Kuehl et al., 2005]. As a representative non-Himalayan sample, I used strontium data for the Chambal River, which is a tributary of the Ganges in southern India that originates in the Deccan Trap basalts and Vindhyan sediments [Rengarajan et al., 2009]. As seen in Figure 2-5, strontium isotope ratios in the Chambal River are fairly low (0.7092-0.7122, average 0.7102), and mixing of three end members (dry season flow, rainwater, and Chambal River water) can reasonably explain the rainy season strontium data obtained in my study. In addition, although I did not collect samples of subsurface flow or floodplain waters in non-Himalayan regions, which should be investigated in the near future, these can be estimated using groundwater data for Bangladesh presented by Paul et al. [2010]. In Bangladesh, the groundwater level is much lower than the river bed [Kuehl et al., 2005]. Therefore, the river water and subsurface water can flow downward to the groundwater flow. According to Paul et al. [2010], the groundwater exhibits Sr isotope ratios and variations (0.7111-0.7305, average 0.7218) that are higher than those of the Chambal River water but still lower than those of the Ganges River water in the dry season. Therefore, in Bangladesh, the

groundwater (and perhaps subsurface flow water) should be affected by the geology of these non-Himalayan regions with low strontium isotope ratios, as well as by that of Himalayan regions, and should contribute to the seasonal variation in pCO_2 in the Ganges and Brahmaputra. When the seasonal variation of Sr isotope ratios and 1/Sr of the Ganges are compared to those of the Brahmaputra, the Ganges River water can be largely affected by the groundwater, while the contribution of rainwater can be larger in the Brahmaputra.

On the other hand, measured strontium isotope ratios in the Meghna River were much lower than those in the Ganges and Brahmaputra rivers, and they exhibited little seasonal variation. The Meghna basin lies entirely within the region of Himalayan alluvium, which may prevent it from being affected by the seasonal water cycle. Tripathy et al. [2010] attributed lower strontium isotope ratios in the upper Ganges basin during the rainy season to a larger area of active weathering in the river basin, increased subsurface flow, a higher dissolution rate of carbonates compared with that of silicates, and a shorter water-rock interaction time.

The impact of lowland waters to the carbonate system in the mainstream waters is also reported in other rivers around the world. Richey et al. [2002] focused on the Amazon River and reported increased pCO_2 and CO_2 degassing fluxes when the river basin was flooded. They suggested that the dissolved CO_2 originates from organic matter transported from upland and flooded forests. Yao et al. [2007] also reported positive relationships between pCO_2 and river water discharge in the Xijiang River, suggesting active soil respiration in the rainy season. In addition, Galy and Eglinton [2011] investigated the sources of terrestrial biospheric carbon in the Ganges and Brahmaputra River basins, by measuring its ^{14}C age. The calendar age of the carbon was old in the Himalayan range (460 to 17000 yr) and young in the floodplain (1600 to 4800 yr). Biospheric carbon in the lowland is more labile, suggesting large CO_2 evasion in this area. They also reported that more refractory organic carbon can be decomposed and released to the atmosphere in the rainy season.

It is also noted that dissolved CO_2 in the river waters can originate from both direct CO_2 input from the soil and organic carbon decomposition in the river waters. However, it is very difficult to distinguish between the two. More detailed studies on not only dissolved CO_2 but also organic carbon in the river waters are needed.

In situ photosynthesis can also affect river water properties. Manaka et al. [2013] have shown that active photosynthesis decreases pCO_2 in some lake waters with long residence times. For example, in Lake Kasumigaura, a eutrophic lake in Japan, high levels of photosynthesis lead to high

CO_2 and nutrient consumption and increased organic matter in the lake water. As a result, pCO_2 is lower in the lake water than in the atmosphere (for details, see Appendix-1). I measured nutrient (nitrate and phosphate) concentrations in river waters in Bangladesh during both the dry and rainy seasons, but I did not find a clear relationship between the nutrient concentrations and pCO_2. Compared with nutrient concentrations in other large rivers around the world, the concentrations I measured were moderate to low, and they showed rather large spatial and seasonal variations [Turner et al., 2003] (Table 2-1). Typically, nutrient concentrations depend on local biological activity, nutrient inputs, and the turbulence of the water. In the rainy season in particular, turbidity in the studied rivers is high [Lakshminarayana, 1965], and suspended particles block sunlight and depress photosynthesis. Furthermore, high flow velocities in rivers tend to reduce in situ biological activity [Yao et al., 2007]. As a result, primary production is reduced in turbid river water, and nutrient concentrations play only minor roles in controlling pCO_2 values in the large rivers of Bangladesh.

2.4.4. Potential CO_2 release from the water to the atmosphere

I compared the pCO_2 values of the Ganges, Brahmaputra, and Meghna River waters with those of not only the Ayeyarwady, Mekong, and Chao Phraya rivers, but also other large river systems. Although I could not calculate annual mean pCO_2 values due to a lack of data and because the data were obtained mainly in dry seasons, the results suggest that pCO_2 values in the river waters evaluated in this study are relatively low (Table 1-1).

With regard to seasonal variations, the potential CO_2 flux from the Ganges and Brahmaputra rivers to the atmosphere should be much larger in the rainy season than in the dry season because the pCO_2 of the rivers is enhanced by the addition of subsurface flow water during this time, when high temperatures increase soil respiration activity. In addition, in the rainy season, the maximum discharge of the Ganges and Brahmaputra rivers is more than three times greater than the mean annual discharge, which leads to an increase in the surface area of the river, where CO_2 exchange between the atmosphere and the water occurs [Webster et al., 2010]. Furthermore, most sandbars that emerge during the dry season are inundated during the rainy season. The surface area of the river reaches a maximum during the rainy season. Normal rainy season flooding inundates 20.5 % (31,000 km^2) of the total area of Bangladesh, whereas catastrophic flooding inundates 34.0-38.5 % (50,000-57,000 km^2) [Mirza, 2002]. Unfortunately, I have no pCO_2 data from floodwaters, but it is likely that these are also mixed with subsurface flow water with high pCO_2. Therefore, the total amount of CO_2 released to the atmosphere

from the terrestrial waters (both river water and floodwaters) in Bangladesh should be much larger in the rainy season than in the dry season.

Approximate calculations can be made of the actual CO_2 fluxes from the river water to the atmosphere, based on the concentration difference of CO_2 between the overlying air and the bulk of the water, and the gas exchange velocity between the water and the atmosphere (k) [Jonsson et al., 2007; Yao et al., 2007; Alin et al., 2011; Raymond et al., 2013]. Alin et al. [2011] measured k_{600} values (temperature-normalized gas transfer velocity values in the Amazon and Mekong rivers, and reported that the influence of wind speed or water current velocity on these values can vary depending on the river size. For large rivers (channels > 100 m wide), they reported k_{600} values of 14.7 ± 8.6 (cm h^{-1}). The k value at a temperature of t (k_T) can be calculated using the following equation:

$$k_{600} = k_T (600 / Sc_T)^{-0.5} \quad (2\text{-}1)$$

$$Sc_T = 1911.1 - 118.11\ T + 3.4527\ T^2 - 0.04132\ T^3 \quad (2\text{-}2)$$

Sc_T represents the Schmidt number for temperature T, and the Schmidt number for 20 °C in freshwater is 600. Assuming an average temperature of the Ganges and Brahmaputra river water of 22 °C, the calculated k_T value is 15.4 ± 9.0 cm h^{-1} (1350 ± 790 m yr^{-1}). CO_2 degassing flux rate (F, unit: mol m^{-2} yr^{-1}) from surface river water to the atmosphere can be simply calculated as follows:

$$F = k_t (C_{air} - C_{water}) \quad (2\text{-}3)$$

C_{air} and C_{water} represent the concentration of CO_2 in the atmosphere and waters (unit: mol m^{-3}). In order to convert pCO_2 (unit: μatm) into a unit of mol m^{-3}, equation 2-3 is used and converted as follows:

$$F = k_t K (pCO_{2air} - pCO_{2water}) \times 10^{-6} \quad (2\text{-}4)$$

K represents Henry's law constants (unit: mol L^{-1} atm^{-1}). For CO_2 gas at a temperature of 25 °C, this value is 3.4×10^{-2} mol L^{-1} atm^{-1} (34 mol m^{-1} atm^{-1}). pCO_{2air} is assumed to be 395 μatm. When pCO_{2water} is 500 and 1000 μatm, the calculated degassing flux is 28 ± 16 mol m^{-2} yr^{-1} and 4.8 ± 2.8 mol m^{-2} yr^{-1}, respectively.

In order to calculate total CO_2 flux from the Ganges and Brahmaputra River waters to the atmosphere, the water surface area of each river must be estimated. Using Google Earth™, I estimated the river width as follows. The water surface area 0 – 140 km from the river mouth is defined as the lower Meghna. For the Ganges, the river width for the following distances from the river mouth: 140-250 km, 250-500 km, 500-1000 km, and 1000-2500 km, is 8 km, 5 km, 3 km, and 1 km, respectively. For the Brahmaputra, the river width for the following distances from the river mouth: 250-700 km,

700-1200 km, 1200-1300 km, and 1300-2800 km, is 8 km, 5 km, 1 km, and 0.3 km, respectively. Compared to the Ganges, the river width of the Brahmaputra shows a larger decrease, even in the middle streams, also observed in the topographic profiles in Figure 2-4. I also hypothesized that the annual average river water pCO_2 is 1000 μatm where the distance from the river mouth is less than 1000 km, and 500 μatm where the distance is greater than 1000 km. For details, see Table 2-3.

As a result, calculated total CO_2 fluxes from the Ganges and Brahmaputra River waters were 0.45-1.7 × 10^{11} mol yr^{-1} (0.54-2.1 TgC yr^{-1}) and 0.62-2.4 × 10^{11} mol yr^{-1} (0.74-2.8 TgC yr^{-1}), respectively. These values are small compared to other major rivers in the world: F values in the Amazon, Mekong, and Mississippi rivers were calculated to be 3.9 × 10^{13} mol yr^{-1} [Richey et al., 2002], 5.6 × 10^{11} mol yr^{-1} [Li et al., 2013], and 8.3 × 10^{11} mol yr^{-1} [Dubois et al., 2010], respectively. However as the total CO_2 fluxes from global river waters are 0.23-1.8 PgC yr^{-1}, as shown in Table 1-2, these two rivers together account for as much as 0.07-2 % of total CO_2 fluxes.

This calculation may include some errors, for example, k_T values may vary between the upper and lower streams. Although I assumed that K values were constant, they show a large variation with temperature. In addition, the river width should be larger in the rainy seasons. For more accurate calculation, more river water samples and geographical datasets of this area are needed.

It should also be noted that this large release of CO_2 can be attributed to terrestrial respiration. CO_2 released from soils to the atmosphere during the dry season may only be released via the waters to the atmosphere during the rainy season. In other words, during the rainy season, terrestrial waters may function as efficient transporters of CO_2 from terrestrial ecosystems to the atmosphere. To clarify the role of ecosystems in this area on the short-term carbon cycle, it would be necessary to measure pCO_2 in more samples from both water and soil during both the dry and rainy seasons.

Ganges River

Distance from the river mouth (km)	River Width (km)	pCO_2 (μatm)
0-140	(Lower Meghna)	
140-250	8	1000
250-500	5	1000
500-1000	3	1000
1000-2500	1	500

Brahmaputra River

Distance from the river mouth (km)	River Width (km)	pCO_2 (μatm)
0-140	(Lower Meghna)	
140-250	(Ganges River)	
250-700	8	1000
700-1000	5	1000
1000-1200	5	500
1200-1300	1	500
1300-2800	0.3	500

Table 2-3.

Assumptions of river width and pCO_2 values for the Ganges and Brahmaputra River.

2.5. Conclusions

To understand the potential importance of CO_2 exchange between river water and the atmosphere over short timescales, I investigated three major rivers in Bangladesh.

(1) The Ganges and Brahmaputra rivers originate in the upper Himalayas, where carbonate weathering is active. However, unexpectedly high pCO_2 values were observed, particularly in the lower streams. This finding suggests that abundant CO_2 can be released from the river water to the atmosphere.

(2) Along the lower reaches of these rivers, soil development and higher temperatures promote soil respiration, which can supply additional CO_2 to the river water.

(3) Seasonal variations in groundwater flow may largely control the chemical composition of the river water. During the dry season, deep groundwater flow, which has a longer residence time underground, contributes relatively more to the river water, resulting in lower pCO_2 values. In contrast, subsurface flow water in the lowlands, which has a shorter underground residence time, is strongly affected by soil respiration. During the rainy season, this subsurface flow plays an important role in the river water system as an efficient transporter of CO_2 from terrestrial ecosystems to the atmosphere, in particular in the Ganges basin.

(4) Total CO_2 fluxes from the Ganges and Brahmaputra River waters were calculated as 0.45-1.7 × 10^{11} mol yr^{-1} and 0.62-2.4 × 10^{11} mol yr^{-1}, respectively. Although these values are low compared to those in other large river systems, they may be important for the short-term carbon cycle. More detailed spatial and seasonal investigation is required.

Appendix-1: A brief review of Manaka et al. [2013]

Manaka et al. [2013] conducted sampling surveys in two types of lake in Japan: eutrophic lakes (e.g., Lake Kasumigaura) and an acidotrophic lake (Lake Inawashiro). They reported significant differences between pCO_2 and nutrient concentration values in the eutrophic lake and those of its input river. Active photosynthesis occurred in the lake with a relatively longer residence time, resulting in high CO_2 and nutrient consumption. In contrast, Lake Inawashiro was affected by volcanic activity in the upper streams, resulting in a lower pH. When the influence of volcanic activity was stronger in the past, precipitation of volcanic-derived iron and aluminum removed nutrients by co-precipitation in the lake. However, during the last three decades, volcanic activity has weakened and the lake water has become alkalized. The study used a simple mixing model and proposed that recent active photosynthesis can contribute greatly to this alkalization. In general, they suggested that nutrients and photosynthesis are potentially important for the carbonate chemistry of terrestrial waters.

Appendix-2: Photographs of sampling surveys

Here I show photographs taken during sampling surveys in Bangladesh, Myanmar, and Thailand.

Figure A2-1.

Photographs of (a) the Ganges at Station G-3, Bangladesh, (b) the Brahmaputra at Station B-3, Bangladesh, (c) the Ayeyarwady at Station A-3, Myanmar, and (d) the Mekong at Station Me-1, Thailand.

Chapter 3. Chemical weathering and long-term CO_2 consumption in the Himalayan rivers reconstructed from major ion chemistry

3.1. Introduction

Terrestrial rivers play an important role in the global carbon cycle, which affects the Earth's surface environment [Sarmiento and Gruber, 2006]. In Chapter 2, I discussed soil respiration and CO_2 evasion from river waters to the atmosphere. Chemical weathering is another important geochemical processes for the global carbon cycle. This weathering consumes atmospheric CO_2 and generates HCO_3^-. The HCO_3^- is transported to the ocean by rivers and released to the atmosphere in the form of CO_2 through oceanic carbonate mineralization processes. On a modern timescale, the amount of CO_2 released from river waters (0.23-1.80 PgC yr^{-1}, Table 1-2) is larger than that consumed by chemical weathering (0.3 PgC yr^{-1}, as discussed by IPCC [2013] and Figure 1-1), highlighting the potential importance of CO_2 evasion on this timescale. On the other hand, on a geological timescale, most carbon on the Earth's surface consumed by biota in the basins is decomposed and returned back to the atmosphere. On this timescale, biological activity cannot act as a net sink of carbon in the global carbon cycle. In contrast, as shown in equation 1-3 and 1-4, the molar ratio of CO_2 consumed by silicate and carbonate weathering is different. Considering this type of weathering and the subsequent carbon transfer and oceanic carbonate mineralization, only silicate weathering contributes to a net reduction in atmospheric CO_2 concentrations on a geological timescale. This process is also closely linked to past climate conditions and temperatures [Berner et al., 1983; Brady, 1991]. Therefore, to understand the Earth's surface environment, it is quite essential to differentiate between silicate and carbonate weathering in the river basins and uncover the long-term role of rivers in the carbon cycle.

Himalayan rivers are among the world's largest and play an important role in both the water and carbon cycles. With regard to the long-term carbon cycle, active weathering occurs as a result of the ongoing uplift of the Himalayan-Tibetan Plateau and the heavy rains associated with the Asian monsoon [Molnar et al., 1993; Yin and Harrison, 2000]. Raymo et al. [1988] and Raymo [1991] have suggested that the global cooling during the Eocene was triggered primarily by active chemical

weathering of the newly uplifted Himalaya Mountains.

In this study, I focus on Himalayan rivers, in particular the Ayeyarwady, Mekong, and Chao Phraya rivers (the Chao Phraya is a local non-Himalayan river in Thailand) (Figure 1-4 and 2-2). Previous studies have reported that the Ayeyarwady is dominated by silicate weathering to an unusual extent, the result being that a large consumption of CO_2 in this area plays an important, long-term role in both the Himalayan and global carbon cycles [Gaillardet et al., 1999; Sarin, 2001]. However, chemical datasets of this river are old and limited, a reflection of political and economic conditions in the river basin. Knowledge of the carbonate system of this river is the last piece of information needed to understand the carbon cycle in the entire Himalayan region. It is therefore important to reevaluate this river's present chemical composition and the long-term impact of all Himalayan watersheds on the carbon cycle. This study therefore involves a sampling survey of these three rivers. I measure the concentrations of major ions to quantify chemical weathering and CO_2 consumption in the river basin. My goal is to use the results of these chemical analyses to improve understanding of the effects of these rivers and the Himalaya Mountains in the global carbon cycle on a long timescale.

3.2. Analytical procedures

The sampling protocol is the same as that detailed in Section 2.2 of this thesis.

3.3. Results

The results related to carbonate systems in all Himalayan rivers have already been presented in Section 2.3 and Table 2-1. Here I briefly report the major ion concentration results. In most samples the concentrations of Ca^{2+} and HCO_3^- were high (Table 2-1 and Figure 3-1): 621-1105 μmol kg^{-1} and 1725-2985 μmol kg^{-1}, respectively, in the Ganges; 353-671 μmol kg^{-1} and 841-1674 μmol kg^{-1}, respectively, in the Brahmaputra; 106-277 μmol kg^{-1} and 373-977 μmol kg^{-1}, respectively, in the Mekong; 146-185 μmol kg^{-1} and 476-718 μmol kg^{-1}, respectively, in the Ayeyarwady; 657 μmol kg^{-1} and 1584 μmol kg^{-1}, respectively, in the Mekong (Me-1); and 407-1120 μmol kg^{-1} and 1264-2848 μmol kg^{-1}, respectively, in the Chao Phraya River systems. In the Me-2 and Me-3 samples, I observed extremely high concentrations of Na^+ (2621-3421 μmol kg^{-1}) and Cl^- (1763-1943 μmol kg^{-1}). For more information on the Ganges, Brahmaputra, and Meghna rivers, see Sections 2.3 and 4.3.

3.4. Discussion

In this section, I discuss chemical properties and chemical weathering in the Ayeyarwady, Mekong, and Chao Phraya rivers. A detailed discussion about the Ganges, Brahmaputra, and Meghna river waters is in Appendix-3.

3.4.1. Chemical characteristics of Himalayan rivers: an overview

A trilinear diagram of major ion compositions demonstrated that most samples taken from these rivers had similar chemical characteristics (Figure 3-1). The water quality of the three rivers can be characterized as calcium bicarbonate. Two exceptions were the Chi River and Mun River samples (Me-2 and Me-3), which were extraordinarily rich in Na^+ and Cl^-. These high Na^+ and Cl^- concentrations have been attributed to local halite dissolution [Shrestha, 2006; Wongpokhom et al., 2008]. However, the lower reach of the Mekong River, downstream of the confluence with these two tributaries, still shows calcium bicarbonate-type characteristics [Li et al., 2014]. Moreover, a comparative analysis with the Ganges, Brahmaputra, and Meghna rivers in Bangladesh suggests that there is a similar trend in the chemical characteristics of river waters throughout the Southeast/South Asian regions. Considering that the balance of cations and anions derives mainly from chemical weathering of continental rocks, the balance is unlikely to undergo major changes unless there is intermixing of waters from drainage basins with different lithologies. Therefore, the cation and anion balances of the Southeast/South Asian rivers presumably reflect the fact that they originate in the same region, the Tibetan Plateau, and the general features of their chemistry have been maintained downstream.

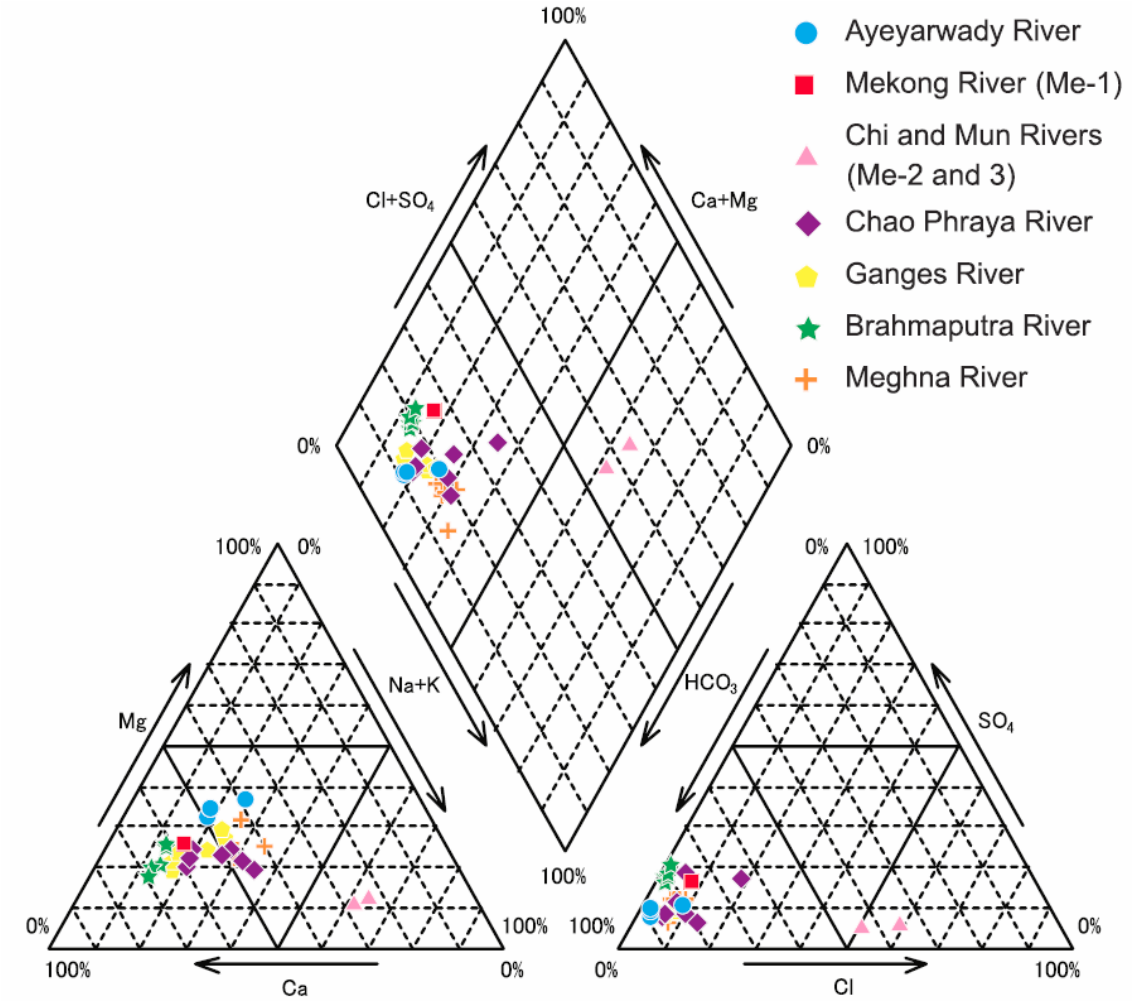

Figure 3-1.

Trilinear diagram of the major ion composition of the river water samples.

3.4.2. Chemical weathering rates of silicate and carbonate

A closer examination of major ion concentrations revealed some factors that distinguished the three rivers (Table 2-1 and Figure 3-1). To determine the factors controlling the intensity of chemical weathering, I plotted Na-normalized HCO_3^- concentrations relative to Na-normalized Ca^{2+} concentrations (Figure 3-2). As first pointed out by Gaillardet et al. [1999], this plot illustrates the mixing between the two main water types: carbonate and silicate drained, given the end-members of silicate, carbonate, and evaporite weathering. It is noted that the end-members were estimated using data on small rivers draining one single lithology. This figure indicates that the Chi/Mun (Me-2 and Me-3) and Brahmaputra River samples plot relatively close to the silicate/evaporate and carbonate

end-members, respectively. Interestingly, my data for the Ayeyarwady plot closer to the carbonate end-member than those of Gaillardet et al. [1999]. Possible explanations for this difference might be spatial variations in water composition, because actual river data for the Ayeyarwady are still scarce. For example, because the geological characteristics of Myanmar differ longitudinally (Figure 1-6) [Bender, 1983; Wandrey and Law, 1997; Hadden, 2008], the chemical composition of Ayeyarwady River water should differ between the mainstream and tributaries (e.g., the Chindwin and Myitnge rivers). However, I took water samples only from the middle to lower reaches of the river, which are representative of the mainstream water that flows into the ocean.

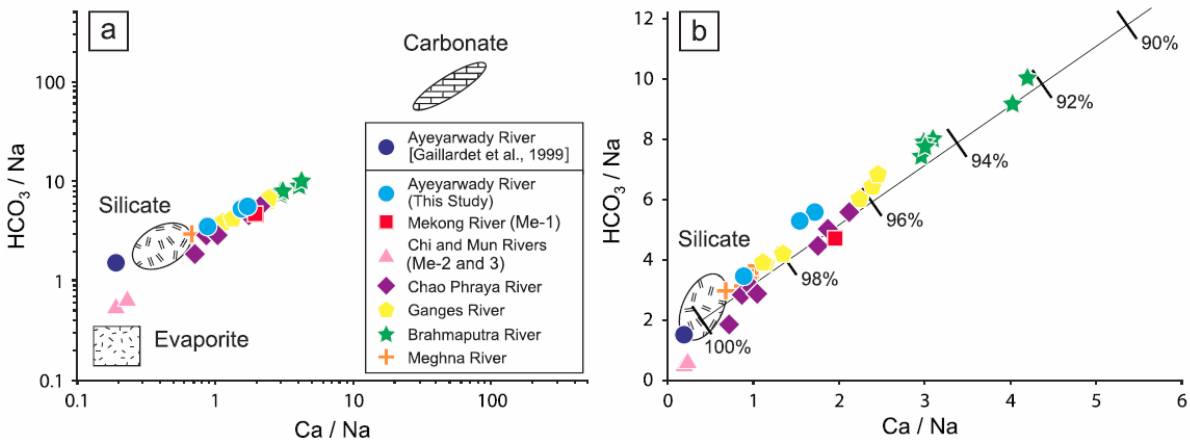

Figure 3-2.

Variations of Na-normalized HCO_3^- relative to Na-normalized Ca^{2+} on (a) logarithmic and (b) linear scales. The datasets of the Ayeyarwady River are based on both this study and Gaillardet et al. [1999]. The end-member reservoirs (silicate, carbonate, and evaporite) were estimated by Gaillardet et al. [1999] based on small rivers draining each lithology. Figure 3-2 (b) also shows a mixing line between silicate and carbonate, assuming that the silicate end-member is HCO_3/Na = 2 and Ca/Na = 0.4, and the carbonate end-member is HCO_3/Na = 100 and Ca/Na = 50, respectively.

Determining the relative contributions of silicate and carbonate to chemical weathering is important for estimating CO_2 consumption by rivers. To determine the ratio of silicate to carbonate weathering, I calculated the contribution of silicate to the total cationic charge balance measured in the river water samples, in other words, total alkalinity budgets (for details, see Section 1.4). Na^+ in river water is mainly derived from halite dissolution and silicate weathering, whereas K^+ is mostly derived from silicate weathering [Wu et al., 2008]. Therefore, the contribution of silicate to these cations can be calculated with the following equation, proposed by Galy and France-Lanord [1999]:

$$[Na^+]_{sil} \approx [Na^+]_{riv} - [Cl^-]_{riv} \quad (3\text{-}1)$$

$$[K^+]_{sil} \approx [K^+]_{riv} \quad (3\text{-}2)$$

where $[Na^+]_{sil}$ and $[K^+]_{sil}$ are metrics of the contributions of silicate weathering to Na^+ and K^+, respectively, in the river water and $[Na^+]_{riv}$, $[K^+]_{riv}$, and $[Cl^-]_{riv}$ are the molar concentrations of the ions measured in the river water samples. An implicit assumption here is that the Na derived from carbonate weathering is minor [Dalai et al., 2002]. The contribution of $[Na^+]_{sil}$ to the total cationic charge balance was 7-19 %. The average contribution was 13 % in the Ayeyarwady and Chao Phraya and 7 % in the Mekong (only Me-1) (Table 3-1). The Ca^{2+} in river water is derived mainly from carbonates, evaporates, and silicates, and Mg^{2+} is derived mainly from carbonates and silicates [Wu et al., 2008]. According to Galy and France-Lanord [1999], the silicates associated with Mg consist mainly of biotite, which does not contain Na, and they found a good, positive correlation between riverine Mg^{2+} and K^+ concentrations in Himalayan rivers draining only silicate formations. Therefore, silicate-derived Ca^{2+} and Mg^{2+} can be expressed by the following two equations:

$$[Ca^{2+}]_{sil} \approx [Na^+]_{sil} \times (Ca / Na)_{sil\text{-}rock} \quad (3\text{-}3)$$

$$[Mg^{2+}]_{sil} \approx [K^+]_{sil} \times (Mg / K)_{sil\text{-}rock} \quad (3\text{-}4)$$

where $[Ca^{2+}]_{sil}$ and $[Mg^{2+}]_{sil}$ are metrics of the cations derived from silicate weathering and $(Ca / Na)_{sil\text{-}rock}$ and $(Mg / K)_{sil\text{-}rock}$ are the molar ratios of the cations released into the river water as a result of congruent weathering of silicate rocks in the river basin. Because I did not conduct sediment sampling, I relied on Galy and France-Lanord's [1999] estimation of $(Ca/Na)_{sil\text{-}rock}$ and $(Mg/K)_{sil\text{-}rock}$: 0.18-0.3 and 0.3-0.7, respectively (for details, see Section 1.4). These ratios are based on relatively high-silicate and relatively low-silicate Himalayan rock, respectively. The minimum values of $[Ca^{2+}]_{sil}$ and $[Mg^{2+}]_{sil}$ in Table 3-1 ($[Ca^{2+}]_{sil\ (min)}$ and $[Mg^{2+}]_{sil\ (min)}$) were calculated based on the minimum values of $(Ca/Na)_{sil\text{-}rock}$ and $(Mg/K)_{sil\text{-}rock}$, respectively, and vice versa for the maximum values. Given these ratios, the total contribution of silicate weathering to the cationic charge balance (total alkalinity

budgets) can be calculated as follows [Dalai et al., 2002],

$$CAT_{sil} = ([Na^+]_{sil} + [K^+]_{sil} + 2 \times [Ca^{2+}]_{sil} + 2 \times [Mg^{2+}]_{sil}) / ([Na^+]_{riv} + [K^+]_{riv} + 2 \times [Ca^{2+}]_{riv} + 2 \times [Mg^{2+}]_{riv}) \quad (3\text{-}5)$$

where CAT_{sil} represents the contribution of the cationic charge derived from silicate weathering to the total alkalinity budgets. The concentrations of Ca^{2+} and Mg^{2+} are both multiplied by 2 because they are divalent. In this calculation, I took account of uncertainties in major ion measurements (less than ± 3 %). In addition, because the $(Ca/Na)_{sil\text{-}rock}$ and $(Mg/K)_{sil\text{-}rock}$ ratios are associated with some uncertainty, my result has a rather large range, but a relative comparison is nevertheless possible. Results showed that the contributions of silicates were larger in the Ayeyarwady and Chao Phraya rivers (21-32 % and 17-41 %, respectively) than in the Mekong River (Me-1, 12-19 %) (Table 3-1).

Table 3-1.

Calculated concentrations of major ions and total cations derived from silicate (sil) and carbonate (carb) weathering.

Locality	Total Cationic Charge Balance	$[Na^+]_{sil}$	$[K^+]_{sil}$	$[Ca^{2+}]_{sil\ (min)}$	$[Mg^{2+}]_{sil\ (min)}$	$[Ca^{2+}]_{sil\ (max)}$	$[Mg^{2+}]_{sil\ (max)}$	CAT_{sil}	CAT_{carb}
	($\mu mol\ kg^{-1}$)							(%)	(%)
Ayeyarwady River system									
A-1	598	70	24	13	7	21	17	21-31	67-77
A-2	812	106	24	19	7	32	17	21-30	68-77
A-3	807	106	24	19	7	32	17	21-30	68-77
A-4	968	126	33	23	10	38	23	21-32	61-70
Mekong River									
Me-1	2286	170	47	31	14	51	33	12-19	73-83
Me-2 (Chi)	4482	556	131	100	39	167	92	17-33	27-33
Me-3 (Mun)	5754	139	260	25	78	42	182	5-21	26-36
Chao Phraya River									
C-1 (Ping)	2321	189	140	34	42	57	98	19-30	64-77
C-2 (Wang)	3996	405	125	73	37	122	87	17-26	68-78
C-3 (Ping)	2208	241	97	43	29	72	68	20-30	65-76
C-4 (Yom)	3292	625	84	112	25	187	59	28-39	58-65
C-5 (Nan)	1704	186	65	34	19	56	45	19-30	58-68
C-6	1856	325	78	58	23	97	54	28-41	52-60
C-7	2709	407	91	73	27	122	63	23-36	51-59

Given this information, I can also calculate the cationic charge contribution from carbonate weathering under the assumption that Ca^{2+} and Mg^{2+} are derived only from silicate and carbonate weathering. The equation is shown below:

$$CAT_{carb} = \{2 \times ([Ca^{2+}]_{riv} - [Ca^{2+}]_{sil}) + 2 \times ([Mg^{2+}]_{riv} - [Mg^{2+}]_{sil})\} / ([Na^{+}]_{riv} + [K^{+}]_{riv} + 2 \times [Ca^{2+}]_{riv} + 2 \times [Mg^{2+}]_{riv}) \quad (3\text{-}6)$$

where CAT_{carb} represents the fraction of all the cationic charge derived from carbonate weathering. Results showed that 61-77 %, 73-83 %, and 51-78 % of the total alkalinity budgets in the Ayeyarwady, Mekong (Me-1), and Chao Phraya rivers, respectively, were derived from carbonate weathering (Table 3-1). In the Chi and Mun rivers, both CAT_{sil} and CAT_{carb} values were relatively low (5-33 % and 26-36 %, respectively) due to the contribution of local halite dissolution.

A large uncertainty is associated with these calculations due to the fact that the major cations are derived not only from silicate and carbonate weathering but also from rainwater, sea spray, evaporite dissolution, etc. In addition, I do not have actual data on the chemical composition of silicate/carbonate rocks in this basin. Therefore, this estimation shows only the upper limit of the possible contributions of silicate and carbonate weathering, and more accurate estimates would require additional information and constraints. However, it should be pointed out that these results appear to controvert the previous results reported by Gaillardet et al. [1999], that carbonate weathering rarely contributed to the total alkalinity budgets in the Ayeyarwady River. Instead, my results show that the Ayeyarwady is dominated by carbonate weathering but with a relatively high contribution from silicate weathering compared to the Mekong. The Chao Phraya River seems to have the highest contribution from silicates among the three rivers.

3.4.3. CO_2 consumption by chemical weathering and its impact on the global cooling

Several studies have suggested that the rise of the Himalayas, which started in the early Cenozoic, could be an explanation for the global cooling seen in deep-sea sedimentary cores from the late Eocene [Raymo et al., 1988; Raymo, 1991; Raymo and Ruddiman, 1992]. According to these studies, the formation of the Himalaya Mountains triggered intense chemical weathering of silicates, which eventually led to an acceleration in the consumption of atmospheric CO_2. This process would of course eventually reduce the atmospheric concentration of CO_2 and contribute to a global-scale cooling.

Moreover, this hypothesis seems consistent with the increase in $^{87}Sr/^{86}Sr$ ratios in marine

carbonates of the same age. Silicate weathering results in a relatively high $^{87}Sr/^{86}Sr$ ratio in river water, whereas weathering of carbonates does not (for details, see Tripathy et al. [2012]). The increase in $^{87}Sr/^{86}Sr$ ratios in marine fossils since the early Cenozoic is important evidence in support of this hypothesis.

However, there have been some interesting challenges to this suggestion. These have been based on the argument that the rise in the $^{87}Sr/^{86}Sr$ ratio was not caused by silicate weathering. It has been suggested that, owing to regional metamorphism in the Himalayas, high $^{87}Sr/^{86}Sr$ ratios can be the result of carbonate as well as silicate weathering [Palmer and Edmond, 1992; Bickle et al., 2001, 2003] (for details, see Section 1.5.2). This is, in fact, a very critical argument, as carbonate weathering does not cause a reduction in atmospheric CO_2 on a long timescale.

Similarly, my results showed that the chemistry of the Ayeyarwady is dominated by carbonate weathering. To determine the total CO_2 consumption of these rivers, I used the cation concentration methodology introduced by Wu et al. [2008]. The assumption that the majority of the cations are derived from silicate and carbonate weathering leads to the following equation for calculating CO_2 consumption due to weathering:

$$[\Phi CO_{2sil}] = ([Na^+]_{sil} + [K^+]_{sil} + 2 \times [Ca^{2+}]_{sil} + 2 \times [Mg^{2+}]_{sil}) \times \text{discharge} \quad (3\text{-}7)$$

$$[\Phi CO_{2carb}] = ([Ca^{2+}]_{carb} + [Mg^{2+}]_{carb}) \times \text{discharge} \quad (3\text{-}8)$$

where $[\Phi CO_{2sil}]$ and $[\Phi CO_{2carb}]$ are measures of CO_2 consumption due to silicate and carbonate weathering, respectively. River discharge data used in the calculations were taken from Meybeck and Ragu [2012]. The calculation is associated with some potential errors, such as (a) uncertainties in major ion measurements (less than ± 3 %) and (b) large variation in $(Ca/Na)_{sol}$ and $(Mg/K)_{sol}$ ratios (0.18-0.3 and 0.3-0.7, respectively). For the Ayeyarwady and Chao Phraya rivers, I also took account of (c) spatial variations in major ion concentrations amongst samples from the same rivers. For example, the maximum and minimum value of $[\Phi CO_{2sil}]$ attributed to (a) i.e., "3 %" errors of each ion concentration, can be calculated as follows:

$$[\Phi CO_{2sil}]_{(max)-(a)}$$

$$= ([Na^+]_{sil\ (max)} \times (1 + 2\ (Ca / Na)_{sil\text{-}rock}) + [K^+]_{sil\ (max)} \times (1 + 2\ (Mg / K)_{sil\text{-}rock}) \times \text{discharge}$$

$$= (([Na^+]_{riv\ (max)} - [Cl^-]_{riv\ (min)}) \times (1 + 2\ (Ca / Na)_{sil\text{-}rock}) + [K^+]_{riv\ (max)} \times (1 + 2\ (Mg / K)_{sil\text{-}rock}) \times \text{discharge}$$

$$= ((1.03\ [Na^+]_{riv} - 0.97\ [Cl^-]_{riv}) \times (1 + 2\ (Ca / Na)_{sil\text{-}rock}) + 1.03\ [K^+]_{riv} \times (1 + 2\ (Mg / K)_{sil\text{-}rock}) \times \text{discharge} \quad (3\text{-}9)$$

$$[\Phi CO_{2sil}]_{(min)\text{-}(a)}$$

$$= ((0.97\,[Na^+]_{riv} - 1.03\,[Cl^-]_{riv}) \times (1 + 2\,(Ca / Na)_{sil\text{-}rock}) + 0.97\,[K^+]_{riv}$$

$$\times (1 + 2\,(Mg / K)_{sil\text{-}rock}) \times \text{discharge} \quad (3\text{-}10)$$

In contrast, the maximum and minimum value of $[\Phi CO_{2sil}]$ attributed to (a) can be calculated as follows:

$$[\Phi CO_{2sil}]_{(max)\text{-}(b)}$$

$$= ([Na^+]_{sil} \times (1 + 2\,(Ca / Na)_{sil\text{-}rock\,(max)}) + [K^+]_{sil} \times (1 + 2\,(Mg / K)_{sil\text{-}rock\,(max)}) \times \text{discharge}$$

$$= ([Na^+]_{sil} \times (1 + 2 \times 0.3) + [K^+]_{sil} \times (1 + 2 \times 0.7) \times \text{discharge} \quad (3\text{-}11)$$

$$[\Phi CO_{2sil}]_{(min)\text{-}(b)}$$

$$= ([Na^+]_{sil} \times (1 + 2 \times 0.18) + [K^+]_{sil} \times (1 + 2 \times 0.3) \times \text{discharge} \quad (3\text{-}12)$$

With regard to the Ayeyarwady River samples, propagated errors of (a)-(c) for the calculation of $[\Phi CO_{2sil}]$ and $[\Phi CO_{2carb}]$ were at most 16×10^9 (maximum relative error of 6 %) and 14×10^9 mol yr^{-1} (5 %), 29×10^9 (12 %) and 15×10^9 mol yr^{-1} (5 %), and 59×10^9 (26 %) and 54×10^9 mol yr^{-1} (19 %), respectively.

In addition, seasonal variations in river water chemistry should be considered. However, Wu et al. [2008] have confirmed that, in their methodology, in the Tibetan Plateau the cation concentration data from the rainy season best match the annual time series estimates. Therefore, my datasets from the rainy season samples should represent annual average CO_2 consumption due to chemical weathering.

In my results, the Mekong River basin consumed 132-192 $\times 10^9$ mol yr^{-1} and 389-438 $\times 10^9$ mol yr^{-1} of CO_2 due to silicate and carbonate weathering, respectively (Table 3-2). Although I had only one sample from the mainstream of the Mekong on which to base the calculations, as a first-order estimation these values of CO_2 consumption were very close to previously reported values (194×10^9 mol yr^{-1} and 409×10^9 mol yr^{-1} by Gaillardet et al. [1999] and 152×10^9 mol yr^{-1} and 228×10^9 mol yr^{-1} by Li et al. [2014], respectively). My methodology and calculations are therefore likely to be fundamentally correct. In addition, I estimated amounts of CO_2 consumed in the Chao Phraya River system by silicate and carbonate weathering of 9-35 $\times 10^9$ mol yr^{-1} and 13-43 $\times 10^9$ mol yr^{-1}, respectively.

However, my results showed that the Ayeyarwady River basin consumed only 63-145 $\times 10^9$ mol yr^{-1} of CO_2 via silicate weathering (Table 3-2 and Figure 3-3). This value is about 10 % of the rate of 832×10^9 mol yr^{-1} reported by Gaillardet et al. [1999], which was originally thought to account for

more than 40 % of total Himalayan CO_2 consumption via silicate weathering. My estimate for the Ayeyarwady River obviously reflects the conclusion that the Ayeyarwady River is, in fact, a river dominated by carbonate weathering, similar to other Himalayan rivers. My results also suggest that CO_2 consumption by silicate weathering within all Himalayan watersheds (the Ganges, Mekong, Yangtze, Brahmaputra, Ayeyarwady, Indus, and Salween river watersheds) could be smaller than reported in previous studies. Unfortunately, neither I nor Gaillardet et al. [1999] have datasets for the Salween River. Although Gaillardet et al. [1999] suggested that Himalayan rivers account for as much as ~20 % of the total global CO_2 consumption by silicate weathering, my calculations indicate that these rivers only actually account for about 10 %. I therefore conclude that the hypothesis of Raymo et al. [1988] and Raymo [1991] that the Himalaya Mountains contribute to global cooling by acting as a huge, long-term sink of CO_2 via silicate weathering, is dubious. However, further studies are needed to address questions about changes in chemical weathering that occur in the Himalaya Mountains over millions of years.

Table 3-2.

Calculated CO_2 consumption by silicate and carbonate weathering from previous studies [Gaillardet et al., 1999; Li et al., 2014] and this study.

Locality		CO_2 consumption (10^9 mol yr^{-1})	
		Silicate	Carbonate
Ayeyarwady River			
	This study	63-145	96-167
	Gaillardet et al. [1999]	832	24
Mekong River			
	This study	132-192	389-438
	Gaillardet et al. [1999]	194	409
	Li et al. [2014]	152	228
Chao Phraya River			
	This study	9-35	13-43

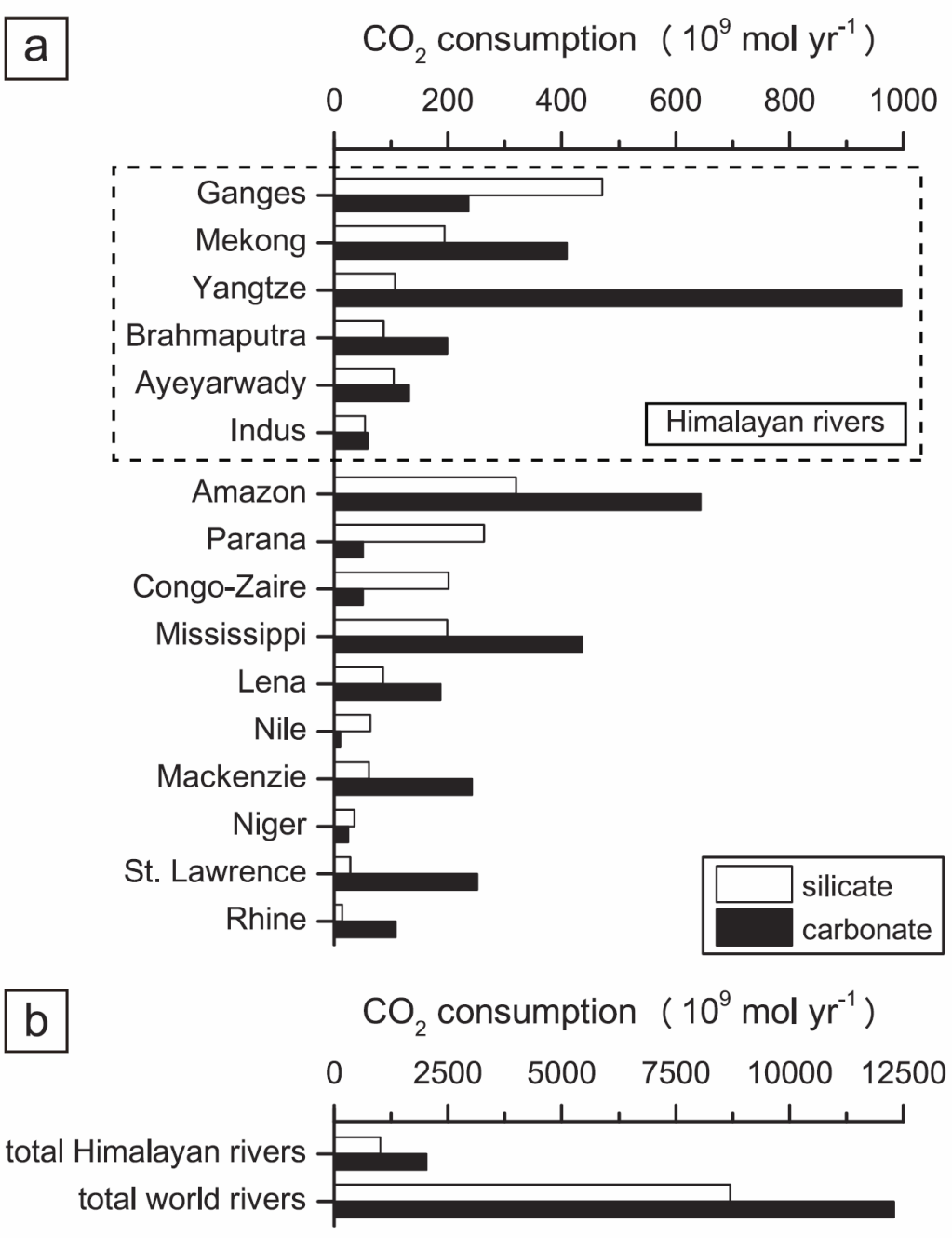

Figure 3-3.

CO_2 consumption by chemical weathering of silicate and carbonate in (a) Himalayan and major world rivers and (b) total Himalayan/world rivers. The original datasets were compiled by Gaillardet et al. [1999], although their data for the Ayeyarwady River have been replaced by data from my study.

3.5. Conclusions

To understand the potential importance of the Himalaya Mountains to the global carbon cycle on a long timescale, I studied two major Himalayan rivers, the Ayeyarwady and Mekong rivers, and one local river in Thailand, the Chao Phraya River. In contrast to previous studies, my results showed that total alkalinity budgets of the Ayeyarwady River were for the most part dominated by carbonate weathering. Long-term CO_2 consumption by silicate weathering in the Ayeyarwady was estimated at only 63-145 $\times$ 10^9 mol yr^{-1}, much smaller than previous estimates by Gaillardet et al. [1999]. These results suggest that long-term carbon consumption by chemical weathering in the Himalaya Mountains should not be that significant and may have played a lesser role in past long-term global cooling than previously thought, although more detailed studies are necessary.

Appendix-3: Chemical weathering rates in the Ganges and Brahmaputra rivers

Using the same method of Sections 3.4.2 and 3.4.3, I calculated chemical weathering rates in the Ganges, Brahmaputra, and Meghna rivers. Table A3-1 shows concentrations of major ions and total cations derived from silicate and carbonate weathering. CAT_{sil} and CAT_{carb} values in the Ganges were similar to those in the Brahmaputra, and little seasonal variation was observed. Relatively large amounts of cations were derived from silicate rocks in the Meghna, inferred from relatively higher concentrations of Na^+ and K^+ shown in Figure 3-1 and 3-2. In addition, the concentrations of SO_4^{2-} were relatively high amongst all dissolved anions in the Brahmaputra River (Table 2-1), which is consistent with the report of Galy and France-Lanord [1999], showing that sulphuric acid largely contributes to chemical weathering and total alkalinity flux in this river (see Section 1.4.2).

CO_2 consumption rates were higher in dry seasons than in rainy seasons. Assuming a ratio of water discharge in dry seasons to rainy seasons of 1:9, [ΦCO_{2sil}] and [ΦCO_{2carb}] values were 170 × 10^9 mol yr^{-1} and 290 × 10^9 mol yr^{-1} in the Ganges, 150 × 10^9 mol yr^{-1} and 320 × 10^9 mol yr^{-1} in the Brahmaputra, and 20 × 10^9 mol yr^{-1} and 20 × 10^9 mol yr^{-1} in the Meghna, respectively. These values are comparable to previous reports shown in Table 1-6.

Table A3-1.

Calculated concentrations of major ions and total cations derived from silicate and carbonate weathering in the Ganges, Brahmaputra, and Meghna rivers.

Locality	Date	Total Cationic Charge Balance	$[Na^+]_{sil}$	$[K^+]_{sil}$	$[Ca^{2+}]_{sil\ (min)}$	$[Mg^{2+}]_{sil\ (min)}$	$[Ca^{2+}]_{sil\ (max)}$	$[Mg^{2+}]_{sil\ (max)}$	CAT_{sil}	CAT_{carb}
	(dd/mm/yyyy)	($\mu mol\ kg^{-1}$)							(%)	(%)
Ganges River										
G-1	11/01/2011	3657	426	104	77	31	128	73	19-28	65-74
G-2	11/01/2011	3678	290	107	52	32	87	75	14-21	72-83
G-3	12/01/2011	3160	390	101	70	30	117	71	20-30	62-71
G-3	07/09/2011	2186	205	92	37	28	61	65	18-27	68-80
G-3	20/02/2012	3635	494	92	89	28	148	65	21-30	64-72
G-3	24/09/2012	2005	174	73	31	22	52	51	16-24	71-82
Brahmaputra River										
B-1	13/01/2011	1961	178	59	32	18	53	41	16-23	74-84
B-2	12/01/2011	2077	173	60	31	18	52	42	15-22	75-86
B-3	14/01/2011	1943	176	61	32	18	53	43	16-24	73-84
B-3	06/09/2011	1379	99	60	18	18	30	42	16-23	73-86
B-3	19/02/2012	2183	184	54	33	16	55	38	14-21	76-86
B-3	22/09/2012	1040	70	44	13	13	21	31	15-22	74-87
Meghna River										
S-1 (Surma)	15/01/2011	945	171	35	31	11	51	25	28-41	56-64
K-1 (Kusiyara)	15/01/2011	1087	238	56	43	17	72	39	35-51	46-53
M-1	16/01/2011	918	175	37	32	11	53	26	30-43	54-61
M-1	17/02/2012	1326	229	34	41	10	69	23	25-36	59-67
M-2	17/01/2011	946	172	38	31	11	51	27	29-42	52-60
M-2	05/09/2011	441	74	26	13	8	22	18	30-44	52-62
M-2	25/09/2012	459	79	19	14	6	24	13	28-40	57-65

Chapter 4. Development of analytical procedures for determination of magnesium and silicon isotope ratios in river water samples

4.1. Introduction

River water plays an important role in the carbon cycle and terrestrial environment on different timescales, by stimulating chemical weathering of terrestrial rocks, conveying terrestrial materials to the ocean, and providing essential chemical components to seawater [Siegenthaler and Sarmiento, 1993; Sarmiento and Gruber, 2006; Hönisch et al., 2012]. This chapter analyzes chemical weathering in the long-term carbon cycle.

In Chapter 3, the chemical weathering rates in the river basins based on major ion concentrations are calculated. However, as discussed in Section 1.5.1, all of the dissolved ions are not conservatively transported downstream, resulting in a misestimation of weathering rates. To improve our understanding of chemical weathering in river basins, stable isotope ratios of major ions are potential proxies. This chapter will focus on Mg and Si. These elements are abundant in the continental crust, and essential for various biogeochemical processes in the carbon cycle, such as chemical weathering and biological activity [Berner et al., 1983; Martin, 1995]. Through chemical weathering processes, Mg is released from both silicate and carbonate rocks to river waters, while Si is released from only silicate rocks, and both are transported to the ocean. Recent advances in analytical devices have enabled us to measure the stable isotope composition of both Mg and Si, and δ^{26}Mg and δ^{30}Si can be used to identify the sources and chemical reaction history of Mg and Si, respectively. With regard to Mg, values of δ^{26}Mg for materials on the surface of the Earth vary widely (from -4.6 ‰ to +1.8 ‰, see Figure 1-8) [e.g., Young and Galy, 2004; Tipper et al., 2006; Immenhauser et al., 2010; Liu et al., 2014], with average values for the upper continental crust of approximately -0.22 ‰ [Li et al., 2010]. δ^{26}Mg values of river waters reflect those of the bedrock. In addition, substantial Mg isotope fractionation takes place during low temperature biogeochemical reactions in the terrestrial environment, mainly secondary mineral formation [Ding et al., 2004; Wimpenny et al., 2011; Huang et al., 2012; Opfergelt et al., 2012; Liu et al., 2014; Saenger and Wang, 2014; Frings et al., 2015] (for

details, see Section 1.5.3). Therefore, by measuring δ^{26}Mg values of the river waters, it should be possible to identify which type of rock has weathered in the basins, as well as what kind of biogeochemical reactions have occurred and eliminated Mg from the dissolved load during river flow. In contrast, δ^{30}Si values of Earth-surface materials vary between -3.7 ‰ and 5.0 ‰ (see Figure 1-10) [e.g., Basile-Doelsch, 2006; Hoefs, 2015], with average values for the upper continental crust of approximately -0.25 ‰ [Savage et al., 2013]. Isotope fractionation occurs through both high and low temperature processes. Although Si is derived from only silicate weathering in the basin, large Si isotope fractionation attributed to biological uptake of dissolved Si is also observed [Ding et al., 2004; Sun et al., 2013]. For these reasons, these isotope ratios can provide insights into the long-term carbon cycle and global climate, as well as Mg/Si cycling during chemical weathering, secondary mineral formation, and biological activity. However, due to the difficulty in measuring these isotope ratios, it remains unclear which factors influence them. In addition, there are a limited number of studies focusing on these isotopes in global river basins and discussing the source rocks and subsequent CO_2 consumption.

With regard to Mg, this study investigates both δ^{26}Mg and $^{87}Sr/^{86}Sr$ in the Ganges, Brahmaputra, and Meghna rivers in the dry and wet seasons. Active chemical weathering processes occur in this area [Molnar et al., 1993; Yin and Harrison, 2000], which is well suited for investigating Mg isotope dynamics during chemical weathering and isotope fractionation processes. In addition, these rivers are an important source of Mg for the ocean. Although Tipper et al. [2008] already reported δ^{26}Mg values mainly in the upper streams (Figure 4-1), little is known about spatial and seasonal variations in the values. Through analysis of samples taken in the downstream and comparison with samples of Tipper et al. [2008], Mg-related processes during river flow are investigated. The possibility of riverine δ^{26}Mg as a proxy for chemical weathering, and to gain insight into both the carbon and Mg cycle, is also assessed.

With regard to Si, this work develops analytical methods of δ^{30}Si in river waters with high accuracy. Although the isotope ratio is not measured because of problems with the analytical equipment, a Si separation and purification method, which is essential for the analysis, is developed. Here, the separation scheme for the preparation of river waters is explained.

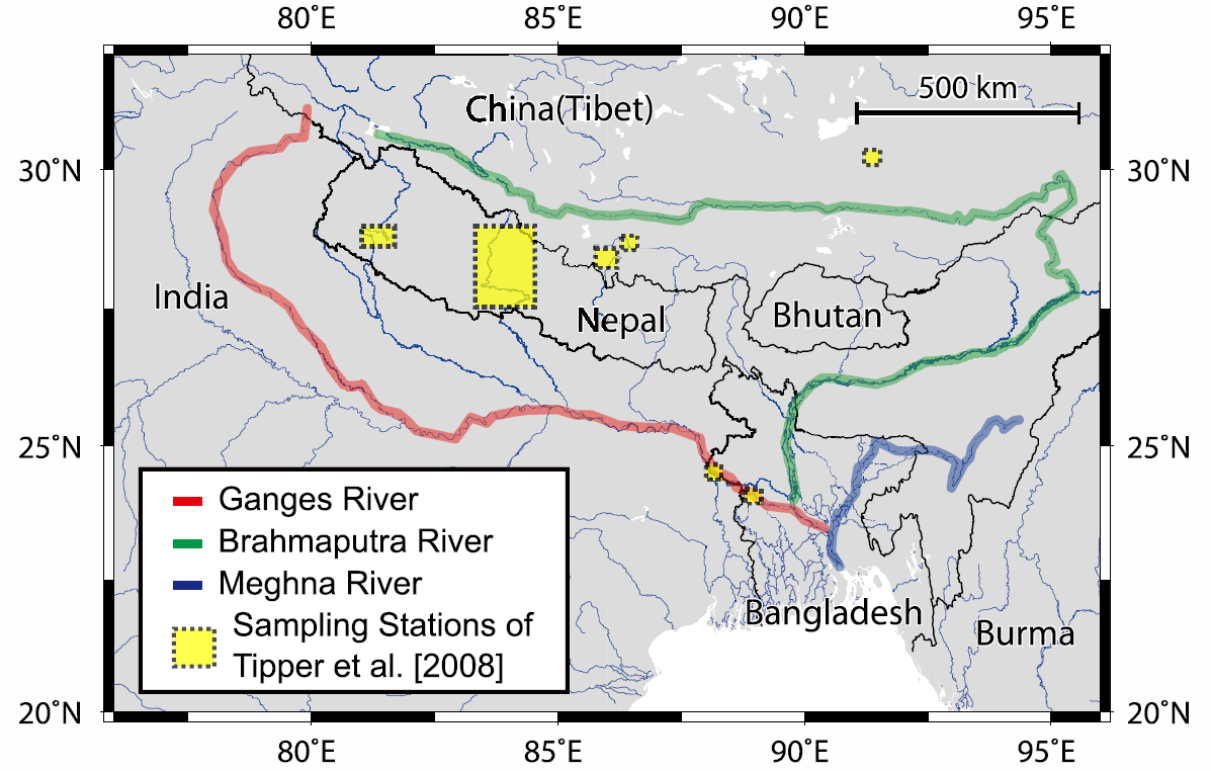

Figure 4-1.

Locations of rivers and sampling stations of Tipper et al. [2008] (for my sampling stations, see Figure 2-1).

4.2. Analytical procedures for Mg isotope measurement

The sampling protocol is shown in Chapter 2. In order to understand the dissolved Mg flux from land to ocean, I analyzed six additional samples from river waters and one from groundwater. I set two sampling stations in the Ganges downstream of the confluence with the Brahmaputra. I took one sample from GB-1 station (23.78°N, 89.90°E) in February 2012, and two samples from GB-2 station (23.46°N, 90.27°E) in January and September 2011. One sampling station, GBM-1 was located in the lower Meghna (23.23°N, 90.63°E). Three samples were taken during both dry and rainy seasons. In addition, I took one groundwater sample (GW-1) from a well near M-2 station (depth: 100 m) (Table 4-1). I also calculated the saturation state of calcite ($\Omega_{calcite}$) using my calcium and carbonate ion concentration data and K_{sp} values from Plummer and Busenberg [1982].

Mg was extracted from the river water and groundwater samples by ion exchange chromatography, as described by Tanimizu [2008] and Yoshimura et al. [2011]. For general information about ion exchange chromatography, see Section 4.5. Mg isotope ratios were measured at KCC with a multiple-collector ICP-MS instrument (NEPTUNE: Thermo Scientific, Germany) using Si-external standardization and standard sample-bracketing methods. Standards and samples were prepared as ~500 ppb Mg solutions in 0.15 M HNO_3. Isotopic data are reported as $\delta^{25}Mg$ or $\delta^{26}Mg$ (see equation 1-16), and the 2σ reproducibility of the seawater reference material BCR403 (Institute for Reference Materials and Measurements, Geel, Belgium) are 0.10 ‰ and 0.09 ‰ for $\delta^{25}Mg$ and $\delta^{26}Mg$, respectively.

Table 4-1.

Physical properties, Mg and Sr isotope ratios, and major ion concentrations in the river water and groundwater samples. Most of the dataset is already shown in Table 2-1.

Locality	Lat (°N)	Long (°E)	Date	Temp. (°C)	$\delta^{26}Mg$ (‰)	2SD	$\delta^{25}Mg$ (‰)	2SD	$^{87}Sr/^{86}Sr$ (2SE, 10^{-7})	Na^+	Mg^{2+}	K^+	Ca^{2+}	Sr^{2+}	Cl^-	SO_4^{2-}	HCO_3^-	$\Omega_{calcite}$
										($\mu mol\ kg^{-1}$)								
Ganges River																		
G-1	24.62	88.16	11/01/2011	16.0	-1.34	0.02	-0.73	0.13	0.7286329 (94)	717	453	104	965	2.02	291	181	2985	6.1
G-2	24.37	88.56	11/01/2011	17.4	-1.16	0.08	-0.60	0.09	0.7287156 (86)	494	434	107	1105	1.76	203	156	2925	9.5
G-3	24.07	89.03	12/01/2011	16.5	-1.14	0.01	-0.57	0.07	0.7286908 (94)	682	430	101	759	1.69	292	172	2602	8.4
G-3	24.07	89.03	07/09/2011	30.6	-1.32	0.05	-0.65	0.11	0.7256897 (94)	290	209	92	693	1.13	85	96	1853	2.3
G-3	24.07	89.03	20/02/2012	22.0	-1.30	0.08	-0.67	0.01	0.7268390 (20)	750	538	92	858	1.77	256	164	2827	12.5
G-3	24.07	89.03	24/09/2012	29.6	-1.21	0.04	-0.60	0.08	0.7248720 (20)	253	218	73	621	1.00	79	86	1725	1.2
Brahmaputra River																		
B-1	25.53	89.69	13/01/2011	16.5	-1.05	0.01	-0.60	0.14	0.7193583 (96)	213	205	59	640	1.09	35	183	1646	1.0
B-2	24.87	89.61	12/01/2011	16.7	-1.07	0.10	-0.58	0.02	0.7200278 (108)	208	261	60	644	1.09	35	174	1652	1.8
B-3	24.38	89.80	14/01/2011	16.1	-1.03	0.08	-0.55	0.00	0.7206957 (88)	211	204	61	632	1.07	35	173	1665	1.0
B-3	24.38	89.80	06/09/2011	31.3	-1.32	0.04	-0.70	0.11	0.7186717 (90)	118	124	60	476	0.76	19	145	1076	0.8
B-3	24.38	89.80	19/02/2012	21.4	-1.18	0.03	-0.72	0.01	0.7200691 (20)	227	280	54	671	1.08	43	191	1674	1.7
B-3	24.38	89.80	22/09/2012	27.5	-1.10	0.01	-0.49	0.10	0.7178980 (30)	84	104	44	353	0.54	14	98	841	0.2
G-B (Ganges River after confluence with the Brahmaputra River)																		
GB-1	23.78	89.80	22/02/2012	22.9	-1.11	0.01	-0.58	0.03	0.7265944 (20)	719	539	91	883	1.74	253	181	2712	10.1
GB-2	23.46	90.27	17/01/2011	16.9	-1.15	0.02	-0.58	0.02	0.7228512 (98)	312	244	69	688	1.20	85	176	1887	2.0
GB-2	23.46	90.27	05/09/2011	30.6	-1.11	0.03	-0.53	0.05	0.7207815 (78)	138	124	63	477	0.80	31	124	1145	1.1
Upper Meghna River																		
S-1	24.21	90.99	15/01/2011	18.8	-0.79	0.02	-0.38	0.08	0.7155291 (88)	230	116	35	224	0.55	59	62	805	0.1
K-1	24.17	91.00	15/01/2011	19.4	-	-	-	-	0.7156579 (94)	321	137	56	218	0.61	82	36	948	0.1
M-1	24.05	91.01	16/01/2011	19.2	-0.68	0.01	-0.35	0.08	0.7157216 (100)	234	103	37	220	0.54	59	60	792	0.1
M-1	24.05	91.01	17/02/2012	22.0	-0.91	0.04	-0.47	0.03	0.7156379 (20)	315	212	34	277	0.65	86	76	977	0.4
M-2	23.61	90.63	17/01/2011	19.4	-0.97	0.09	-0.49	0.02	0.7162142 (84)	258	103	38	222	0.51	87	58	765	0.1
M-2	23.61	90.63	05/09/2011	31.6	-0.98	0.09	-0.42	0.11	0.7163666 (96)	102	50	26	106	0.25	29	23	373	0.0
M-2	23.61	90.63	25/09/2012	31.0	-0.66	0.01	-0.28	0.09	0.7163973 (60)	104	60	19	108	0.24	25	29	395	0.0
G-B-M (Lower Meghna River)																		
GBM-1	23.23	90.63	18/01/2011	17.5	-1.19	0.10	-0.61	0.04	0.7212142 (104)	368	226	65	577	1.02	120	149	1660	1.3
GBM-1	23.23	90.63	08/09/2011	30.2	-1.19	0.08	-0.53	0.03	0.7221272 (88)	169	129	65	479	0.78	41	108	1217	0.7
GBM-1	23.23	90.63	18/02/2012	21.7	-1.25	0.05	-0.67	0.02	0.7224677 (20)	357	355	61	726	1.25	95	184	1989	2.1
Groundwater																		
GW-1	23.60	90.62	17/01/2011	27.3	-0.59	0.02	-0.30	0.04	0.714767 (47)	3150	284	27	505	1.59	1570	6	3270	1.1

4.3. Results of Mg analysis

4.3.1. General Chemistry

All of the samples had a high calcium concentration and, in particular, a high bicarbonate concentration (Table 4-1). Taking a closer look at the values of major ion concentrations, the Ganges River samples (G-1 to G-3) were relatively enriched in Na^+, K^+, and Cl^-, whereas the Brahmaputra River samples (B-1 to B-3) showed relatively high concentrations of Ca^{2+} and SO_4^{2-} ion. In contrast, the Meghna River samples (S-1, M-1, and M-2) and the groundwater sample (GW-1) were rich in sodium and potassium. In the same season, the general chemistry of sample GB-1 (including the concentrations of major ions and the Mg and Sr isotope ratios) was similar to that of samples G-1 to G-3. A possible explanation for this similarity is that the GB-1 sample was not well mixed due to the fact that the GB-1 sampling station was close to the confluence of the Ganges and Brahmaputra rivers. In contrast, the chemical composition of the GB-2 sample reflected the mixed chemical compositions of the rivers. The general chemistry of GBM-1 is also similar to that of GB-2, the indication being that the major ion flux from the upper Meghna River is small compared to the fluxes from the Ganges and Brahmaputra rivers.

The concentrations of all major ions were lower in the rainy season than in the dry season (Table 4-1). In Ganges River water samples, the percentage of calcium ions in total cations was higher in the rainy season than in the dry season. $\Omega_{calcite}$ values for the G-1 to G-3 and GB-1 samples were high (> 6.1) in the dry season. For Ganges River water samples in the rainy season and samples from other rivers in both seasons, the $\Omega_{calcite}$ values were low (< 2.3). For more information, see Sections 2.3 and 3.3.

4.3.2. Mg^{2+} concentrations and isotope ratios

A wide range of Mg^{2+} concentrations was observed in the three rivers (Table 4-1). In Ganges River water samples, the dry and rainy season values were 430-538 μmol kg^{-1} (average 464 μmol kg^{-1}) and 209-218 μmol kg^{-1} (average 214 μmol kg^{-1}), respectively. In Brahmaputra river water samples, the values were 204-280 μmol kg^{-1} (average 237 μmol kg^{-1}) and 104-124 μmol kg^{-1} (average 114 μmol kg^{-1}), respectively, and in samples from the upper Meghna River system, the values were 103-212 μmol kg^{-1} (average 134 μmol kg^{-1}) and 50-60 μmol kg^{-1} (average 55 μmol kg^{-1}), respectively. The dry and rainy season Mg^{2+} concentrations in the GBM-1 and GW-1 samples were 129-355 and 284 μmol kg^{-1}, respectively. In all of these river water samples, I observed higher concentrations of Mg^{2+} in the

dry season than in the rainy season.

Spatial variations in δ^{26}Mg values were large only within the upper Meghna River system (Table 4-1). The δ^{26}Mg values of the samples increased in the following order: Ganges River samples (-1.34 ‰ to -1.14 ‰, average -1.24 ‰) < Brahmaputra River samples (-1.32 ‰ to -1.03 ‰, average -1.13 ‰) < upper Meghna River system samples (-0.66 ‰ to -0.98 ‰, average -0.83 ‰) < groundwater sample (-0.59 ‰). I observed small seasonal variations in δ^{26}Mg values in all of the river samples.

4.3.3. Sr^{2+} concentrations and isotope ratios

The dry and rainy season Sr^{2+} concentrations in the GBM-1 and GW-1 samples were 0.78-1.25 and 1.59 μmol kg^{-1}, respectively (Table 4-1). The $^{87}Sr/^{86}Sr$ ratios for the GBM-1 and GW-1 samples were 0.722 and 0.715, respectively. For other samples, see Section 2.3.

4.4. Discussion of Mg isotopes

4.4.1. Major factors: the Ganges River

$^{87}Sr/^{86}Sr$ ratios in the Ganges River show large spatial variations (Table 4-1, Figure 4-2). In the upper streams, Sr isotope ratios are high (e.g., 0.734-0.746 at Rishikesh [Bickle et al., 2003]) because of regional metamorphism [Palmer and Edmond, 1992; Tripathy et al., 2010]. The elevated $^{87}Sr/^{86}Sr$ ratios have been attributed to the presence of radiogenic silicate and carbonate rocks in every major lithotectonic unit in the basin (e.g., TSS, HHCS, and LHS) [Galy et al., 1999; Galy and France-Lanord, 1999; Bickle et al., 2001, 2003]. In contrast, lower stream samples showed relatively low $^{87}Sr/^{86}Sr$ ratios, which can be explained by the dissolution of detrital carbonate with low $^{87}Sr/^{86}Sr$ ratios (< 0.72) [Galy et al., 1999] and inputs from less radiogenic tributaries from the south [Bickle et al., 2003]. The relative contribution of these sources causes seasonal variation in Sr isotope ratios [Singh et al., 2010; Tripathy et al., 2010].

The fact that the $\delta^{26}Mg$ values of the samples exhibited neither clear seasonal differences nor downstream changes (Table 4-1) implies that Mg isotope ratios in the Ganges River systems behave conservatively. Tipper et al. [2008] studied the Mg isotope composition of rocks and water in the Marsyandi catchment (i.e., the upper tributaries of the Ganges River) and reported that LHS dolostone strongly influenced the riverine Mg isotope composition. They proposed that dissolution of dolostone occurred congruently with limited isotope fractionation and that $\delta^{26}Mg$ values in their river water samples were close to those in LHS dolostone ($\delta^{26}Mg$ values for LHS dolostone range between -1.66 ‰ and -1.34 ‰). The $\delta^{26}Mg$ values reported by Tipper et al. [2008] are surprisingly close to those in my samples from the lower streams (Table 4-1). Although there are other factors controlling the riverine Mg isotope composition (see Section 1.5.3), a simple explanation for this small spatial variation in $\delta^{26}Mg$ values is that the overall riverine Mg composition in the Ganges River is primarily due to dissolution of dolostone in the upper streams. This explanation also suggests that lithological controls and source rocks of riverine Mg^{2+} are quite different from those of riverine Sr^{2+}.

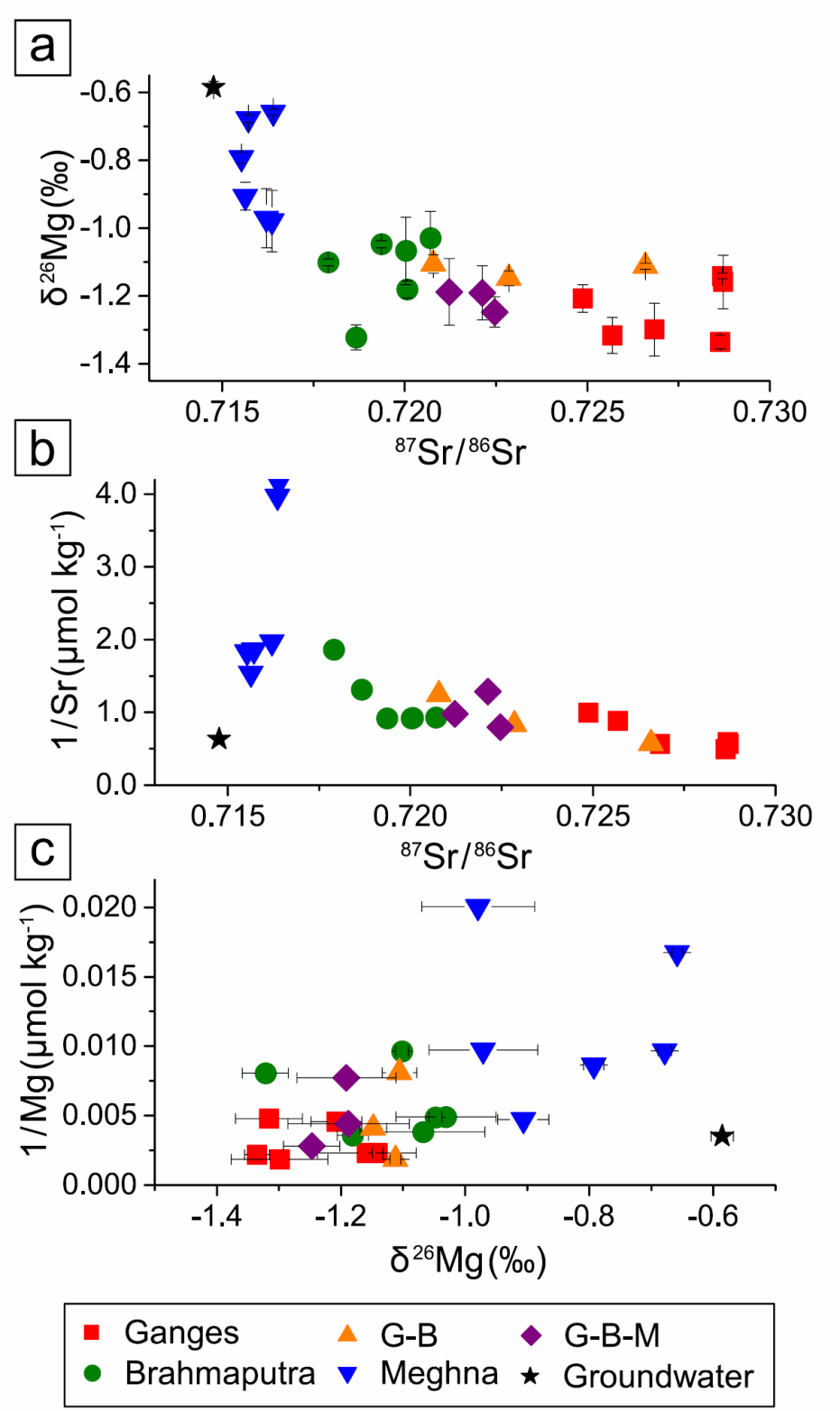

Figure 4-2.

Variations in (a) δ^{26}Mg (‰) relative to $^{87}Sr/^{86}Sr$, (b) 1/Sr (μmol kg^{-1}) relative to $^{87}Sr/^{86}Sr$, and (c) 1/Mg (μmol kg^{-1}) relative to δ^{26}Mg (‰) of the river water and groundwater samples.

4.4.2. Major factors: the Brahmaputra River

Strontium isotope ratios are lower in the Brahmaputra River than in the Ganges River (e.g., the ratios are 0.715-0.730 in the Brahmaputra main channel [Singh et al., 2006]) (Table 4-1, Figure 4-2). In the lower part of the Brahmaputra River, Sr isotope ratios are relatively low because of a significant contribution of Sr from non-Himalayan-type rocks with low $^{87}Sr/^{86}Sr$ ratios [Singh et al., 2006]. Brahmaputra River water is relatively rich in calcium compared to Ganges River water. This fact indicates that the chemical composition of the Brahmaputra River is largely affected by the dissolution of limestone.

However, my results show that $\delta^{26}Mg$ values for Brahmaputra River water are slightly higher than those for Ganges River water (Table 4-1, Figure 4-2). In general, limestone contains light Mg isotopes (< -2.5‰) [Galy et al., 2002; Young and Galy, 2004; Tipper et al., 2006, 2008; Bolou-Bi et al., 2009] and shows little isotope fractionation during dissolution [Brenot et al., 2008; Lee et al., 2014]. Thus, considering the dominant influence of limestone, $\delta^{26}Mg$ values seem too high.

This discrepancy suggests the presence of another Mg source rock with a heavier Mg isotope. In general, $\delta^{26}Mg$ values of silicate rocks are larger than those of limestone and dolostone and range between -0.89 ‰ and 0.00 ‰ [Tipper et al., 2006, 2008; Brenot et al., 2008; Bolou-Bi et al., 2009; Huang et al., 2009, 2012; Teng et al., 2010a]. Such high $\delta^{26}Mg$ values in this river can be attributed to silicate weathering and related secondary mineral formation, as well as limestone weathering. This kind of combination has also been reported for the small upper tributaries of the Ganges, which drain limestone [Tipper et al., 2008].

4.4.3. Major factors: the Meghna River

Upper Meghna River water is enriched in sodium and potassium, and its chemical composition should be mainly affected by silicate weathering of the lowland deposits (Table 4-1). The low Sr isotope ratios for upper Meghna River water are consistent with a relatively high silicate contribution of non-Himalayan, less radiogenic sediment in the river basin [Bickle et al., 2003]. The $\delta^{26}Mg$ values are also consistent with high silicate contributions: $\delta^{26}Mg$ values for upper Meghna River water are higher than those for Ganges and Brahmaputra River water. Spatial variations in $\delta^{26}Mg$ values in the Meghna river system were large, which may be attributed to the relatively large contribution of locally distributed water sources that may control Mg isotope composition in the river water. In addition, adsorption and desorption processes during extreme silicate weathering lead to

substantial isotope fractionation [Huang et al., 2012], which also contributes to the large variability in $\delta^{26}Mg$ values of local rocks and river waters.

4.4.4. Minor factors

Relatively large spatial variations in calcium concentrations were observed in Ganges River water samples during the dry season only (Table 4-1). In contrast, Sr isotope ratios were constant, the indication being that source rocks of the major ions and Sr were homogeneously distributed within the river. The spatial variation in calcium concentration can be explained by a single in situ process: precipitation of calcite. In the Ganges River, the fact that $\Omega_{calcite}$ values become extremely high in the dry season can lead to a decrease in the concentration of dissolved calcium. However, no significant spatial or seasonal variation in $\delta^{26}Mg$ was observed in the Ganges River water samples. This result suggests that a small percentage of Mg^{2+} is removed from the river water through precipitation of calcite, which probably has only a minor effect on the Mg isotope composition. In turn, because $\Omega_{calcite}$ values of the Ganges River water samples were relatively low in the rainy season, and low in other rivers during both seasons, precipitation of calcite seems unlikely.

Sarin et al. [1989] reported that alkaline and saline soils add sodium, potassium, and chlorine to the middle reaches of the Ganges in India. However, $\delta^{26}Mg$ values for upper and lower stream water are essentially the same [Tipper et al., 2008]. Therefore, although the major ion composition of Ganges River water can vary in this area, the alkaline and saline soils are not a significant source of Mg^{2+} in the river water.

The contribution of saline soils to the chlorine concentration of Brahmaputra River water samples was small. Assuming that the chlorine in my samples came entirely from sea spray and subsequent precipitation and that the chlorine concentration did not change during riverine transport [Feth, 1981], I used the equations proposed by Lee et al. [2014] to calculate atmospheric-corrected riverine $\delta^{26}Mg$ values. In calculating these values, I used the concentration of chlorine in the B-1 sample (a representative Brahmaputra River water sample) and the average value of $\delta^{26}Mg$ in seawater (-0.82 ‰ [Foster et al., 2010]). The difference between the corrected and uncorrected $\delta^{26}Mg$ values was at most 0.036, which is less than my analytical error. Therefore, I concluded that the contribution of atmospheric Mg input to the riverine $\delta^{26}Mg$ values is negligible.

Biological processes, which preferentially involve uptake of heavy isotopes of Mg [Bolou-Bi et al., 2010], played a minor role in the Mg isotope composition, as suggested by other riverine

studies [Brenot et al., 2008; Pogge von Strandmann et al., 2008b; Tipper et al., 2008, 2012a; Wimpenny et al., 2011]. In the lower basin of the Ganges, vegetative growth is rapid during the rainy season. Therefore, if vegetation had a strong influence on the riverine Mg isotope composition, I would anticipate large spatial and seasonal variations of $\delta^{26}Mg$ values, neither of which were found.

4.4.5. Implications for the oceanic Mg budget

To evaluate the Mg isotope flux from the Ganges, Brahmaputra, and Meghna River systems to the ocean, I calculated the Mg mass balance as follows:

$$F_{Mg\text{-}total} = D_G [Mg^{2+}]_G + D_B [Mg^{2+}]_B + D_M [Mg^{2+}]_M \quad (4\text{-}1)$$

$$\delta^{26}Mg_{total} = (\delta^{26}Mg_G \times D_G [Mg^{2+}]_G + \delta^{26}Mg_B \times D_B [Mg^{2+}]_B + \delta^{26}Mg_M \times D_M [Mg^{2+}]_M) / F_{Mg\text{-}total} \quad (4\text{-}2)$$

where D_x, $[Mg^{2+}]_x$, and $\delta^{26}Mg_x$ represent the average annual discharge, Mg^{2+} concentration, and $\delta^{26}Mg$ value in river x (i.e., Ganges (x = G), Brahmaputra (x = B), and Meghna rivers (x = M)), respectively. $F_{Mg\text{-}total}$ represents the total Mg^{2+} flux of these three river systems, and $\delta^{26}Mg_{total}$ represents the average Mg isotope ratio of the systems. Based on Mg^{2+} concentration and isotope data and the mean annual water discharge data reported by Parua [2010] and Webster et al. [2010], the calculated values of $F_{Mg\text{-}total}$ and $\delta^{26}Mg_{total}$ are 2.4×10^{11} mol yr^{-1} and -1.17 ‰, respectively. The calculated $F_{Mg\text{-}total}$ value is very close to the value proposed by Galy and France-Lanord [1999] (1.9×10^{11} mol yr^{-1}, the sum of the Mg^{2+} flux of the Ganges and Brahmaputra rivers). Moreover, the calculated $\delta^{26}Mg_{total}$ value is close to $\delta^{26}Mg$ values for the GB-2 and GBM-1 samples. These results suggest not only that my calculation is adequate but also that upper Meghna River water with low Mg^{2+} concentrations and high $\delta^{26}Mg$ values accounts for only a small fraction of the total Mg^{2+} flux of lower Meghna River water to the ocean. Previous studies have reported that the global riverine Mg^{2+} flux and its average $\delta^{26}Mg$ value are 5.6×10^{12} mol yr^{-1} and -1.09 ‰ [Wilkinson and Algeo, 1989; Tipper et al., 2006]. Therefore, I conclude that the Ganges, Brahmaputra, and Meghna rivers play an important role in the global Mg cycle: they transport to the ocean as much as 4 % of the total riverine Mg^{2+} flux with a slightly lower than average $\delta^{26}Mg$ value.

Although I collected only one groundwater sample, I used the GW-1 sample data to estimate the groundwater Mg^{2+} flux to the ocean. Dowling et al. [2003] reported a subsurface water discharge into the Bay of Bengal of 1.5×10^{11} m^3 yr^{-1}, or 15 % of the surface Ganges-Brahmaputra River flux. Assuming the Mg isotope composition of GW-1 represents the average Mg isotope composition of

groundwater in the sampling area, my calculation shows that groundwater in the sampling area annually transports 4.3×10^{10} mol of Mg^{2+} with high $\delta^{26}Mg$ values (-0.59 ‰) to the ocean.

Previous studies have reported a discrepancy between the Mg isotope composition of seawater and that of global river water, which is the major means for transporting Mg to the ocean [Tipper et al., 2006; Teng et al., 2010a]. In addition, whether the modern ocean is in a steady state with respect to Mg isotope ratios is unknown [Tipper et al., 2006]. Dowling et al. [2003] have reported a much higher concentration of Mg in the groundwater in my sampling area (> 23,365 μmol kg^{-1}) than was found in GW-1, so my calculated Mg^{2+} flux may be an underestimate. However, my calculated flux for groundwater is still large compared to the riverine flux. This unexpectedly large flux of Mg^{2+} with $\delta^{26}Mg$ values larger than those in river water supports my analysis of the oceanic Mg cycle. To further elucidate the global Mg cycle and the related Earth-surface environment, more detailed information is needed on the Mg isotope compositions of both river water and groundwater in various seasons.

4.4.6. Future studies for further understandings of chemical weathering

Although previous studies detailed in Section 1.4.2 reported chemical weathering rates of silicate and carbonate rocks based on major ion concentrations, contributions of other processes to the dissolved load (e.g., secondary mineral formation and vegetation) are not clear, which can lead to misestimation of CO_2 consumption in the basin. Through $\delta^{26}Mg$ measurements, I highlighted the potential importance of both bedrock and secondary minerals on the Mg flux, which can lead to a precise estimate of the Mg budget derived from silicate or carbonate weathering. However, the volume of Mg exchanged between river waters and minerals and its fractionation factors, which may depend on mineral type, remain undefined.

For future work, it would be beneficial to measure $\delta^{26}Mg$ values of both dissolved and particulate load in different geological conditions. Theoretical and experimental knowledge of mineral crystal structure and reaction kinetics is also necessary to constrain fractionation factors of various Mg-related processes. In addition, the combination of major ion concentrations and Mg^{2+} and Si isotope composition (discussed in the next chapter) can provide not only important information on the behavior of Mg^{2+} and Si in river waters but also an accurate consumption rate of CO_2 by silicate and carbonate weathering, which plays an important role in the long-term global carbon cycle.

4.5. Analytical procedures for Si isotope measurement

It is necessary to separate Si from other elements in the river water and groundwater prior to $\delta^{30}Si$ measurement. The ion exchange process using polymer resins is a common and effective approach for this separation. In the case of cation exchange, when a water sample comes into contact with the resin, positively charged ions in the solute bond to the resin and a hydrogen ion is released to the solute, as follows:

$$R^-H^+ + A^+ \rightarrow R^-A^+ + H^+ \quad (4\text{-}3)$$

where R and A represent an ion exchanger in the resin and a positively charged ion, respectively. Cation exchange resins are prepared by the copolymerization of styrene and divinylbenzene (DVB). Most of the benzene rings have sulfonic acid ($-SO_3H$) or carboxylic groups (-COOH), which work as cation exchangers. While exchangers with carboxylic groups are not active in acidic environments, those with sulfonic acid are active over the entire pH range. In contrast, anion exchange resins have base exchangers such as quaternary ammonium groups ($-NR_3^+$) that absorb dissolved anions.

Each ion has a unique size and charge, which determines their affinity for the resin. For dilute solutions, the orders of affinity for some common cations and anions are as follows [Naushad and Al-Othman, 2013]:

$$Hg^{2+} < Li^+ < H^+ < Na^+ < K^+ \approx NH_4^+ < Cd^{2+} < Cs^+ < Ag^+ < Mn^{2+} < Mg^{2+} < Zn^{2+} < Cu^{2+} < Ni^{2+} < Co^{2+} < Ca^{2+} < Sr^{2+} < Pb^{2+} < Al^{3+} < Fe^{3+} \quad (4\text{-}4)$$

$$OH^- \approx F^- < HCO_3^- < Cl^- < Br^- < NO_3^- < HSO_4^- < PO_4^{3-} < CrO_4^{2-} < SO_4^{2-} \quad (4\text{-}5)$$

In addition, ion exchange distribution coefficients with resins (D), which is shown in the following equation, can vary depending on the type of solution and its concentration.

$$D = C_R / C_S \quad (4\text{-}6)$$

where C_R and C_S represent the concentration of each element in the resin and solution, respectively. Nelson [1964] proposed variations of D values for cation exchange resin (a sulfonic acid-polystyrene-DVB resin) for various elements in HCl and $HClO_4$ solutions (concentration of each acid: 0 to 12 mol kg^{-1}). For example, Mg tends to be absorbed by the resin in dilute acid, but it tends to be released to the solution in concentrated acid. Using these characteristics of the resins and elements, it is possible to separate each element in the solution, when the type of resin and solution is varied [Strelow et al., 1971; Na et al., 1995].

For Si separation from both water and sediment samples, Georg et al. [2006] proposed a one-pass separation method using cation exchange resin in columns. They avoided using HF, which is

often used to fuse solid samples but which requires special safety considerations and HF-resistant sample introduction equipment. In addition, this chemical sometimes causes significant loss of beam intensity and mass-bias stability. They fused solid samples using the alkaline fusion method, while water samples were acidified (to a pH of 2-3) by HCl before separation. Because dissolved Si exists as a form of $Si(OH)_4$ (in equilibrium with $H_3SiO_4^-$) in neutral to acidified waters, most of the dissolved Si is not captured by the cation exchange resin. In contrast, Engström et al. [2006] used anion exchange chromatography. The dissolved Si is loaded on the resin either in $Si(OH)_4$ or in the form of SiF_6^{2-}, both of which exhibit high affinity for the resin. Detailed information about Si behavior and anion exchange processes in this resin can be found in Ben Sik Ali et al. [2004].

Through the method of Georg et al. [2006], it is impossible to separate major anions from the solute. However, they proposed that concentrations of anions were low in river waters, and their impact for $\delta^{30}Si$ measurements (e.g., matrix problem) was negligible. Compared to the method of Engström et al. [2006], this method is safer and more simple, using only HCl, HNO_3, and pure water. For this reason, I chose to use and revise the method of Georg et al. [2006] for $\delta^{30}Si$ measurement in the river water samples.

Special attention should be paid to the selection of columns and resins in different laboratory environments. The size of columns and the amount of resins can affect ion exchange capacity and the time required for elution. Resins having low cross-linking (proportion of DVB) tend to be watery and change dimensions noticeably depending on which type of ions are bound to it [Naushad and Al-Othman, 2013]. In addition, temperature and purity of the laboratory can influence the recovery rate of each ion. It is therefore vital to repeatedly conduct pilot studies to test the recovery rate of silicon and the removal rate of major cations using test samples, prior to analyzing the sample of interest.

In the following experiment, I used pure acid and water for resin cleaning and sample acidification after separation as follows: TAMAPURE-AA-100-grade HNO_3 (Tama Chemicals Co.), ultrapure100-grade HCl (Kanto Chemical Co.), and deionized water from a MilliQ-element (Millipore) system, referred to here as MQ. Every process was conducted in a clean room at AIST (Figure 4-3). The Si separation and purification was achieved using a sulfonic acid-polystyrene-DVB resin (Bio-Rad, AG 50W-X12, 200-400 mesh) filled to a 1.8 mL resin bed in plastic columns (Figure 4-3).

Before sample loading, the resin was washed repeatedly with HCl, HNO_3, and pure water (Table 4-2). Compared to the original method of Georg et al. [2006] this cleaning process was

simplified. 2 mL of “acidified” (discussed later) samples were then loaded on the resin, which were eluted by 4 mL of MQ. Most of the dissolved cations in each sample were retained in the resin, and Si and other anions are eluted.

In order to complete Si separation, the following three questions were asked: (1) Has all the Si been recovered and are all the cations removed? (2) How does the acidity of loaded samples affect the recovery rate of Si and major cations? (3) Can I apply this separation method to samples with high major ion and/or Si concentrations?

In order to examine question (1), I used a Canadian lake water sample (CRANBERRY-05, lot No. 0313, Environment Canada) as a test material. Chemical components of this sample are shown in Table 4-3. A small portion of 3M HCl was mixed with this standard to a pH of 2 (= 0.01 M HCl), and the separation processes were conducted. The volume of elution was 6 mL, as shown in Table 4-2. After separation, the concentrations of major ions and Si in the elution were measured by using an inductively coupled plasma atomic emission spectrometer (ICP-AES, Seiko Instruments, SPS7800) at AIST. Analytical error of this device is approximately 5 %. The results of this separation process are shown in Table 4-4. The intensity values are the raw data. The recovery rates (percentages) are defined as the ratio of concentration values in samples processed for Si separation to those in unprocessed samples. Recovery rates approach 100 % when all of the element was recovered through the process. In this process, the recovery rates of Si were 102.3 ± 4.2 % (n = 24), while those of Na^{+}, Mg^{2+}, and Ca^{2+} were lower than 1 % on average. The ratios of cation concentrations ($[Na^{+}] + [Mg^{2+}] + [Ca^{2+}]$) to Si concentration (unit: Eq kg^{-1}) were 21 in the original sample, and less than 0.16 in the operated samples. Given analytical errors of ICP-AES measurement, this result indicates that this Si separation process is applicable for my samples and laboratory environment. It was not possible to calculate the recovery rates of K. The emission wavelength of K (767 nm) was much greater than that of other cations (< 589 nm) and the intensity values for K measurement were too small for my samples, generating abundant errors. However, the concentrations of K were small compared to other cations, resulting in negligible matrix effects for the measurement of Si.


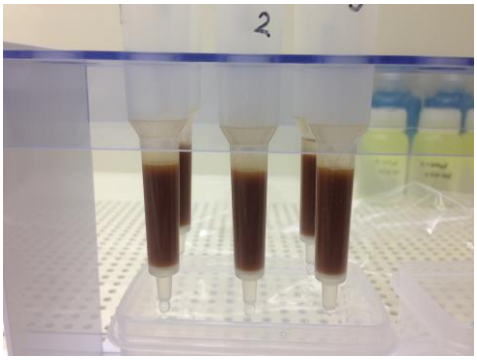

Figure 4-3.

Photographs of (a) the clean room in AIST and (b) 1.8 mL resin beds in plastic columns.

Table 4-2.

Si separation method for river water samples.

Separation stage	Solution matrix	Volume (mL)
Pre-cleaning	10M HCl	5mL
	7M HNO_3	3mL
	6M HCl	3mL
	3M HCl	3mL
Conditioning	MQ	6mL
Sample load	Acidified sample	2mL
Elution	MQ	4mL
Result	6mL Elution	

Table 4-3.

Chemical componentry of Canadian lake water sample (CRANBERRY-05, lot No. 0313, Environment Canada). The concentration of HCO_3^- is officially reported as that of DIC.

Na^+	Mg^{2+}	K^+	Ca^{2+}	Cl^-	SO_4^{2-}	HCO_3^-	Si
(μmol kg^{-1})							
874	232	18	324	999	92	778	96

Table 4-4. (Continued on the following page)

Sample No.	Sample type		Si		
		Acidity	Intensity	Concentration	Recovery
		(μmol/L)		(mg/L)	(%)
Experiment-1					
#1-1	Blank		8938	0.03	
#1-2	Lake Water	0.01 (HCl)	32764	2.47	107
#1-3	Lake Water	0.01 (HCl)	31877	2.38	103
#1-4	Lake Water	0.01 (HCl)	32464	2.44	106
#1-5	Lake Water	0.01 (HCl)	31825	2.38	103
#1-6	Lake Water	0.01 (HCl)	32327	2.41	105
#1-7	Lake Water	0.01 (HCl)	31378	2.32	101
#1-8	Lake Water	0.01 (HCl)	32391	2.42	105
#1-9	Lake Water	0.01 (HCl)	32007	2.38	103
#1-10	Lake Water	0.01 (HCl)	32255	2.41	104
Experiment-2					
#2-1	Lake Water	0.01 (HCl)	30520	2.40	102
#2-2	Lake Water	0.01 (HCl)	29969	2.34	99
#2-3	Lake Water	0.01 (HCl)	30248	2.37	100
#2-4	Lake Water	0.01 (HCl)	30651	2.42	102
#2-5	Lake Water	0.01 (HCl)	30198	2.37	100
#2-6	Lake Water	0.01 (HCl)	30362	2.39	101
#2-7	Lake Water	0.01 (HCl)	30758	2.43	103
#2-8	Lake Water	0.01 (HCl)	30182	2.37	100
Experiment-3					
#3-1	Blank		5976	0.10	
#3-2	Lake Water	none	25078	2.28	104
#3-3	Lake Water	none	25460	2.33	106
#3-4	Lake Water	none	25088	2.28	104
#3-5	Lake Water	0.01 (HCl)	25140	2.29	102
#3-6	Lake Water	0.01 (HCl)	25013	2.29	102
#3-7	Lake Water	0.01 (HCl)	25152	2.30	103
#3-8	Lake Water	0.32 (HNO_3)	23600	2.24	102
#3-9	Lake Water	0.32 (HNO_3)	23985	2.28	104
#3-10	Lake Water	0.32 (HNO_3)	23876	2.27	104
Experiment-4					
#4-1	Blank		5186	0.00	
#4-2	Groundwater-A	0.01 (HCl)	246967	28.62	100
#4-3	Groundwater-A	0.01 (HCl)	246900	28.63	100
#4-4	Groundwater-B	0.01 (HCl)	161905	18.57	101
#4-5	Groundwater-B	0.01 (HCl)	160172	18.37	100
#4-6	Groundwater-C	0.01 (HCl)	125441	14.27	104
#4-7	Groundwater-C	0.01 (HCl)	123080	13.99	102
#4-8	Lake Water	0.01 (HCl)	24988	2.28	101
#4-9	Lake Water	0.01 (HCl)	25177	2.30	102
#4-10	Lake Water	0.01 (HCl)	25346	2.31	102
Experiment-5					
#5-1	Blank		4761	0.00	
#5-2	Lake Water	0.01 (HCl)	23233	2.29	99
#5-3	Lake Water	0.1 (HCl)	22430	2.26	101
#5-4	Lake Water	0.5 (HCl)	19898	2.25	103
#5-5	Lake Water	0.32 (HNO_3)	24633	2.44	100
#5-6	Lake Water	0.5 (HNO_3)	24256	2.45	111
#5-7	Lake Water	1 (HNO_3)	22896	2.46	120
#5-8	Lake Water	2 (HNO_3)	19114	2.33	136

Table 4-4. (Preceding page)

Results of Si separation experiments using both a test material (Lake water) and Bangladeshi groundwater samples (Groundwater-A to C). Samples were acidified prior to loading, resulting in different concentrations of HCl or HNO_3. The intensity values are the raw data of ICP-AES measurements. These data were then converted to concentration values using linear regressions of standard materials (not shown here) as well as a baseline correction. Concentration values were calculated taking account of sample dilution prior to ICP-AES measurements. The recovery rates (percentages) are defined as the ratio of concentration values in samples processed for Si separation to those in the unprocessed samples (not shown here). Recovery rates approach 100 % when all of the element was recovered through the process.

The timing of Si elution in this process was also examined, by collecting every 0.5 mL of the elution (Table 4-5, Figure 4-4). The results of two experiments are shown in Figure 4-4. The total Si recovery rate in 6 mL of elution was 103.2 %, and concentrations of other cations were negligible. Most of the Si was recovered in the first 3 mL elution. I also observed a small fraction of Si in the succeeding 1 mL. Although Si content in the succeeding 1 mL corresponds to less than 1.5 % of total Si in the unprocessed sample, the larger volume of elution should lead to better Si recovery rates.

The acidity of the lake water sample was altered before loading in order to examine question (2). The different acid concentrations are as follows: without acid, 0.01 M HCl, 0.1 M HCl, 0.5 M HCl, 0.32 M HNO_3 (= 2 %w), 0.5 M HNO_3, 1 M HNO_3, and 2 M HNO_3. Extremely high acidity in the loaded sample can cause retention of major cations on the resin (e.g., elution of Mg is conducted using both 0.6 and 1.2 μmol kg^{-1} HCl, as shown by Tanimizu [2008]). The removal rates of cations were still low in all samples, while those of Si exceed 100 % in samples with large concentrations of HNO_3 (Table 4-4). Therefore, this Si separation process should be operated on samples acidified using only small amounts of HCl or HNO_3.

Table 4-5.

Elution profile during Si separation for a Canadian lake water sample (CRANBERRY-05, lot No. 0313, Environment Canada). The datasets are indicated graphically in Figure 4-4.

Sample No.		Solution	Si		
			Intensity	Content	Recovery
				(10^9 g)	(%)
Experiment-1					
	#1-1	Conditioning by MQ	8479	D.L.	D.L.
	#1-2	Conditioning by MQ	8480	D.L.	D.L.
	#1-3	Lake Water	8571	18	0.4
	#1-4	Lake Water	12346	696	15.2
	#1-5	Lake Water	14537	1119	24.5
	#1-6	Lake Water	15029	1193	26.1
	#1-7	Elution by MQ	14731	1156	25.3
	#1-8	Elution by MQ	10980	437	9.6
	#1-9	Elution by MQ	8691	D.L.	D.L.
	#1-10	Elution by MQ	8756	2	0.0
	#1-11	Elution by MQ	8688	D.L.	D.L.
	#1-12	Elution by MQ	8689	D.L.	D.L.
	#1-13	Elution by MQ	8677	D.L.	D.L.
	#1-14	Elution by MQ	8726	30	0.7
	#1-15	Elution by MQ	8717	42	0.9
	#1-16	Elution by MQ	8655	D.L.	D.L.
Experiment-2					
	#2-1	Conditioning by MQ	8540	D.L.	D.L.
	#2-2	Conditioning by MQ	8426	D.L.	D.L.
	#2-3	Lake Water	8703	7	0.2
	#2-4	Lake Water	12016	637	13.9
	#2-5	Lake Water	14736	1154	25.2
	#2-6	Lake Water	14986	1188	26.0
	#2-7	Elution by MQ	15039	1204	26.3
	#2-8	Elution by MQ	11545	536	11.7
	#2-9	Elution by MQ	8711	D.L.	D.L.
	#2-10	Elution by MQ	8714	D.L.	D.L.
	#2-11	Elution by MQ	8746	D.L.	D.L.
	#2-12	Elution by MQ	8646	D.L.	D.L.
	#2-13	Elution by MQ	8746	26	0.6
	#2-14	Elution by MQ	8753	42	0.9
	#2-15	Elution by MQ	8736	53	1.2
	#2-16	Elution by MQ	8798	14	0.3

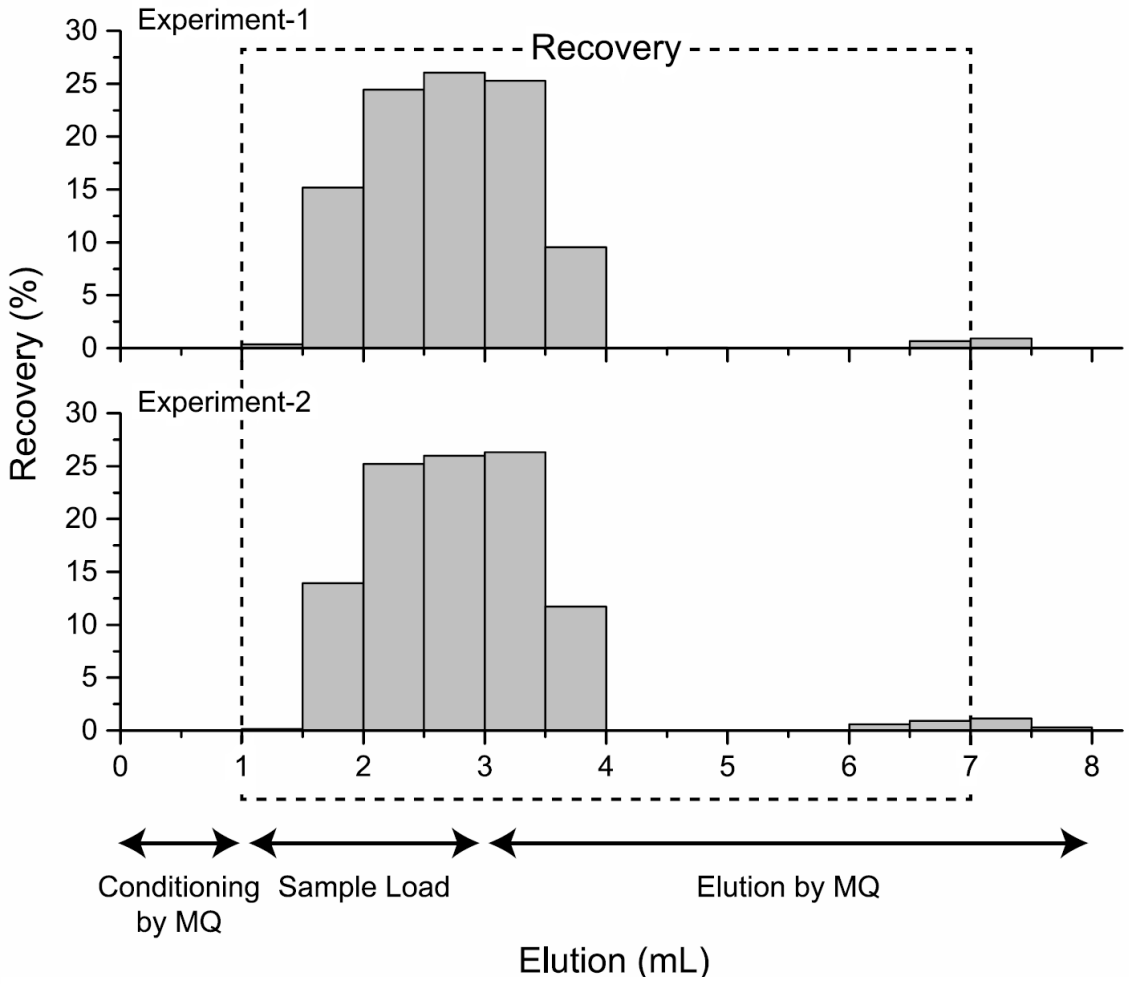

Figure 4-4.

Elution profile during Si separation for a Canadian lake water sample (CRANBERRY-05, lot No. 0313, Environment Canada). The detailed datasets are shown in Table 4-5. The areas surrounded by the dashed line indicate 6 mL volume of sample elution shown in Table 4-2.

This process was also employed for groundwater samples in Bangladesh (Groundwater-A to C), containing the highest concentrations of Si and major cations. The most concentrated samples have Si concentrations of approximately 1000 μmol kg^{-1} and total cation concentrations over 10000 μeq kg^{-1}. Si can be completely separated from other cations in these samples (Table 4-4), suggesting that this method can be applied to every sample I have collected.

It is noted that evaporation to dryness, which is often applied to separate other elements, including Mg, should not be applied to Si separation. When Si elution water is evaporated, Si tends to

precipitate in the form of amorphous silica (SiO_2). I fused the evaporation residue by HNO_3, resulting in a Si recovery rate of less than 40 %. Therefore, HF or the alkaline fusion method should be used for complete fusion of the residue. Engström et al. [2006] also proposed that Fe and Ni must be isolated from samples because they could deteriorate the accuracy of the measurements by forming doubly charged ions, which have the same m/z (weight/charge) values as Si isotopes. With regard to river waters, the concentration of these elements is low, and their impact can be negligible.

Si separation was completed for all of samples from the Ganges, Brahmaputra, and Meghna rivers. Unfortunately, isotope ratios could not be measured because of problems with the analytical equipment. In future work the aim is to measure these isotope ratios and discuss Si-related processes, including chemical weathering in the basin.

4.6. Conclusion

To understand chemical weathering and Mg-related processes, I determined Mg isotope compositions and the concentrations of major ions in Ganges, Brahmaputra, and Meghna River water during the dry and rainy seasons. My main findings and conclusions are as follows:

(1) The Mg isotope composition of Ganges and Brahmaputra River water is mainly controlled by the lithology (dolostone/silicate) and chemical weathering in the upper streams draining the Himalayan-Tibetan region, and is almost constant in both the dry and rainy seasons.

(2) Spatial and seasonal variations in the concentrations of Mg^{2+}, Sr^{2+}, and other major ions were observed. This observation suggests that results obtained using the Mg isotope ratio as a proxy for chemical weathering are not always consistent with results obtained using other chemical proxies. To understand the riverine Mg cycle, close attention should be paid to the Mg isotope ratio.

(3) The magnesium isotope composition in lower Meghna River water is similar to that of both Ganges River water and Brahmaputra River water. The Ganges, Brahmaputra, and Meghna rivers play an important role in the riverine Mg cycle and Mg isotope composition of seawater: they transport to the ocean as much as 4 % of the total riverine flux of Mg^{2+} with a $\delta^{26}Mg$ value (-1.2 ‰), slightly lower than the global riverine average.

A Si separation method, which is essential for Si isotope measurement, was also developed. The cation-exchange method proposed by Georg et al. [2006] was revised and multiple pilot studies were conducted. The Si recovery rate in this study was 102.3 ± 4.2 % (n = 24), suggesting that this process is applicable for my samples and laboratory environment.

Appendix-4: Lithium isotope ratios in the Ganges, Brahmaputra, and Meghna rivers

Lithium isotopes in river waters are one of the most promising tracers of silicate weathering in river basins. Based on previous studies, most dissolved Li in major rivers is derived from weathering of silicate, not carbonate, in the basin. Li has only two stable isotopes (^{6}Li and ^{7}Li) with a relatively large mass difference, which leads to a large range in isotope composition among various biogeochemical materials. The per mil notation for Li isotope ratios is defined as follows:

$$\delta^{7}Li = \{(^{7}Li / {}^{6}Li)_{sample} / (^{7}Li / {}^{6}Li)_{standard} - 1\} \times 1000 \quad \text{(A4-1)}$$

Recent studies use the NIST L-SVEC standard material. The degree of lithium isotope fractionation can be used as a proxy for weathering intensity at the scale of the basin because ^{6}Li is preferentially incorporated or absorbed into/on secondary minerals while the influence of the isotope composition of the bedrock is minor. For example, Pistiner and Henderson [2003] conducted laboratory experiments and reported large Li isotope fractionation (fractionation factor (α) of 0.986) during sorption of Li onto a gibbsite surface.

Araoka [2014] reported Li^{+} concentrations and isotope ratios of my samples from the Ganges, Brahmaputra, and Meghna rivers. The study also reported data of four groundwater samples (GW-1 to 4), one of which (GW-1) I measured for Mg isotope ratios. For details, see Table A4-1. The uncertainty of the $\delta^{7}Li$ value was better than ± 0.3 ‰, as estimated from its long-term reproducibility, and 8.14 ± 0.29 ‰ (2 SD, n =15) using an in-house lithium standard (Kanto Chemical Co.).

$\delta^{7}Li$ values of the Ganges River waters were 23.1-27.6 ‰ during the dry season and 22.5 ‰ during the rainy season (Table A4-1, Figure A4-1). Those of Brahmaputra and Meghna River waters were 25.4-29.8 ‰ (dry season) and 22.2 ‰ (rainy season), and 23.8-34.2 ‰ (dry season) and 19.1 ‰ (rainy season), respectively. The groundwater showed relatively small $\delta^{7}Li$ values (5.1-11.6 ‰).

Kısakűrek et al. [2005] reported $\delta^{7}Li$ values of the upper streams of the Ganges River, including TSS, HHCS, and LHS areas. Values range between 6.1 ‰ and 31.0 ‰ (average: 17.1 ‰), which is lower than those of Araoka [2014] in the lower streams (Table A4-1, Figure A4-1). In addition, the upper continental crust has even lighter values of $\delta^{7}Li$ (about 0 ‰) [Tang et al., 2010]. Therefore, relatively light Li has been removed during the silicate weathering and subsequent secondary mineral formation from the upper to lower streams of the river. Araoka [2014] also reported seasonal variations in $\delta^{7}Li$ values i.e., those from the dry season were larger than those in rainy seasons. This difference may be attributed to the water residence time. The short residence time in the rainy season reduces interactions between dissolved and suspended matter, resulting in relatively light Li in the dissolved

load.

I also compared δ^7Li values of the Ganges, Brahmaputra, and Meghna rivers with my δ^{26}Mg datasets (Figure A4-2). While δ^7Li values in my samples were higher than those in the upper streams [Kısakűrek et al., 2005], δ^{26}Mg values of my samples plotted within the same range as those of the upper streams [Tipper et al., 2008]. This result indicates that, compared to Mg, Li is more likely to be removed from the dissolved load and cause isotope fractionation along the river flow. In other words, Li isotopes in river waters may be a more promising tracer of geochemical processes occurring along the river, while Mg isotopes may be more useful to trace the source rocks in the river basin.

Table A4-1.

Physical properties, Mg and Li isotope ratios, and Li^+ concentrations in the river water and groundwater samples.

Locality	Lat (°N)	Long (°E)	Date	Temp. (°C)	$\delta^{26}Mg$ (‰)	2SD	$\delta^{25}Mg$ (‰)	2SD	$^{87}Sr/^{86}Sr$ (2SE, 10^{-7})	Li^+ (μmol kg^{-1})	δ^7Li (‰)
Ganges River											
G-1	24.62	88.16	11/01/2011	16.0	-1.34	0.02	-0.73	0.13	0.7286329 (94)	0.58	23.1
G-2	24.37	88.56	11/01/2011	17.4	-1.16	0.08	-0.60	0.09	0.7287156 (86)	0.29	27.6
G-3	24.07	89.03	12/01/2011	16.5	-1.14	0.01	-0.57	0.07	0.7286908 (94)	0.43	24.3
G-3	24.07	89.03	07/09/2011	30.6	-1.32	0.05	-0.65	0.11	0.7256897 (94)	0.21	22.5
G-3	24.07	89.03	20/02/2012	22.0	-1.30	0.08	-0.67	0.01	0.7268390 (20)	-	-
G-3	24.07	89.03	24/09/2012	29.6	-1.21	0.04	-0.60	0.08	0.7248720 (20)	-	-
Brahmaputra River											
B-1	25.53	89.69	13/01/2011	16.5	-1.05	0.01	-0.60	0.14	0.7193583 (96)	0.66	25.4
B-2	24.87	89.61	12/01/2011	16.7	-1.07	0.10	-0.58	0.02	0.7200278 (108)	0.59	28.0
B-3	24.38	89.80	14/01/2011	16.1	-1.03	0.08	-0.55	0.00	0.7206957 (88)	0.54	29.8
B-3	24.38	89.80	06/09/2011	31.3	-1.32	0.04	-0.70	0.11	0.7186717 (90)	0.35	22.2
B-3	24.38	89.80	19/02/2012	21.4	-1.18	0.03	-0.72	0.01	0.7200691 (20)	-	-
B-3	24.38	89.80	22/09/2012	27.5	-1.10	0.01	-0.49	0.10	0.7178980 (30)	-	-
G-B (Ganges River after confluence with the Brahmaputra River)											
GB-1	23.78	89.80	22/02/2012	22.9	-1.11	0.01	-0.58	0.03	0.7265944 (20)	-	-
GB-2	23.46	90.27	17/01/2011	16.9	-1.15	0.02	-0.58	0.02	0.7228512 (98)	0.48	30.4
GB-2	23.46	90.27	05/09/2011	30.6	-1.11	0.03	-0.53	0.05	0.7207815 (78)	0.26	26.5
Upper Meghna River											
S-1	24.21	90.99	15/01/2011	18.8	-0.79	0.02	-0.38	0.08	0.7155291 (88)	0.06	28.7
K-1	24.17	91.00	15/01/2011	19.4	-	-	-	-	0.7156579 (94)	0.08	34.2
M-1	24.05	91.01	16/01/2011	19.2	-0.68	0.01	-0.35	0.08	0.7157216 (100)	0.07	28.3
M-1	24.05	91.01	17/02/2012	22.0	-0.91	0.04	-0.47	0.03	0.7156379 (20)	-	-
M-2	23.61	90.63	17/01/2011	19.4	-0.97	0.09	-0.49	0.02	0.7162142 (84)	0.07	23.8
M-2	23.61	90.63	05/09/2011	31.6	-0.98	0.09	-0.42	0.11	0.7163666 (96)	0.04	19.1
M-2	23.61	90.63	25/09/2012	31.0	-0.66	0.01	-0.28	0.09	0.7163973 (60)	-	-
G-B-M (Lower Meghna River)											
GBM-1	23.23	90.63	18/01/2011	17.5	-1.19	0.10	-0.61	0.04	0.7212142 (104)	0.37	30.5
GBM-1	23.23	90.63	08/09/2011	30.2	-1.19	0.08	-0.53	0.03	0.7221272 (88)	0.20	25.7
GBM-1	23.23	90.63	18/02/2012	21.7	-1.25	0.05	-0.67	0.02	0.7224677 (20)	-	-
Groundwater											
GW-1	23.60	90.62	17/01/2011	27.3	-0.59	0.02	-0.30	0.04	0.714767 (47)	1.15	6.4
GW-2	23.47	90.26	05/09/2011	27.5	-	-	-	-	0.7181977 (78)	1.41	11.6
GW-3	23.76	90.35	09/09/2011	27.0	-	-	-	-	0.7179618 (82)	1.67	5.1
GW-4	23.76	90.36	09/09/2011	29.1	-	-	-	-	0.7161535 (98)	1.26	5.3

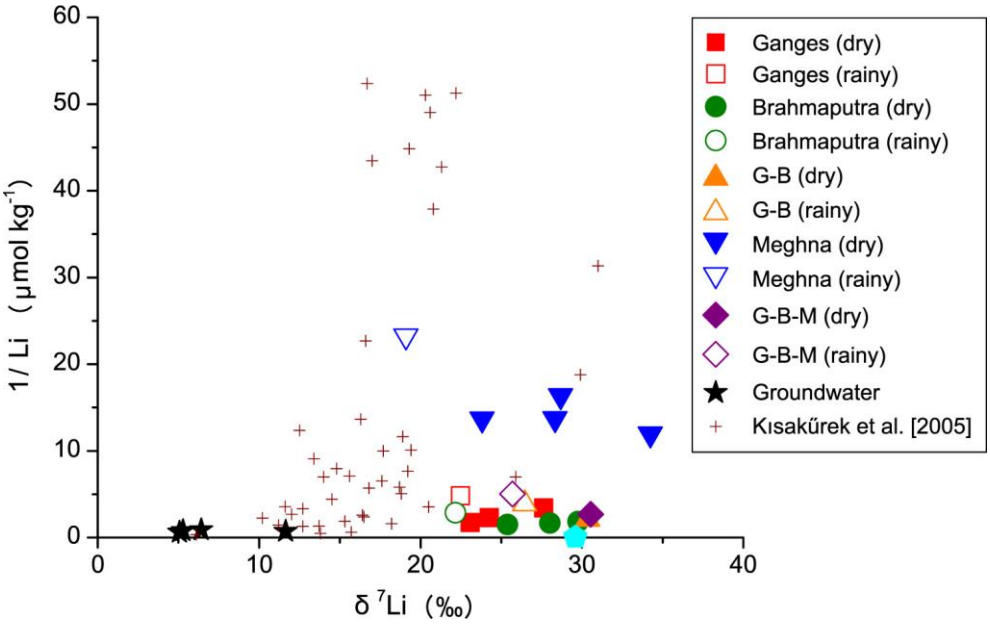

Figure A4-1.

Variations in δ^{7}Li (‰) relative to 1/Li (μmol kg^{-1}) of the river water and groundwater samples.

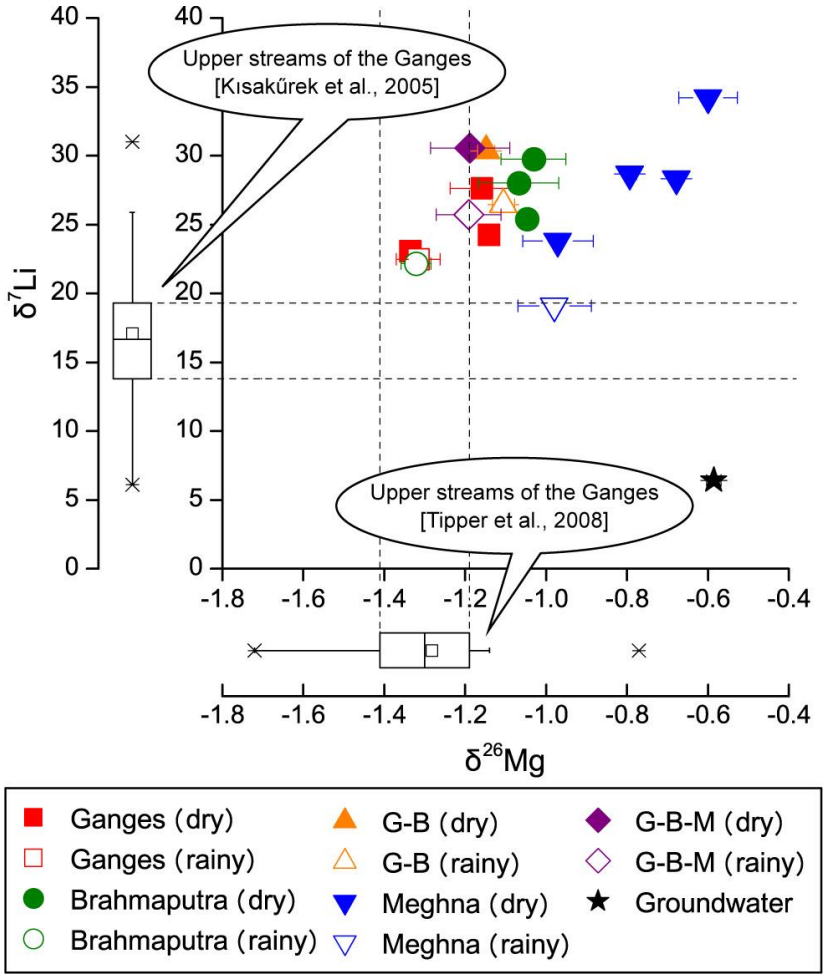

Figure A4-2.

Variations in δ^{26}Mg (‰) relative to δ^{7}Li (‰) of the river water and groundwater samples. Boxplots at the bottom and left of the plot indicate variation in δ^{26}Mg (‰) and δ^{7}Li (‰), respectively, previously reported in the upper streams of the Ganges.

Chapter 5. Conclusions and future perspectives

5.1. General conclusions

In this thesis, the carbon cycle in Himalayan rivers on both modern and geological timescales is examined. Chapter 2 focuses on the carbon cycle on a modern timescale, as well as biological activity and CO_2 evasion from river waters to the atmosphere. My findings showed higher pCO_2 values in the lowland waters of the Ganges, Brahmaputra, and Meghna rivers, in particular in rainy seasons. This result is attributed to enhanced biological activity in the soil. In Chapter 3, I calculated CO_2 consumption by silicate and carbonate weathering, which plays an important role in the long-term carbon cycle, based on major ion compositions in the dissolved load. Previous studies have reported that the Ayeyarwady river basin is dominated by silicate weathering to an unusual extent. Another finding of this study is that chemical weathering in this river basin is actually dominated by carbonate weathering, and that all Himalayan watersheds account for only approximately 10 % of total global CO_2 consumption by silicate weathering. In Chapter 4, I examined new potential proxies for a more precise understanding of chemical weathering, that is, stable isotope ratios of Mg and Si. I reported Mg isotope compositions of Ganges and Brahmaputra River water. The average δ^{26}Mg value was -1.2 ‰, mainly controlled by the lithology (dolostone/silicate) and chemical weathering in the upper streams. A Si separation method from river water samples, using cation-exchange resins, was also developed.

5.2. Impact of global warming on the riverine carbon cycle

Global warming is one of the most serious environmental issues confronting the world today. CO_2 fluxes from Himalayan river waters to the atmosphere, which are discussed in the context of the short-term carbon cycle, can be increased by global warming. In order to evaluate the effect of global warming on river water pCO_2, I simulated a virtual situation whereby temperature rises by 2 °C, with no change in alkalinity, using the CO_2calc program [Robbins et al., 2010]. The results show that a 2 °C increase in water temperature raises pCO_2 by 6 % on average in the Ganges, Brahmaputra, and Meghna rivers. Since alkalinity itself has a positive correlation with rising temperature (shown by Raymond and Cole [2003], see also Figure 2-3), this estimation is likely to be a lower limit and actual pCO_2 values are expected to be higher. In addition, increases in atmospheric temperatures are expected to

enhance soil respiration, which is shown in the lower streams of the rivers.

Global warming is predicted to cause extreme rainfall events and rainy season flooding in the Bangladesh region [Lal and Harasawa, 2001; Mirza, 2002]. Such increased rainfall would also increase the contribution of subsurface flow water to rivers and further increase the pCO_2 of river water. Galy and Eglinton [2011] also reported abundant refractory soil carbon within the Himalayan system. This carbon can be decomposed through global warming and associated extreme rainfall, and released in the form of DOC or CO_2.

It is also observed that global warming can affect chemical weathering rates in the Himalayan river basins, although the timescale of this process is different from that of biological activity. Dissolved CO_2 in the soil and water can enhance chemical weathering, which can act as a negative feedback for global warming [Walker et al., 1981]. In addition, riverine transport and burial of organic carbon may also function as a huge carbon sink [France-Lanord and Derry, 1997; Galy et al., 2007].

In this study, the potential importance of CO_2 evasion from the Himalayan river waters to the atmosphere are highlighted. In order to understand the positive feedback of this CO_2 evasion and future climate change, I aim to conduct more detailed studies on the carbonate system in both river water and river basins, through continuous sampling in multiple locations, precise calculation of the CO_2 exchange flux through biological activity and/or chemical weathering, and monitoring of future precipitation changes in this area.

Acknowledgements

First of all, I express great appreciation to my supervisor, Dr. Hodaka Kawahata for overall support in my academic life. I am very grateful to Dr. Atsushi Suzuki and Dr. Daisuke Araoka of AIST, and Dr. Toshihiro Yoshimura and Dr. Hiroyuki Ushie of AORI for their empathic coaching. I also thank Mr. Souya Otani (AORI) for overall support in studies of rivers in Myanmar and Thailand.

I would like to express my gratitude to Dr. H. M. Zakir Hossain, Mr. Kengo Higashi, Mr. Daisaku Ishikawa, Mr. Takeshige Ishiwa (AIST), Mr. Md. Nahid Nowsher, Mr. Sabbir Ahamed, Mr. Mostafa Tarek (Jessore University of Science and Technology, Bangladesh), Dr. Thura Aung (Myanmar Earthquake Committee, Myanmar), Dr. Raywadee Roachanakanan, and Ms. Preedamon Kamwachirapitak (Mahidol University, Thailand) for their support in my sampling surveys. Dr. Harue Masuda (Osaka City University) and Dr. Kyaw Moe (JAMSTEC) provided constructive comments and advice for the surveys.

I am very grateful to Associate Dr. Hiroshi Ogawa, Ms. Yoko Fujimoto, and Ms. Megumi Shinozuka (AORI) for their support in analyses of nutrients. Dr. Masaya Yasuhara (Rissho University) and Dr. Akihiko Inamura (AIST) made enormous contributions to my analyses of major ions. I received generous support for isotope analyses from Dr. Naohiko Ohkouchi, Dr. Tsuyoshi Ishikawa, Dr. Shigeyuki Wakaki (JAMSTEC), Dr. Jun Matsuoka, Dr. Kazuya Nagaishi (Marine Works Japan Ltd.), Dr. Masaharu Tanimizu (Kwansei Gakuin University), Dr. Kyoko Yamaoka, and Ms. Yumiko Yoshinaga (AIST). I would also like to express my gratitude to Dr. Yusuke Yokoyama and Dr. Miyairi Yosuke (AORI) for overall support for my experiments in AORI.

I gratefully acknowledge reviews of my work by Dr. Yoshio Takahashi, Dr. Ryuji Tada, Dr. Takashi Murakami (the University of Tokyo), Dr. Junichiro Kuroda, and Dr. Yoshinori Takano (JAMSTEC).

My special thanks are expressed to Dr. Toshihiro Yamazaki, Dr. Kyoko Okino, Dr. Juichiro Ashi, and Dr. Asuka Yamaguchi (AORI). The support of Ms. Kyoko Koda, Ms. Mayumi Koga, and Ms. Rica Uchida for my paperwork were invaluable. Advice and comments given by Mr. Arata Kioka, Mr. Kazuhiro Yagasaki, and Mr. Yuta Isaji has been a great help in my English writing. I also thank all members of Kawahata laboratory and my colleagues at the Department of Ocean Floor Geoscience and Center for Earth Surface System Dynamics in AORI for assistance in the laboratory and

considerable academic assistance. I would like to express my gratitude to the editors and anonymous reviewers for my previously published works.

Last of all, I am really grateful to my friends and my parents for their supports and encouragements. This study was supported by the Japan Society for the Promotion of Science Grants-in-Aid for Research Fellowship (14J10963) and Sasagawa Scientific Research Grant.

Declaration of previously published work

Chapter 2. was conducted during my master's program and has been published in its entirety in the following paper:

- Manaka, T., H. Ushie, D. Araoka, S. Otani, A. Inamura, A. Suzuki, H. M. Zakir Hossain, and H. Kawahata (2015), Spatial and seasonal variation in surface water pCO_2 in the Ganges, Brahmaputra, and Meghna Rivers on the Indian subcontinent, Aquat. Geochemistry, 21(5), 437-458, doi:10.1007/s10498-015-9262-2.

Chapter 3. has been published in its entirety in the following paper. S. Otani and I contributed equally; S. Otani mainly conducted chemical analysis, and I wrote the majority of the text.

- Manaka, T., S. Otani, A. Inamura, A. Suzuki, T. Aung, R. Roachanakanan, T. Ishiwa, and H. Kawahata (2015), Chemical weathering and long-term CO_2 consumption in the Ayeyarwady and Mekong river basins in the Himalayas, J. Geophys. Res. Biogeosciences, 120(6), 1165-1175, doi:10.1002/2015JG002932.

Chapter 4 will soon be submitted for publication as the following:

- Manaka, T., T. Yoshimura, D. Araoka, A. Suzuki, H. M. Zakir Hossain, and H. Kawahata (in prep.) Tracing the sources of magnesium and silicon in the Himalayan rivers from spatial and seasonal variations of isotope compositions, Geophys. Res. Lett.

References

Aitkenhead, J. A., and W. H. McDowell (2000), Soil C:N ratio as a predictor of annual riverine DOC flux at local and global scales, *Global Biogeochem. Cycles*, *14*(1), 127–138, doi:10.1029/1999GB900083.

Alin, S. R., M. de F. F. L. Rasera, C. I. Salimon, J. E. Richey, G. W. Holtgrieve, A. V. Krusche, and A. Snidvongs (2011), Physical controls on carbon dioxide transfer velocity and flux in low-gradient river systems and implications for regional carbon budgets, *J. Geophys. Res.*, *116*(G1), G01009, doi:10.1029/2010JG001398.

Amante, C., and B. W. Eakins (2009), ETOPO1 1 Arc-Minute Global Relief Model: Procedures, Data Sources and Analysis, , doi:10.7289/V5C8276M.

Amiotte Suchet, P., J.-L. Probst, and W. Ludwig (2003), Worldwide distribution of continental rock lithology: Implications for the atmospheric/soil CO_2 uptake by continental weathering and alkalinity river transport to the oceans, *Global Biogeochem. Cycles*, *17*(2), n/a–n/a, doi:10.1029/2002GB001891.

André, L., D. Cardinal, L. Alleman, and S. Moorbath (2006), Silicon isotopes in ~3.8 Ga West Greenland rocks as clues to the Eoarchaean supracrustal Si cycle, *Earth Planet. Sci. Lett.*, *245*(1-2), 162–173, doi:10.1016/j.epsl.2006.02.046.

Araoka, D. (2014), Lithium isotope ratios in playas, submarine hydrothermal fluids, and rivers: implication for global lithium cycles at earth surface environment, Ph. D. thesis, Graduate School of Frontier Sciences, The University of Tokyo, Tokyo, Japan

Archer, D. (2003), Biological Fluxes in the Ocean and Atmospheric pCO_2, in *Treatise on Geochemistry*, edited by H. D. Holland and K. K. Turekian, pp. 275–291, Elsevier.

Aucour, A., S. M. F. Sheppard, O. Guyomar, and J. Wattelet (1999), Use of ^{13}C to trace origin and cycling of inorganic carbon in the Rhône river system, *Chem. Geol.*, *159*(1-4), 87–105, doi:10.1016/S0009-2541(99)00035-2.

Aucour, A.-M., C. France-Lanord, K. Pedoja, A.-C. Pierson-Wickmann, and S. M. F. Sheppard (2006), Fluxes and sources of particulate organic carbon in the Ganga-Brahmaputra river system, *Global Biogeochem. Cycles*, *20*(2), GB2006, doi:10.1029/2004GB002324.

Aufdenkampe, A. K., E. Mayorga, P. A. Raymond, J. M. Melack, S. C. Doney, S. R. Alin, R. E. Aalto,

and K. Yoo (2011), Riverine coupling of biogeochemical cycles between land, oceans, and atmosphere, *Front. Ecol. Environ.*, *9*(1), 53–60, doi:10.1890/100014.

Bangladesh Meteorological Department (2016), Rainfall in 2014, Available from: http://www.bmd.gov.bd/?/home

Basile-Doelsch, I. (2006), Si stable isotopes in the Earth's surface: A review, *J. Geochemical Explor.*, *88*(1–3), 252–256, doi:10.1016/j.gexplo.2005.08.050.

Battin, T. J., S. Luyssaert, L. A. Kaplan, A. K. Aufdenkampe, A. Richter, and L. J. Tranvik (2009), The boundless carbon cycle, *Nat. Geosci.*, *2*(9), 598–600, doi:10.1038/ngeo618.

Bender, F. (1983), *Geology of Burma*, Gebr. Borntraeger, Berlin.

Berner, E. K., and R. A. Berner (1987), *Global water cycle: geochemistry and environment*, Prentice-Hall.

Berner, R. A., A. C. Lasaga, and R. M. Garrels (1983), The carbonate-silicate geochemical cycle and its effect on atmospheric carbon dioxide over the past 100 million years, *Am. J. Sci.*, *283*(7), 641–683, doi:10.2475/ajs.283.7.641.

Beucher, C. P., M. A. Brzezinski, and J. L. Jones (2008), Sources and biological fractionation of Silicon isotopes in the Eastern Equatorial Pacific, *Geochim. Cosmochim. Acta*, *72*(13), 3063–3073, doi:10.1016/j.gca.2008.04.021.

Bickle, M. J., N. B. W. Harris, J. M. Bunbury, H. J. Chapman, I. J. Fairchild, and T. Ahmad (2001), Controls on the $^{87}Sr/^{86}Sr$ ratios of carbonates in the Garhwal Himalaya, Headwaters of the Ganges, *J. Geol.*, *109*(6), 737–753, doi:10.1086/323192.

Bickle, M. J., J. Bunbury, H. J. Chapman, N. B. W. Harris, I. J. Fairchild, and T. Ahmad (2003), Fluxes of Sr into the headwaters of the Ganges, *Geochim. Cosmochim. Acta*, *67*(14), 2567–2584, doi:10.1016/S0016-7037(03)00029-2.

Bolou-Bi, E. B., N. Vigier, A. Brenot, and A. Poszwa (2009), Magnesium isotope compositions of natural reference materials, *Geostand. Geoanalytical Res.*, *33*(1), 95–109, doi:10.1111/j.1751-908X.2009.00884.x.

Bolou-Bi, E. B., A. Poszwa, C. Leyval, and N. Vigier (2010), Experimental determination of magnesium isotope fractionation during higher plant growth, *Geochim. Cosmochim. Acta*, *74*(9), 2523–2537, doi:10.1016/j.gca.2010.02.010.

Bolou-Bi, E. B., N. Vigier, A. Poszwa, J.-P. Boudot, and E. Dambrine (2012), Effects of biogeochemical processes on magnesium isotope variations in a forested catchment in the

Vosges Mountains (France), *Geochim. Cosmochim. Acta*, *87*, 341–355, doi:10.1016/j.gca.2012.04.005.

Bourdon, B., E. T. Tipper, C. Fitoussi, and A. Stracke (2010), Chondritic Mg isotope composition of the Earth, *Geochim. Cosmochim. Acta*, *74*(17), 5069–5083, doi:10.1016/j.gca.2010.06.008.

Brady, P. V (1991), The effect of silicate weathering on global temperature and atmospheric CO_2, *J. Geophys. Res.*, *96*(B11), 18101, doi:10.1029/91JB01898.

Brenot, A., C. Cloquet, N. Vigier, J. Carignan, and C. France-Lanord (2008), Magnesium isotope systematics of the lithologically varied Moselle river basin, France, *Geochim. Cosmochim. Acta*, *72*(20), 5070–5089, doi:10.1016/j.gca.2008.07.027.

Buhl, D., R. D. Neuser, D. K. Richter, D. Riedel, B. Roberts, H. Strauss, and J. Veizer (1991), Nature and nurture: Environmental isotope story of the River Rhine, *Naturwissenschaften*, *78*(8), 337–346, doi:10.1007/BF01131605.

Butman, D., and P. a. Raymond (2011), Significant efflux of carbon dioxide from streams and rivers in the United States, *Nat. Geosci.*, *4*(12), 839–842, doi:10.1038/ngeo1294.

Capo, R. C., B. W. Stewart, and O. A. Chadwick (1998), Strontium isotopes as tracers of ecosystem processes: theory and methods, *Geoderma*, *82*(1-3), 197–225, doi:10.1016/S0016-7061(97)00102-X.

Catling, H. D., P. R. Hobbs, Z. Islam, and B. Alam (1983), Agronomic practices and yield assessments of deepwater rice in Bangladesh, *F. Crop. Res.*, *6*, 109–132, doi:10.1016/0378-4290(83)90052-7.

Chang, V. T.-C., A. Makishima, N. S. Belshaw, and R. K. O'Nions (2003), Purification of Mg from low-Mg biogenic carbonates for isotope ratio determination using multiple collector ICP-MS, *J. Anal. At. Spectrom.*, *18*(4), 296–301, doi:10.1039/B210977H.

Chapman, H., M. Bickle, S. H. Thaw, and H. N. Thiam (2015), Chemical fluxes from time series sampling of the Irrawaddy and Salween Rivers, Myanmar, *Chem. Geol.*, *401*, 15–27, doi:10.1016/j.chemgeo.2015.02.012.

Chatterjee, J., and S. K. Singh (2012), $^{87}Sr/^{86}Sr$ and major ion composition of rainwater of Ahmedabad, India: Sources of base cations, *Atmos. Environ.*, *63*, 60–67, doi:10.1016/j.atmosenv.2012.08.060.

Cockerton, H. E., F. A. Street-Perrott, M. J. Leng, P. A. Barker, M. S. A. Horstwood, and V. Pashley (2013), Stable-isotope (H, O, and Si) evidence for seasonal variations in hydrology and Si

cycling from modern waters in the Nile Basin: implications for interpreting the Quaternary record, *Quat. Sci. Rev.*, *66*, 4–21, doi:10.1016/j.quascirev.2012.12.005.

Cole, J. J., and N. F. Caraco (2001), Carbon in catchments: connecting terrestrial carbon losses with aquatic metabolism, *Mar. Freshw. Res.*, *52*(1), 101–110, doi:10.1071/MF00084.

Cole, J. J. et al. (2007), Plumbing the global carbon cycle: Integrating inland waters into the terrestrial carbon budget, *Ecosystems*, *10*(1), 172–185, doi:10.1007/s10021-006-9013-8.

Dalai, T. K., S. Krishnaswami, and M. M. Sarin (2002), Major ion chemistry in the headwaters of the Yamuna river system:: Chemical weathering, its temperature dependence and CO_2 consumption in the Himalaya, *Geochim. Cosmochim. Acta*, *66*(19), 3397–3416, doi:10.1016/S0016-7037(02)00937-7.

Department of Meteorology and Hydrology (Myanmar) (2014), Rainfall data in Myanmar, (September). Available from: http://www.dmh.gov.mm/

Depetris, P. J., and S. Kempe (1993), Carbon dynamics and sources in the Paraná River, *Limnol. Oceanogr.*, *38*(2), 382–395.

de Villiers, S., J. A. D. Dickson, and R. M. Ellam (2005), The composition of the continental river weathering flux deduced from seawater Mg isotopes, *Chem. Geol.*, *216*(1-2), 133–142, doi:10.1016/j.chemgeo.2004.11.010.

Dheeradilok, P., T. Wongwanich, W. Tansathien, and P. Chaodumrong (1992), An introduction to geology of Thailand, in *Proceedings of the National Conference on Geologic Resources of Thailand: Potential for Future Development*, pp. 737–752, Dep. of Miner. Resour., Bangkok.

Dickson, A. G., C. L. Sabine, and J. R. Christian (2007), *Guide to best practices for ocean CO_2 measurements*, PICES Special Publication 3, IOCCP Report No.8, North Pacific Marine Science Organization.

Ding, T., D. Wan, C. Wang, and F. Zhang (2004), Silicon isotope compositions of dissolved silicon and suspended matter in the Yangtze River, China, *Geochim. Cosmochim. Acta*, *68*(2), 205–216, doi:10.1016/S0016-7037(03)00264-3.

Dowling, C. B., R. J. Poreda, and A. R. Basu (2003), The groundwater geochemistry of the Bengal Basin: Weathering, chemsorption, and trace metal flux to the oceans, *Geochim. Cosmochim. Acta*, *67*(12), 2117–2136, doi:10.1016/S0016-7037(02)01306-6.

Dubois, K. D., D. Lee, and J. Veizer (2010), Isotopic constraints on alkalinity, dissolved organic carbon, and atmospheric carbon dioxide fluxes in the Mississippi River, *J. Geophys. Res.*, *115*(G2),

G02018, doi:10.1029/2009JG001102.

Engström, E., I. Rodushkin, D. C. Baxter, and B. Öhlander (2006), Chromatographic Purification for the Determination of Dissolved Silicon Isotopic Compositions in Natural Waters by High-Resolution Multicollector Inductively Coupled Plasma Mass Spectrometry, *Anal. Chem.*, *78*(1), 250–257, doi:10.1021/ac051246v.

Evans, M. J., L. A. Derry, and C. France-Lanord (2004), Geothermal fluxes of alkalinity in the Narayani river system of central Nepal, *Geochemistry, Geophys. Geosystems*, *5*(8), Q08011, doi:10.1029/2004GC000719.

Evans, M. J., L. A. Derry, and C. France-Lanord (2008), Degassing of metamorphic carbon dioxide from the Nepal Himalaya, *Geochemistry, Geophys. Geosystems*, *9*(4), Q04021, doi:10.1029/2007GC001796.

Feely, R., S. Doney, and S. Cooley (2009), Ocean Acidification: Present Conditions and Future Changes in a High- CO_2 World, *Oceanography*, *22*(4), 36–47, doi:10.5670/oceanog.2009.95.

Feth, J. H. (1981), *Chloride in natural continental water-A review*, USGS Water Supply Paper: 2176.

Fontorbe, G., C. L. De La Rocha, H. J. Chapman, and M. J. Bickle (2013), The silicon isotopic composition of the Ganges and its tributaries, *Earth Planet. Sci. Lett.*, *381*, 21–30, doi:10.1016/j.epsl.2013.08.026.

Foster, G. L., P. a. E. Pogge von Strandmann, and J. W. B. Rae (2010), Boron and magnesium isotopic composition of seawater, *Geochemistry, Geophys. Geosystems*, *11*(8), Q08015, doi:10.1029/2010GC003201.

France-Lanord, C., and L. A. Derry (1997), Organic carbon burial forcing of the carbon cycle from Himalayan erosion, *Nature*, *390*(6655), 65–67, doi:10.1038/36324.

Frings, P. J., W. Clymans, G. Fontorbe, W. Gray, G. Chakrapani, D. J. Conley, and C. De La Rocha (2015), Silicate weathering in the Ganges alluvial plain, *Earth Planet. Sci. Lett.*, *427*, 136–148, doi:10.1016/j.epsl.2015.06.049.

Fujii, T., E. A. Pringle, M. Chaussidon, and F. Moynier (2015), Isotope fractionation of Si in protonation/deprotonation reaction of silicic acid: A new pH proxy, *Geochim. Cosmochim. Acta*, *168*, 193–205, doi:10.1016/j.gca.2015.07.003.

Gaillardet, J., B. Dupré, P. Louvat, and C. J. Allègre (1999), Global silicate weathering and CO_2 consumption rates deduced from the chemistry of large rivers, *Chem. Geol.*, *159*(1–4), 3–30, doi:10.1016/S0009-2541(99)00031-5.

Gaillardet, J., J. Viers, and B. Dupré (2003), Trace Elements in River Waters, in *Treatise on Geochemistry*, edited by H. D. Holland and K. K. Turekian, pp. 225–272, Elsevier.

Galy, A., and C. France-Lanord (1999), Weathering processes in the Ganges–Brahmaputra basin and the riverine alkalinity budget, *Chem. Geol.*, *159*(1-4), 31–60, doi:10.1016/S0009-2541(99)00033-9.

Galy, A., C. France-Lanord, and L. A. Derry (1999), The strontium isotopic budget of Himalayan rivers in Nepal and Bangladesh, *Geochim. Cosmochim. Acta*, *63*(13–14), 1905–1925, doi:10.1016/S0016-7037(99)00081-2.

Galy, A., M. Bar-Matthews, L. Halicz, and R. K. O'Nions (2002), Mg isotopic composition of carbonate: insight from speleothem formation, *Earth Planet. Sci. Lett.*, *201*(1), 105–115, doi:10.1016/S0012-821X(02)00675-1.

Galy, V., and T. Eglinton (2011), Protracted storage of biospheric carbon in the Ganges–Brahmaputra basin, *Nat. Geosci.*, *4*(12), 843–847, doi:10.1038/ngeo1293.

Galy, V., C. France-Lanord, O. Beyssac, P. Faure, H. Kudrass, and F. Palhol (2007), Efficient organic carbon burial in the Bengal fan sustained by the Himalayan erosional system, *Nature*, *450*(7168), 407–U6, doi:10.1038/nature06273.

Georg, R. B., B. C. Reynolds, M. Frank, and A. N. Halliday (2006), New sample preparation techniques for the determination of Si isotopic compositions using MC-ICPMS, *Chem. Geol.*, *235*(1-2), 95–104, doi:10.1016/j.chemgeo.2006.06.006.

Georg, R. B., A. J. West, A. R. Basu, and A. N. Halliday (2009), Silicon fluxes and isotope composition of direct groundwater discharge into the Bay of Bengal and the effect on the global ocean silicon isotope budget, *Earth Planet. Sci. Lett.*, *283*(1-4), 67–74, doi:10.1016/j.epsl.2009.03.041.

Hadden, R. L. (2008), *The geology of Burma (Myanmar): an annotated bibliography of Burma's geology, geography and earth science*, Topographic Engineering Center, US Army Corps of Engineers, Alexandria, VA.

Hartmann, J. (2009), Bicarbonate-fluxes and CO_2-consumption by chemical weathering on the Japanese Archipelago — Application of a multi-lithological model framework, *Chem. Geol.*, *265*(3-4), 237–271, doi:10.1016/j.chemgeo.2009.03.024.

Hartmann, J., N. Jansen, H. H. Dürr, S. Kempe, and P. Köhler (2009), Global CO_2-consumption by chemical weathering: What is the contribution of highly active weathering regions?, *Glob.*

Planet. Change, *69*(4), 185–194, doi:10.1016/j.gloplacha.2009.07.007.

Hélie, J.-F., C. Hillaire-Marcel, and B. Rondeau (2002), Seasonal changes in the sources and fluxes of dissolved inorganic carbon through the St. Lawrence River - isotopic and chemical constraint, *Chem. Geol.*, *186*(1-2), 117–138, doi:10.1016/S0009-2541(01)00417-X.

Heroy, D. C., S. A. Kuehl, and S. L. Goodbred Jr. (2003), Mineralogy of the Ganges and Brahmaputra Rivers: implications for river switching and Late Quaternary climate change, *Sediment. Geol.*, *155*(3–4), 343–359, doi:10.1016/S0037-0738(02)00186-0.

Hoefs, J. (2015), *Stable Isotope Geochemistry*, Springer International Publishing, Cham.

Hönisch, B. et al. (2012), The geological record of ocean acidification, *Science (80-.).*, *335*(6072), 1058–1063, doi:10.1126/science.1208277.

Hope, D., S. M. Palmer, M. F. Billett, and J. J. C. Dawson (2004), Variations in dissolved CO_2 and CH_4 in a first-order stream and catchment: an investigation of soil-stream linkages, *Hydrol. Process.*, *18*(17), 3255–3275, doi:10.1002/hyp.5657.

Hren, M. T., C. P. Chamberlain, G. E. Hilley, P. M. Blisniuk, and B. Bookhagen (2007), Major ion chemistry of the Yarlung Tsangpo–Brahmaputra river: Chemical weathering, erosion, and CO_2 consumption in the southern Tibetan plateau and eastern syntaxis of the Himalaya, *Geochim. Cosmochim. Acta*, *71*(12), 2907–2935, doi:10.1016/j.gca.2007.03.021.

Huang, F., J. Glessner, A. Ianno, C. Lundstrom, and Z. Zhang (2009), Magnesium isotopic composition of igneous rock standards measured by MC-ICP-MS, *Chem. Geol.*, *268*(1-2), 15–23, doi:10.1016/j.chemgeo.2009.07.003.

Huang, K.-J., F.-Z. Teng, G.-J. Wei, J.-L. Ma, and Z.-Y. Bao (2012), Adsorption- and desorption-controlled magnesium isotope fractionation during extreme weathering of basalt in Hainan Island, China, *Earth Planet. Sci. Lett.*, *359–360*, 73–83, doi:10.1016/j.epsl.2012.10.007.

Huang, X., M. Sillanpää, E. T. Gjessing, S. Peräniemi, and R. D. Vogt (2011), Water quality in the southern Tibetan Plateau: chemical evaluation of the Yarlung Tsangpo (Brahmaputra), *River Res. Appl.*, *27*(1), 113–121, doi:10.1002/rra.1332.

Huizing, H. G. J. (1971), A reconnaissance study of the mineralogy of sand fractions from East Pakistan sediments and soils, *Geoderma*, *6*(2), 109–133, doi:10.1016/0016-7061(71)90029-2.

Immenhauser, A., D. Buhl, D. Richter, A. Niedermayr, D. Riechelmann, M. Dietzel, and U. Schulte (2010), Magnesium-isotope fractionation during low-Mg calcite precipitation in a limestone

cave – Field study and experiments, *Geochim. Cosmochim. Acta*, *74*(15), 4346–4364, doi:10.1016/j.gca.2010.05.006.

Immerzeel, W. W., L. P. H. van Beek, and M. F. P. Bierkens (2010), Climate change will affect the Asian water towers, *Science (80-.).*, *328*(5984), 1382–1385, doi:10.1126/science.1183188.

IPCC (2013), *Climate Change 2013: The Physical Science Basis*, Contribution of Working Group I to the Fifth Assessment Report of the Intergovernmental Panel on Climate Change, Cambridge University Press, Cambridge, United Kingdom and New York, NY, USA.

IPCC (2014), *Climate Change 2014: Synthesis Report*, Contribution of Working Groups I, II and III to the Fifth Assessment Report of the Intergovernmental Panel on Climate Change, Cambridge University Press, Cambridge, United Kingdom and New York, NY, USA.

Islam, K. R., and R. R. Weil (2000), Land use effects on soil quality in a tropical forest ecosystem of Bangladesh, *Agric. Ecosyst. Environ.*, *79*(1), 9–16, doi:10.1016/S0167-8809(99)00145-0.

Jiang, L., Z. Yao, R. Wang, Z. Liu, L. Wang, and S. Wu (2015), Hydrochemistry of the middle and upper reaches of the Yarlung Tsangpo River system: weathering processes and CO_2 consumption, *Environ. Earth Sci.*, *74*(3), 2369–2379, doi:10.1007/s12665-015-4237-6.

Jonsson, A., J. Åberg, and M. Jansson (2007), Variations in pCO_2 during summer in the surface water of an unproductive lake in northern Sweden, *Tellus*, *59*(5), 797–803, doi:10.1111/j.1600-0889.2007.00307.x.

Karim, A., and J. Veizer (2000), Weathering processes in the Indus River Basin: implications from riverine carbon, sulfur, oxygen, and strontium isotopes, *Chem. Geol.*, *170*(1-4), 153–177, doi:10.1016/S0009-2541(99)00246-6.

Kawahata, H., I. Yukino, and A. Suzuki (2000), Terrestrial influences on the Shiraho fringing reef, Ishigaki Island, Japan: high carbon input relative to phosphate, *Coral Reefs*, *19*(2), 172–178, doi:10.1007/s003380000093.

Kempe, S. (1982), Long-term records of CO_2 pressure fluctuations in fresh waters, in *Transport of carbon and minerals in major world rivers, part 1*, edited by E. T. Degens, pp. 91–332, Geologisch-Paläontologisches Institut Universität Hamburg, Hamburg.

Kısakűrek, B., R. H. James, and N. B. W. Harris (2005), Li and δ^7Li in Himalayan rivers: Proxies for silicate weathering?, *Earth Planet. Sci. Lett.*, *237*(3–4), 387–401, doi:10.1016/j.epsl.2005.07.019.

Kuehl, S. A., M. A. Allison, S. L. Goodbred, and H. Kudrass (2005), The Ganges-Brahmaputra Delta,

in *SEPM Special Publication, No.83,* pp. 413–434.

Lakshminarayana, J. S. S. (1965), Studies on phytoplankton of the River Ganges, Varanasi, India PartI: The physico-chemical characteristics of River Ganges, *Hydrobiologia*, *25*(1-2), doi:10.1007/BF00189858.

Lal, M., and H. Harasawa (2001), Future climate change scenarios for Asia as inferred from selected coupled atmosphere-ocean global climate models, *J. Meteorol. Soc. Japan. Ser. II*, *79*(1), 219–227.

Larsen, I. J., P. C. Almond, A. Eger, J. O. Stone, D. R. Montgomery, and B. Malcolm (2014), Rapid soil production and weathering in the Southern Alps, New Zealand, *Science (80-.).*, *343*(6171), 637–640, doi:10.1126/science.1244908.

Lee, S.-W., J.-S. Ryu, and K.-S. Lee (2014), Magnesium isotope geochemistry in the Han River, South Korea, *Chem. Geol.*, *364*, 9–19, doi:10.1016/j.chemgeo.2013.11.022.

Li, S., X. X. Lu, M. He, Y. Zhou, R. Bei, L. Li, and A. D. Ziegler (2011), Major element chemistry in the upper Yangtze River: A case study of the Longchuanjiang River, *Geomorphology*, *129*(1-2), 29–42, doi:10.1016/j.geomorph.2011.01.010.

Li, S., X. X. Lu, and R. T. Bush (2013), CO_2 partial pressure and CO_2 emission in the Lower Mekong River, *J. Hydrol.*, *504*, 40–56, doi:10.1016/j.jhydrol.2013.09.024.

Li, S., X. X. Lu, and R. T. Bush (2014), Chemical weathering and CO_2 consumption in the Lower Mekong River, *Sci. Total Environ.*, *472*, 162–177, doi:10.1016/j.scitotenv.2013.11.027.

Li, W.-Y., F.-Z. Teng, S. Ke, R. L. Rudnick, S. Gao, F.-Y. Wu, and B. W. Chappell (2010), Heterogeneous magnesium isotopic composition of the upper continental crust, *Geochim. Cosmochim. Acta*, *74*(23), 6867–6884, doi:10.1016/j.gca.2010.08.030.

Liu, S.-A., F.-Z. Teng, Y. He, S. Ke, and S. Li (2010), Investigation of magnesium isotope fractionation during granite differentiation: Implication for Mg isotopic composition of the continental crust, *Earth Planet. Sci. Lett.*, *297*(3–4), 646–654, doi:10.1016/j.epsl.2010.07.019.

Liu, X.-M., F.-Z. Teng, R. L. Rudnick, W. F. McDonough, and M. L. Cummings (2014), Massive magnesium depletion and isotope fractionation in weathered basalts, *Geochim. Cosmochim. Acta*, *135*, 336–349, doi:10.1016/j.gca.2014.03.028.

Liu, Z., C. Colin, A. Trentesaux, G. Siani, N. Frank, D. Blamart, and S. Farid (2005), Late Quaternary climatic control on erosion and weathering in the eastern Tibetan Plateau and the Mekong Basin, *Quat. Res.*, *63*(3), 316–328, doi:10.1016/j.yqres.2005.02.005.

Löffler, E., W. P. Thompson, and M. Liengsakul (1984), Quaternary geomorphological development of the lower Mun River Basin, North East Thailand, *Catena*, *11*(4), 321–330, doi:10.1016/0341-8162(84)90030-4.

Lupker, M., C. France-Lanord, V. Galy, J. Lavé, J. Gaillardet, A. P. Gajurel, C. Guilmette, M. Rahman, S. K. Singh, and R. Sinha (2012), Predominant floodplain over mountain weathering of Himalayan sediments (Ganga basin), *Geochim. Cosmochim. Acta*, *84*, 410–432, doi:10.1016/j.gca.2012.02.001.

Manaka, T., H. Ushie, D. Araoka, A. Inamura, A. Suzuki, and H. Kawahata (2013), Rapid alkalization in Lake Inawashiro, Fukushima, Japan: implications for future changes in the carbonate system of terrestrial waters, *Aquat. Geochemistry*, *19*(4), 281–302, doi:10.1007/s10498-013-9195-6.

Manaka, T., and T. Yoshimura (2015), Behavior of magnesium isotopes in chemical weathering and rivers (in Japanese), *Chikyukagaku (Geochemistry)*, *49*(1), 45–58, doi:10.14934/chikyukagaku.49.45.

Martin, R. E. (1995), Cyclic and secular variation in microfossil biomineralization: clues to the biogeochemical evolution of Phanerozoic oceans, *Glob. Planet. Change*, *11*(1–2), 1–23, doi:10.1016/0921-8181(94)00011-2.

Mavromatis, V., Q. Gautier, O. Bosc, and J. Schott (2013), Kinetics of Mg partition and Mg stable isotope fractionation during its incorporation in calcite, *Geochim. Cosmochim. Acta*, *114*, 188–203, doi:10.1016/j.gca.2013.03.024.

Mavromatis, V., A. S. Prokushkin, O. S. Pokrovsky, J. Viers, and M. A. Korets (2014), Magnesium isotopes in permafrost-dominated Central Siberian larch forest watersheds, *Geochim. Cosmochim. Acta*, *147*, 76–89, doi:10.1016/j.gca.2014.10.009.

McArthur, J. M., D. T. Donovan, M. F. Thirlwall, B. W. Fouke, and D. Mattey (2000), Strontium isotope profile of the early Toarcian (Jurassic) oceanic anoxic event, the duration of ammonite biozones, and belemnite palaeotemperatures, *Earth Planet. Sci. Lett.*, *179*(2), 269–285, doi:10.1016/S0012-821X(00)00111-4.

Metcalfe, I. (1988), Origin and assembly of south-east Asian continental terranes, *Geol. Soc. London, Spec. Publ.*, *37*(1), 101–118, doi:10.1144/GSL.SP.1988.037.01.08.

Meybeck, M. (1987), Global chemical weathering of surficial rocks estimated from river dissolved loads, *Am. J. Sci.*, *287*(5), 401–428, doi:10.2475/ajs.287.5.401.

Meybeck, M. (2003), Global Occurrence of Major Elements in Rivers, in *Treatise on Geochemistry*, edited by H. D. Holland and K. K. Turekian, pp. 207–223, Elsevier.

Meybeck, M., and A. Ragu (2012), *GEMS-GLORI world river discharge database*, Laboratoire de Géologie Appliquée, Université Pierre et Marie Curie, Paris, France.

Millero, F. J. (1979), The thermodynamics of the carbonate system in seawater, *Geochim. Cosmochim. Acta*, *43*(11-12), 1651–1661, doi:10.1016/0016-7037(79)90184-4.

Millero, F. J. (2003), Physicochemical Controls on Seawater, in *Treatise on Geochemistry*, edited by H. D. Holland and K. K. Turekian, pp. 1–21, Elsevier, Oxford.

Milliman, J. D., and R. H. Meade (1983), World-wide delivery of river sediment to the oceans, *J. Geol.*, *91*(1), 1–21.

Milliman, J. D., C. Rutkowski, and M. Meybeck (1995), *River discharge to the sea: a global river index (GLORI)*, Texel, NIOZ.

Mirza, M. M. Q. (2002), Global warming and changes in the probability of occurrence of floods in Bangladesh and implications, *Glob. Environ. Chang.*, *12*(2), 127–138, doi:10.1016/S0959-3780(02)00002-X.

Molnar, P., P. England, and J. Martinod (1993), Mantle dynamics, uplift of the Tibetan Plateau, and the Indian Monsoon, *Rev. Geophys.*, *31*(4), 357–396, doi:10.1029/93RG02030.

Mouret, C. (1994), Geological history of northeastern Thailand since the Carboniferous: relations with Indochina and Carboniferous to early Cenozoic evolution model, in *Proceedings of the International Symposium on: Stratigraphic correlation of southeast Asia*, edited by T. Thanasuthipitak and P. Ounchanum, pp. 132–157, Dep. of Mineral Resour., Bangkok.

Na, C., T. Nakano, K. Tazawa, M. Sakagawa, and T. Ito (1995), A systematic and practical method of liquid chromatography for the determination of Sr and Nd isotopic ratios and REE concentrations in geological samples, *Chem. Geol.*, *123*(1–4), 225–237, doi:10.1016/0009-2541(95)00005-7.

Nagahora, S., H. Mikami, Y. Ishikawa, S. Igarashi, T. Fujita, K. Murata, and K. Sakata (2002), Characterization of dissolved fulvic acid extracted from the stream water in the Kushiro Bog (in Japanese), *J. Jpn Soc. Water Environ.*, *25*(4), 229–233, doi:10.2965/jswe.25.229.

Nakapadungrat, S., and P. Putthapiban (1992), Granites and associated mineralisation in Thailand, in *Proceedings of the National Conference on Geologie Resources of Thailand: Potential for Future Development*, pp. 153–171, Dep. of Miner. Resour., Bangkok.

National Oceanic and Atmospheric Administration (NOAA) (2013), NNDC Climate Data Online, Available from: http://www7.ncdc.noaa.gov/CDO/cdo

National Research Council (1992), *Restoration of Aquatic Ecosystems: Science, Technology, and Public Policy*, National Academies Press, Washington, D.C.

Naushad, M., and Z. A. Al-Othman (2013), *A Book on Ion Exchange, Adsorption and Solvent Extraction*, Nova Science Pub Inc.

Négrel, P., C. J. Allègre, B. Dupré, and E. Lewin (1993), Erosion sources determined by inversion of major and trace element ratios and strontium isotopic ratios in river water: The Congo Basin case, *Earth Planet. Sci. Lett.*, *120*(1), 59–76, doi:10.1016/0012-821X(93)90023-3.

Nelson, D. M., P. Tréguer, M. A. Brzezinski, A. Leynaert, and B. Quéguiner (1995), Production and dissolution of biogenic silica in the ocean: Revised global estimates, comparison with regional data and relationship to biogenic sedimentation, *Global Biogeochem. Cycles*, *9*(3), 359–372, doi:10.1029/95GB01070.

Nelson, F., T. Murase, and K. A. Kraus (1964), Ion exchange procedures, *J. Chromatogr. A*, *13*, 503–535, doi:10.1016/S0021-9673(01)95146-5.

Nishio, Y., K. Okamura, M. Tanimizu, T. Ishikawa, and Y. Sano (2010), Lithium and strontium isotopic systematics of waters around Ontake volcano, Japan: Implications for deep-seated fluids and earthquake swarms, *Earth Planet. Sci. Lett.*, *297*(3-4), 567–576, doi:10.1016/j.epsl.2010.07.008.

Nixon, S. W. (1995), Coastal marine eutrophication: definition, social causes, and future concerns, *Ophelia*, *41*, 199–219.

Noh, H., Y. Huh, J. Qin, and A. Ellis (2009), Chemical weathering in the Three Rivers region of Eastern Tibet, *Geochim. Cosmochim. Acta*, *73*(7), 1857–1877, doi:10.1016/j.gca.2009.01.005.

Oelze, M., F. von Blanckenburg, D. Hoellen, M. Dietzel, and J. Bouchez (2014), Si stable isotope fractionation during adsorption and the competition between kinetic and equilibrium isotope fractionation: Implications for weathering systems, *Chem. Geol.*, *380*, 161–171, doi:10.1016/j.chemgeo.2014.04.027.

Oliver, L., N. Harris, M. Bickle, H. Chapman, N. Dise, and M. Horstwood (2003), Silicate weathering rates decoupled from the $^{87}Sr/^{86}Sr$ ratio of the dissolved load during Himalayan erosion, *Chem. Geol.*, *201*(1–2), 119–139, doi:10.1016/S0009-2541(03)00236-5.

Opfergelt, S., R. B. Georg, B. Delvaux, Y.-M. Cabidoche, K. W. Burton, and A. N. Halliday (2012), Mechanisms of magnesium isotope fractionation in volcanic soil weathering sequences, Guadeloupe, *Earth Planet. Sci. Lett.*, *341–344*, 176–185, doi:10.1016/j.epsl.2012.06.010.

Palmer, M. R., and J. M. Edmond (1992), Controls over the strontium isotope composition of river water, *Geochim. Cosmochim. Acta*, *56*(5), 2099–2111, doi:10.1016/0016-7037(92)90332-D.

Parkhurst, D. L., and C. A. J. Appelo (2013), Description of input and examples for PHREEQC version 3—A computer program for speciation, batch-reaction, one-dimensional transport, and inverse geochemical calculations, Available from: http://pubs.usgs.gov/tm/06/a43/

Parua, P. K. (2010), *The Ganga: Water Use in the Indian Subcontinent*, Water Science and Technology Library, Springer.

Paul, M., L. Reisberg, N. Vigier, Y. Zheng, K. M. Ahmed, L. Charlet, and M. R. Huq (2010), Dissolved osmium in Bengal plain groundwater: Implications for the marine Os budget, *Geochim. Cosmochim. Acta*, *74*(12), 3432–3448, doi:10.1016/j.gca.2010.02.034.

Pistiner, J. S., and G. M. Henderson (2003), Lithium-isotope fractionation during continental weathering processes, *Earth Planet. Sci. Lett.*, *214*(1–2), 327–339, doi:10.1016/S0012-821X(03)00348-0.

Plummer, L. N., and E. Busenberg (1982), The solubilities of calcite, aragonite and vaterite in CO_2, *Geochim. Cosmochim. Acta*, *46*(6), 1011–1040, doi:10.1016/0016-7037(82)90056-4.

Pogge von Strandmann, P. A. E., R. H. James, P. van Calsteren, S. R. Gíslason, and K. W. Burton (2008a), Lithium, magnesium and uranium isotope behaviour in the estuarine environment of basaltic islands, *Earth Planet. Sci. Lett.*, *274*(3–4), 462–471, doi:10.1016/j.epsl.2008.07.041.

Pogge von Strandmann, P. A. E., K. W. Burton, R. H. James, P. van Calsteren, S. R. Gislason, and B. Sigfússon (2008b), The influence of weathering processes on riverine magnesium isotopes in a basaltic terrain, *Earth Planet. Sci. Lett.*, *276*(1–2), 187–197, doi:10.1016/j.epsl.2008.09.020.

Pogge von Strandmann, P. A. E., S. Opfergelt, Y.-J. Lai, B. Sigfússon, S. R. Gislason, and K. W. Burton (2012), Lithium, magnesium and silicon isotope behaviour accompanying weathering in a basaltic soil and pore water profile in Iceland, *Earth Planet. Sci. Lett.*, *339–340*, 11–23, doi:10.1016/j.epsl.2012.05.035.

Rai, S. K., S. K. Singh, and S. Krishnaswami (2010), Arsenic migration to deep groundwater in

Bangladesh influenced by adsorption and water demand, *Geochim. Cosmochim. Acta*, *74*(8), 2340–2355, doi:10.1016/j.gca.2010.01.008.

Raich, J. W., and W. H. Schlesinger (1992), The global carbon dioxide flux in soil respiration and its relationship to vegetation and climate, *Tellus B*, *44*(2), 81–99, doi:10.1034/j.1600-0889.1992.t01-1-00001.x.

Raymahashay, B. C. (1970), Characteristics of stream erosion in the Himalayan region of India, in *Proceedings of Symposium on Hydrogeochemistry and Biogeochemistry, Volume 1 - Hydrogeochemistry*, pp. 82–92, the Clarke Company.

Raymo, M. E. (1991), Geochemical evidence supporting T. C. Chamberlin's theory of glaciation, *Geology*, *19*(4), 344–347, doi:10.1130/0091-7613(1991)019<0344:GESTCC>2.3.CO;2.

Raymo, M. E., and W. F. Ruddiman (1992), Tectonic forcing of late Cenozoic climate, *Nature*, *359*(6391), 117–122, doi:10.1038/359117a0.

Raymo, M. E., W. F. Ruddiman, and P. N. Froelich (1988), Influence of late Cenozoic mountain building on ocean geochemical cycles, *Geology*, *16*(7), 649–653, doi:10.1130/0091-7613(1988)016<0649:IOLCMB>2.3.CO;2.

Raymond, P. A., and J. J. Cole (2003), Increase in the export of alkalinity from North America's largest river, *Science (80-.).*, *301*(5629), 88–91, doi:10.1126/science.1083788.

Raymond, P. A. et al. (2013), Global carbon dioxide emissions from inland waters, *Nature*, *503*(7476), 355–359, doi:10.1038/nature12760.

Regnier, P. et al. (2013), Anthropogenic perturbation of the carbon fluxes from land to ocean, *Nat. Geosci.*, *6*(8), 597–607, doi:10.1038/ngeo1830.

Rengarajan, R., S. K. Singh, M. M. Sarin, and S. Krishnaswami (2009), Strontium isotopes and major ion chemistry in the Chambal River system, India: Implications to silicate erosion rates of the Ganga, *Chem. Geol.*, *260*(1–2), 87–101, doi:10.1016/j.chemgeo.2008.12.013.

Reynolds, B., M. Frank, and A. Halliday (2006), Silicon isotope fractionation during nutrient utilization in the North Pacific, *Earth Planet. Sci. Lett.*, *244*(1-2), 431–443, doi:10.1016/j.epsl.2006.02.002.

Richey, J. E., J. M. Melack, A. K. Aufdenkampe, V. M. Ballester, and L. L. Hess (2002), Outgassing from Amazonian rivers and wetlands as a large tropical source of atmospheric CO_2, *Nature*, *416*(6881), 617–620, doi:10.1038/416617a.

Riebe, C. S., J. W. Kirchner, and R. C. Finkel (2004), Erosional and climatic effects on long-term

chemical weathering rates in granitic landscapes spanning diverse climate regimes, *Earth Planet. Sci. Lett.*, *224*(3–4), 547–562, doi:10.1016/j.epsl.2004.05.019.

River Survey Project (1996), *Spatial representation and analysis of hydraulic and morphologic data: water resources planning organization*, Dhaka flood plan coordination organization, River Survey Study Rep. 5, Water Resour. Planning Project, Gov. of Bangladesh, Dhaka.

Robbins, L. L., M. E. Hansen, J. A. Kleypas, and S. C. Meylan (2010), *CO_2calc: a user-friendly seawater carbon calculator for Windows, Mac OS X, and iOS (iPhone)*, U.S. Geological Survey Open-File Report 2010–1280.

Robert, F., and M. Chaussidon (2006), A palaeotemperature curve for the Precambrian oceans based on silicon isotopes in cherts, *Nature*, *443*(7114), 969–972, doi:10.1038/nature05239.

Robinson, R. A. J., C. A. Brezina, R. R. Parrish, M. S. A. Horstwood, N. W. Oo, M. I. Bird, M. Thein, A. S. Walters, G. J. H. Oliver, and K. Zaw (2014), Large rivers and orogens: The evolution of the Yarlung Tsangpo–Irrawaddy system and the eastern Himalayan syntaxis, *Gondwana Res.*, *26*(1), 112–121, doi:10.1016/j.gr.2013.07.002.

Rudnick, R. L., and S. Gao (2003), Composition of the Continental Crust, in *Treatise on Geochemistry*, edited by H. D. Holland and K. K. Turekian, pp. 1–64, Elsevier, Oxford.

Saenger, C., and Z. Wang (2014), Magnesium isotope fractionation in biogenic and abiogenic carbonates: implications for paleoenvironmental proxies, *Quat. Sci. Rev.*, *90*, 1–21, doi:10.1016/j.quascirev.2014.01.014.

Sarin, M. M. (2001), Biogeochemistry of Himalayan rivers as an agent of climate change, *Curr. Sci.*, *81*(11), 1446–1450.

Sarin, M. M., S. Krishnaswami, K. Dilli, B. L. K. Somayajulu, and W. S. Moore (1989), Major ion chemistry of the Ganga-Brahmaputra river system: Weathering processes and fluxes to the Bay of Bengal, *Geochim. Cosmochim. Acta*, *53*(5), 997–1009, doi:10.1016/0016-7037(89)90205-6.

Sarma, V. V. S. S., M. S. Krishna, V. D. Rao, R. Viswanadham, N. A. Kumar, T. R. Kumari, L. Gawade, S. Ghatkar, and A. Tari (2012), Sources and sinks of CO_2 in the west coast of Bay of Bengal, *Tellus*, *64*, 10961, doi:10.3402/tellusb.v64i0.10961.

Sarmiento, J. L., and N. Gruber (2006), *Ocean Biogeochemical Dynamics*, Princeton University Press, Princeton, NJ.

Saulnier, S., C. Rollion-Bard, N. Vigier, and M. Chaussidon (2012), Mg isotope fractionation during

calcite precipitation: An experimental study, *Geochim. Cosmochim. Acta*, *91*, 75–91, doi:10.1016/j.gca.2012.05.024.

Savage, P. S., R. B. Georg, H. M. Williams, and A. N. Halliday (2013), The silicon isotope composition of the upper continental crust, *Geochim. Cosmochim. Acta*, *109*, 384–399, doi:10.1016/j.gca.2013.02.004.

Schmitt, A.-D., N. Vigier, D. Lemarchand, R. Millot, P. Stille, and F. Chabaux (2012), Processes controlling the stable isotope compositions of Li, B, Mg and Ca in plants, soils and waters: A review, *Comptes Rendus Geosci.*, *344*(11–12), 704–722, doi:10.1016/j.crte.2012.10.002.

Senga, Y., M. Hiroki, Y. Nakamura, Y. Watarai, Y. Watanabe, and S. Nohara (2010), Vertical profiles of DIN, DOC, and microbial activities in the wetland soil of Kushiro Mire, northeastern Japan, *Limnology*, *12*(1), 17–23, doi:10.1007/s10201-010-0316-2.

Shrestha, R. P. (2006), Relating soil electrical conductivity to remote sensing and other soil properties for assessing soil salinity in northeast Thailand, *L. Degrad. Dev.*, *17*(6), 677–689, doi:10.1002/ldr.752.

Siegenthaler, U., and J. L. Sarmiento (1993), Atmospheric carbon dioxide and the ocean, *Nature*, *365*(6442), 119–125, doi:10.1038/365119a0.

Ben Sik Ali, M., B. Hamrouni, S. Bouguecha, and M. Dhahbi (2004), Silica removal using ion-exchange resins, *Desalination*, *167*, 273–279, doi:10.1016/j.desal.2004.06.136.

Singh, S., M. Singh, A. K. Choudhary, A. Saxena, I. B. Singh, and A. K. Jain (2010), Sr isotopic signature of the Ganga Alluvial Plain and its implication to Sr flux of the Ganga River System, *Int. J. Earth Sci.*, *99*(8), 1991–1997, doi:10.1007/s00531-009-0479-4.

Singh, S. K., J. R. Trivedi, K. Pande, R. Ramesh, and S. Krishnaswami (1998), Chemical and strontium, oxygen, and carbon isotopic compositions of carbonates from the Lesser Himalaya: implications to the strontium isotope composition of the source waters of the Ganga, Ghaghara, and the Indus rivers, *Geochim. Cosmochim. Acta*, *62*(5), 743–755, doi:10.1016/S0016-7037(97)00381-5.

Singh, S. K., M. M. Sarin, and C. France-Lanord (2005), Chemical erosion in the eastern Himalaya: Major ion composition of the Brahmaputra and $\delta^{13}C$ of dissolved inorganic carbon, *Geochim. Cosmochim. Acta*, *69*(14), 3573–3588, doi:10.1016/j.gca.2005.02.033.

Singh, S. K., A. Kumar, and C. France-Lanord (2006), Sr and $^{87}Sr/^{86}Sr$ in waters and sediments of the Brahmaputra river system: Silicate weathering, CO_2 consumption and Sr flux, *Chem. Geol.*,

234(3-4), 308–320, doi:10.1016/j.chemgeo.2006.05.009.

Singh, S. P., S. K. Singh, R. Bhushan, and V. K. Rai (2015), Dissolved silicon and its isotopes in the water column of the Bay of Bengal: Internal cycling versus lateral transport, *Geochim. Cosmochim. Acta*, *151*, 172–191, doi:10.1016/j.gca.2014.12.019.

Sobek, S., G. Algesten, A.-K. Bergstrom, M. Jansson, and L. J. Tranvik (2003), The catchment and climate regulation of pCO_2 in boreal lakes, *Glob. Chang. Biol.*, *9*(4), 630–641, doi:10.1046/j.1365-2486.2003.00619.x.

Steiger, R. H., and E. Jäger (1977), Subcommission on geochronology: Convention on the use of decay constants in geo- and cosmochronology, *Earth Planet. Sci. Lett.*, *36*(3), 359–362, doi:10.1016/0012-821X(77)90060-7.

Stewart, R. J., B. Hallet, P. K. Zeitler, M. A. Malloy, C. M. Allen, and D. Trippett (2008), Brahmaputra sediment flux dominated by highly localized rapid erosion from the easternmost Himalaya, *Geology*, *36*(9), 711–714, doi:10.1130/G24890A.1.

Strelow, F. W. E., A. H. Victor, C. R. Van Zyl, and C. Eloff (1971), Distribution coefficients and cation exchange behavior of elements in hydrochloric acid-acetone, *Anal. Chem.*, *43*(7), 870–876, doi:10.1021/ac60302a015.

Sun, X., P. S. Andersson, C. Humborg, M. Pastuszak, and C.-M. Mörth (2013), Silicon isotope enrichment in diatoms during nutrient-limited blooms in a eutrophied river system, *J. Geochemical Explor.*, *132*, 173–180, doi:10.1016/j.gexplo.2013.06.014.

Suzuki, A., T. Nakamori, and H. Kayanne (1995), The mechanism of production enhancement in coral reef carbonate systems: model and empirical results, *Sediment. Geol.*, *99*(3-4), 259–280, doi:10.1016/0037-0738(95)00048-D.

Tang, Y.-J., H.-F. Zhang, and J.-F. Ying (2007), Review of the lithium isotope system as a geochemical tracer, *Int. Geol. Rev.*, *49*(4), 374–388, doi:10.2747/0020-6814.49.4.374.

Tanimizu, M. (2008), Determination of Mg isotopic composition of seawater with a rapid Mg purification technique, *J. Nucl. Sci. Technol.*, 51–54.

Telmer, K., and J. Veizer (1999), Carbon fluxes, pCO_2 and substrate weathering in a large northern river basin, Canada: carbon isotope perspectives, *Chem. Geol.*, *159*(1-4), 61–86, doi:10.1016/S0009-2541(99)00034-0.

Teng, F.-Z., W. F. McDonough, R. L. Rudnick, and B. A. Wing (2007), Limited lithium isotopic fractionation during progressive metamorphic dehydration in metapelites: A case study from

the Onawa contact aureole, Maine, *Chem. Geol.*, *239*(1–2), 1–12, doi:10.1016/j.chemgeo.2006.12.003.

Teng, F.-Z., W.-Y. Li, R. L. Rudnick, and L. R. Gardner (2010a), Contrasting lithium and magnesium isotope fractionation during continental weathering, *Earth Planet. Sci. Lett.*, *300*(1–2), 63–71, doi:10.1016/j.epsl.2010.09.036.

Teng, F.-Z., W.-Y. Li, S. Ke, B. Marty, N. Dauphas, S. Huang, F.-Y. Wu, and A. Pourmand (2010b), Magnesium isotopic composition of the Earth and chondrites, *Geochim. Cosmochim. Acta*, *74*(14), 4150–4166, doi:10.1016/j.gca.2010.04.019.

Terai, H., K. Ohta, S. Shidara, M. Kasuya, and D. Adams, Donald (2002), CH_4-, N_2O- and H_2- fluxes and microbial processes in Kushiro Wetland, *Annu. Rep. Res. Inst. Biol. Funct.*, *2*, 7–15.

Thailand Meteorological Department (2014), Climate Charts, Available from: http://www.tmd.go.th/en/

Tipper, E. T., A. Galy, J. Gaillardet, M. J. Bickle, H. Elderfield, and E. A. Carder (2006), The magnesium isotope budget of the modern ocean: Constraints from riverine magnesium isotope ratios, *Earth Planet. Sci. Lett.*, *250*(1-2), 241–253, doi:10.1016/j.epsl.2006.07.037.

Tipper, E. T., A. Galy, and M. J. Bickle (2008), Calcium and magnesium isotope systematics in rivers draining the Himalaya-Tibetan-Plateau region: Lithological or fractionation control?, *Geochim. Cosmochim. Acta*, *72*(4), 1057–1075, doi:10.1016/j.gca.2007.11.029.

Tipper, E. T., D. Calmels, J. Gaillardet, P. Louvat, F. Capmas, and B. Dubacq (2012a), Positive correlation between Li and Mg isotope ratios in the river waters of the Mackenzie Basin challenges the interpretation of apparent isotopic fractionation during weathering, *Earth Planet. Sci. Lett.*, *333–334*, 35–45, doi:10.1016/j.epsl.2012.04.023.

Tipper, E. T., E. Lemarchand, R. S. Hindshaw, B. C. Reynolds, and B. Bourdon (2012b), Seasonal sensitivity of weathering processes: Hints from magnesium isotopes in a glacial stream, *Chem. Geol.*, *312–313*, 80–92, doi:10.1016/j.chemgeo.2012.04.002.

Tripathy, G., S. Singh, and S. Krishnaswami (2012), Sr and Nd isotopes as tracers of chemical and physical erosion, in *Handbook of Environmental Isotope Geochemistry SE - 26*, edited by M. Baskaran, pp. 521–552, Springer Berlin Heidelberg.

Tripathy, G. R., and S. K. Singh (2010), Chemical erosion rates of river basins of the Ganga system in the Himalaya: Reanalysis based on inversion of dissolved major ions, Sr, and 87Sr/86Sr, *Geochemistry, Geophys. Geosystems*, *11*(3), doi:10.1029/2009GC002862.

Tripathy, G. R., V. Goswami, S. K. Singh, and G. J. Chakrapani (2010), Temporal variations in Sr and $^{87}Sr/^{86}Sr$ of the Ganga headwaters: estimates of dissolved Sr flux to the mainstream, *Hydrol. Process.*, *24*(9), 1159–1171, doi:10.1002/hyp.7572.

Turner, R. E., N. N. Rabalais, D. Justic, and Q. Dortch (2003), Global patterns of dissolved N, P and Si in large rivers, *Biogeochemistry*, *64*(3), 297–317, doi:10.1023/A:1024960007569.

Ushie, H., H. Kawahata, A. Suzuki, S. Murayama, and M. Inoue (2010), Enhanced riverine carbon flux from carbonate catchment to the ocean: A comparative hydrogeochemical study on Ishigaki and Iriomote islands, southwestern Japan, *J. Geophys. Res.*, *115*(G2), G02017, doi:10.1029/2009JG001039.

Vollenweider, R. A. (1968), *Scientific fundamentals of the eutrophication of lakes and flowing waters, with particular reference to nitrogen and phosphorus as factors in eutrophication*, Organisation for Economic Co-operaion and Development, Paris.

Walker, J. C. G., P. B. Hays, and J. F. Kasting (1981), A negative feedback mechanism for the long-term stabilization of Earth's surface temperature, *J. Geophys. Res. Ocean.*, *86*(C10), 9776–9782, doi:10.1029/JC086iC10p09776.

Wandrey, C. J., and B. E. Law (1997), *Maps showing geology, oil and gas fields and geological provinces of South Asia*, U. S. Geological Survey Open File Report 97-470C.

Wang, Z., P. Hu, G. Gaetani, C. Liu, C. Saenger, A. Cohen, and S. Hart (2013a), Experimental calibration of Mg isotope fractionation between aragonite and seawater, *Geochim. Cosmochim. Acta*, *102*, 113–123, doi:10.1016/j.gca.2012.10.022.

Wang, Z. A., D. J. Bienvenu, P. J. Mann, K. a. Hoering, J. R. Poulsen, R. G. M. Spencer, and R. M. Holmes (2013b), Inorganic carbon speciation and fluxes in the Congo River, *Geophys. Res. Lett.*, *40*(3), 511–516, doi:10.1002/grl.50160.

Webster, P. J., J. Jian, T. M. Hopson, C. D. Hoyos, P. a. Agudelo, H.-R. Chang, J. a. Curry, R. L. Grossman, T. N. Palmer, and a. R. Subbiah (2010), Extended-range probabilistic forecasts of Ganges and Brahmaputra floods in Bangladesh, *Bull. Am. Meteorol. Soc.*, *91*(11), 1493–1514, doi:10.1175/2010BAMS2911.1.

Whittaker, R., and G. Likens (1973), Primary production: The biosphere and man, *Hum. Ecol.*, *1*(4), 357–369, doi:10.1007/BF01536732.

Wilkinson, B. H., and T. J. Algeo (1989), Sedimentary carbonate record of calcium-magnesium cycling, *Am. J. Sci.*, *289*(10), 1158–1194, doi:10.2475/ajs.289.10.1158.

Wilkinson, S. R., R. M. Welch, H. F. Mayland, and D. L. Grunes (1990), Magnesium in plants: uptake, distribution, function, and utilization by man and animals, in *Metal Ions in Biological Systems:*, vol. 26, edited by H. Sigel and S. Astrid, pp. 33–56, Marcel Dekker, Inc.

Wimpenny, J., K. W. Burton, R. H. James, A. Gannoun, F. Mokadem, and S. R. Gíslason (2011), The behaviour of magnesium and its isotopes during glacial weathering in an ancient shield terrain in West Greenland, *Earth Planet. Sci. Lett.*, *304*(1–2), 260–269, doi:10.1016/j.epsl.2011.02.008.

Wongpokhom, N., I. Kheoruenromne, A. Suddhiprakarn, and R. J. Gilkes (2008), Micromorphological properties of salt affected soils in Northeast Thailand, *Geoderma*, *144*(1–2), 158–170, doi:10.1016/j.geoderma.2007.10.026.

Wu, W., S. Xu, J. Yang, and H. Yin (2008), Silicate weathering and CO_2 consumption deduced from the seven Chinese rivers originating in the Qinghai-Tibet Plateau, *Chem. Geol.*, *249*(3-4), 307–320, doi:10.1016/j.chemgeo.2008.01.025.

Yang, W., F.-Z. Teng, H.-F. Zhang, and S.-G. Li (2012), Magnesium isotopic systematics of continental basalts from the North China craton: Implications for tracing subducted carbonate in the mantle, *Chem. Geol.*, *328*, 185–194, doi:10.1016/j.chemgeo.2012.05.018.

Yao, G., Q. Gao, Z. Wang, X. Huang, T. He, Y. Zhang, S. Jiao, and J. Ding (2007), Dynamics of CO_2 partial pressure and CO_2 outgassing in the lower reaches of the Xijiang River, a subtropical monsoon river in China, *Sci. Total Environ.*, *376*(1-3), 255–266, doi:10.1016/j.scitotenv.2007.01.080.

Yin, A., and T. M. Harrison (2000), Geologic evolution of the Himalayan-Tibetan orogen, *Annu. Rev. Earth Planet. Sci.*, *28*, 211–280, doi:10.1146/annurev.earth.28.1.211.

Yoshimura, T., M. Tanimizu, M. Inoue, A. Suzuki, N. Iwasaki, and H. Kawahata (2011), Mg isotope fractionation in biogenic carbonates of deep-sea coral, benthic foraminifera, and hermatypic coral, *Anal. Bioanal. Chem.*, *401*(9), 2755–2769, doi:10.1007/s00216-011-5264-0.

Young, E. D., and A. Galy (2004), The isotope geochemistry and cosmochemistry of magnesium, *Rev. Mineral. Geochemistry*, *55*, 197–230, doi:10.2138/gsrmg.55.1.197.

Zachos, J., M. Pagani, L. Sloan, E. Thomas, and K. Billups (2001), Trends, rhythms, and aberrations in global climate 65 Ma to present, *Science (80-.).*, *292*(5517), 686–693, doi:10.1126/science.1059412.

Zhai, W., M. Dai, and X. Guo (2007), Carbonate system and CO_2 degassing fluxes in the inner estuary

of Changjiang (Yangtze) River, China, *Mar. Chem.*, *107*(3), 342–356, doi:10.1016/j.marchem.2007.02.011.

Ziegler, K., O. A. Chadwick, M. A. Brzezinski, and E. F. Kelly (2005), Natural variations of $\delta^{30}Si$ ratios during progressive basalt weathering, Hawaiian Islands, *Geochim. Cosmochim. Acta*, *69*(19), 4597–4610, doi:10.1016/j.gca.2005.05.008.